DOE/PC/91008-3
(DE97008693)

IN SITU PERMEABILITY MODIFICATION USING GELLED POLYMER SYSTEMS

Topical Report
June 10, 1996 to April 10, 1997

By
D. W. Green
G. P. Willhite
C. S. McCool
J. A. Heppert
S. Vossoughi

October 1997

Performed Under Contract No. DE-AC22-94PC91008
Subcontract No. G4S60331

The University of Kansas
Lawrence, KS

National Petroleum Technology Office
U. S. DEPARTMENT OF ENERGY
Tulsa, Oklahoma

DOE/PC/91008-3
Distribution Category UC-122

In Situ Permeability Modification Using Gelled Polymer Systems

Topical Report
June 10, 1996 to April 10, 1997

By
D. W. Green
G. P. Willhite
C. S. McCool
J. A. Heppert
S.Vossoughi

October 1997

Work Performed Under Contract No. DE-AC22-94PC91008
Subcontract No. G4S60331
Mike Madden, BDM Program Manager

Prepared for
BDM-Oklahoma/
U.S. Department of Energy
Assistant Secretary for Fossil Energy

Jerry Casteel, Project Manager
National Petroleum Technology Office
P.O. Box 3628
Tulsa, OK 74101

Prepared by:
The University of Kansas
4006 Learned Hall
Lawrence, KS 66045-2223

Table of Contents

List of Figures

List of Tables

Abstract

The research program is directed at improving the understanding of gelled polymer systems and how these systems can be used to increase oil recovery from petroleum reservoirs. The research is focused on five areas: (1) Gel treatment in fractured systems; (2) Gel treatment in carbonate rocks; (3) In-depth placement of gels; (4) Gel systems for application in carbon dioxide flooding; and (5) Gel treatment in production wells. A physical model was developed to study gel treatments that are applied to fractures. The model was designed to examine the effect of leakoff on the placement and effectiveness of gelled polymer treatments. Chemistry of the sulfomethylated resorcinol-formaldehyde (SMRF) system was studied using mass spectrometry and nuclear magnetic resonance (NMR) tests to determine the composition of the sulfomethylated resorcinol solution. Modifications of the SMRF protocol were explored to make the system less expensive and more environmentally friendly. Results indicate that some of the alternate systems might gel at higher temperatures. In carbonate rocks, the buffering effect of carbonate minerals is widely recognized and is detrimental to some gel systems. Interactions between brines and a Baker dolomite core plug were investigated to determine the composition and pH of solutions after contact with the rock. A mathematical model of the dissolution of dolomite and other chemical equilibria gave a good match with experimental data taken at low flow rates. A method to extend the application of the polyacrylamide-chromium(III) acetate system to in-depth matrix treatments was studied at 25C. Screening tests showed that gel times can be increased significantly by the addition of acetate ion to the system and gelation can be prevented if the acetate/chromium ratio is large enough. A series of displacement experiments was completed to evaluate a system based on the gelation of KUSP1 biopolymer with orthoboric acid. The syneresis of this system was studied in bottle tests and in unconsolidated sandpacks. This gel system exhibits strong syneresis but the gel reduced the brine permeability in a sandpack even when there was significant syneresis. The effectiveness of KUSP1-boric acid gel in reducing permeability during a carbon dioxide flood was investigated in a Berea sandstone core. Residual resistance factors of 6.3 and 4.7 were observed for supercritical carbon dioxide and brine respectively after four WAG cycles. An experimental protocol for experiments to simulate the flows near a production well was developed. Gel treatments applied to production wells were studied using a Berea core slab (60 cm in length by 10 cm wide) and a microwave apparatus that allowed for determination of in situ water saturation as a function of slab length. Saturation profiles were determined following an oil flood after one quarter of the slab was treated with a gelled polymer system.

Executive Summary

Results from a research program on the application of gelled polymer technology for in situ permeability modification are presented in this report. The objective of this technology when used with displacement processes such as waterflooding is to reduce the permeability in fractures and/or high permeability matrix zones to improve volumetric sweep efficiency of the displacement process. In production wells, the objective is to reduce water influx.

The research program is focused on five areas:

- Gel treatment in fractured systems
- Gel treatment in carbonate rocks
- In-depth placement of gels
- Gel systems for application in carbon dioxide flooding
- Gel treatment in production wells

The research program is primarily an experimental program directed at improving the understanding of gelled polymer systems and how these systems can be used to increase oil recovery from petroleum reservoirs. A summary of progress for research conducted in the first 10 months of a 28 month program is described in the following sections.

Summary of Progress

Gel treatment in fractured systems: A physical model was developed to study gel treatments that are applied to fractures. The model was designed to examine the effect of leakoff on the placement and effectiveness of gelled polymer treatments. A Berea sandstone slab was fractured, equipped with entrance and exit flow compartments, and encapsulated with epoxy. Flow was regulated through the fracture such that leak-off occurred from the fracture and in to the porous matrix. Flow in the cell was characterized by permeability determinations, by tracer tests and by a series of flow experiments in which a viscous liquid displaced resident brine through the model.

Gel treatment in carbonate rocks: In previous research, we discovered that sulfomethylation of resorcinol lead to increased salinity and pH tolerance of a gel system based on the reaction of sulfomethylated resorcinol with formaldehyde. This system provides superior permeability reduction in carbonate rocks compared to current systems.

Chemistry of the sulfomethylated resorcinol-formaldehyde (SMRF) system was studied using mass spectrometry and nuclear magnetic resonance (NMR) tests to determine the composition of the sulfomethylated resorcinol solution. Modifications of the SMRF protocol were explored to make the system less expensive and more environmentally friendly. The alternate chemicals tested to-date failed to gel under conditions observed for SMRF. Results indicated that some of the alternate systems might gel at higher temperatures.

Many gel systems are sensitive to the pH environment when injected into matrix rock. In carbonate rocks, the buffering effect of carbonate minerals is widely recognized and is detrimental to some gel systems. Interactions between brines and a Baker dolomite core plug were investigated to determine the composition and pH of solutions after contact with the rock. Effects

of injected pH and flow rate on the composition of KCl brine displaced through the dolomite plug were determined. The effects of adding calcium and magnesium ions to the injected solutions were also studied. Both pH and divalent ion content varied with flow rate, indicating that there were rate effects at high flow rates. A mathematical model of the dissolution of dolomite and other chemical equilibria gave a good match with experimental data taken at low flow rates.

In-depth placement of gels: A method to extend the application of the polyacrylamide-chromium(III) acetate system to in-depth matrix treatments was studied at 25C. Bottle tests showed that gel times can be increased significantly by the addition of acetate ion to the system. Screening tests showed that gelation can be prevented if the acetate/chromium ratio is large enough. Flow tests in sandpacks showed that in situ gelation occurred sooner than in the bottle tests. Further work is required to determine if the system can be injected without significant development of flow resistance until after a shut-in period is applied.

Gel systems for application in carbon dioxide flooding: A series of displacement experiments was completed to evaluate a system based on the gelation of KUSP1 biopolymer with orthoboric acid. The syneresis of this system was studied in bottle tests and in unconsolidated sandpacks. This gel system exhibited strong syneresis and the rate of syneresis increased with increasing temperature, boric acid content and decreasing pH. However, the gel reduced the brine permeability in a sandpack even when there was significant syneresis. The effectiveness of KUSP1-boric acid gel in reducing permeability was also investigated in a Berea sandstone core at 41°C and a back pressure of 1200 psi by injecting supercritical carbon dioxide and brine into the core. Residual resistance factors of 6.3 and 4.7 were observed for supercritical carbon dioxide and brine respectively after four WAG cycles.

Gel treatment in production wells: An experimental protocol for experiments to simulate the flows near a production well was developed. Gel treatments applied to production wells were studied using a Berea core slab (60 cm in length by 10 cm wide) and a microwave apparatus that allowed for determination of in situ water saturation as a function of slab length. Oil and water relative permeability curves were determined at selected locations in the slab before gel treatment. Saturation profiles were determined following an oil flood after one quarter of the slab was treated with a gelled polymer system.

Chapter 1

Introduction

Research was conducted on the application of gelled polymer technology for in situ permeability modification. The objective of this technology when used in injection wells is to reduce the permeability of fractures and/or high permeability zones in order to improve the volumetric sweep efficiency of oil-recovery processes. In production wells, the objective is to reduce water influx.

Chemistry of the sulfomethylated resorcinol-formaldehyde (SMRF) system and related systems were investigated and the results are presented in Chapter 2. Low gelant viscosity and superior performance for reduction of permeability are two desirable characteristics of these systems. Knowledge of the chemistry will allow the selection of alternate chemicals that are less expensive and more environmentally friendly.

A physical model was developed to study gel treatments that are applied to fractures. The model was designed to simulate the flow encountered in and around a fracture that is near an injection well. The model allows flow through the fracture with leak-off into the adjoining porous matrix. Progress on the study of gel performance in fractures is presented in Chapter 3.

The chemical interactions between gelant and carbonate reservoirs can affect the performance of a gelled polymer treatment. The interactions between brines and Baker dolomite material were investigated and are reported in Chapter 4. Experimental results and simulations using geo-chemical equlibria reaction model are presented.

A method to increase the gel time of polyacrylamide-chromium(III) acetate systems in order to improve the application of the system to in-depth matrix treatments was studied and the progress is described in Chapter 5. Bottle tests and flow tests in sandpacks are reported.

The performance of the KUSP1-boric acid system for controlling carbon dioxide mobility during carbon dioxide flooding was studied and the results are described Chapter 6.

Gel treatments that are applied to production wells were studied using a Berea core slab and a microwave apparatus that allowed for determination of in situ water saturations as a function of slab length. Results of this investigation are presented in Chapter 7.

Chapter 2

The Chemistry of Sulfomethylated Resorcinol Formaldehyde Gels

Principal Investigator: J. Heppert
Graduate Research Assistant: Tim Baroni

Introduction

Sulfomethylated resorcinol formaldehyde gels (SMRF's) have been known for several years as potential permeability modifiers in tertiary oil recovery schemes.[1] These gels are closely related to phenol formaldehyde gels, which have been used in oil recovery applications,[2] as water soluble polymers, in controlled drug release applications and as precursors for bakelite-like phenol-formaldehyde resins. Under mild temperatures and basic reaction conditions, phenols react with formaldehyde to generate low molecular weight water soluble oligomers. These initial reactions presumably occur because of the potential nucleophilicity of phenoxide anion (**I**), which is formed under basic conditions (Eq. 2.1).

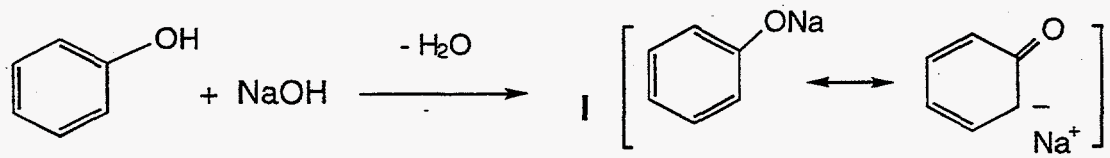

(Eq. 2.1)

Phenoxide anion engages in a range of coupling reactions with formaldehyde(Eq. 2.2), initially producing hydroxymethylated phenols (**II**).

(Eq. 2.2)

The coupling reactions eventually link phenol subunits (Eq. 2.3), generating low molecular weight methylene (CH_2)-bridged oligomers (**III**).

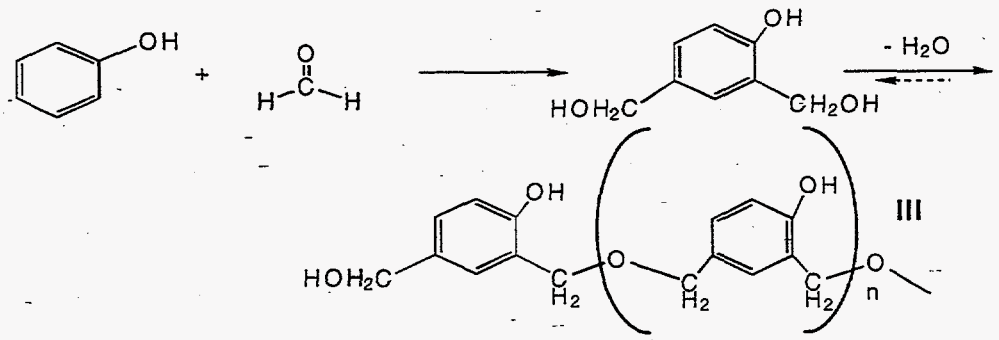

(Eq. 2.3)

As the molecular weight of these oligomers increases, they eventually form hydrogen-bonded gel networks with water that show significant resistance to sheer forces at concentrations between 2 and 3 weight percent. It is a combination of this toughness and the economics of the resorcinol and formaldehyde precursors that make resorcinol formaldehyde gels (RF's) interesting candidates in tertiary oil recovery.

Sulfomethylated resorcinol is formed by pre-treating resorcinol with sulfite and formaldehyde (Eq. 2.4). This pre-treatment generates a resorcinol monomer bearing a highly polar functional group (**IV**).

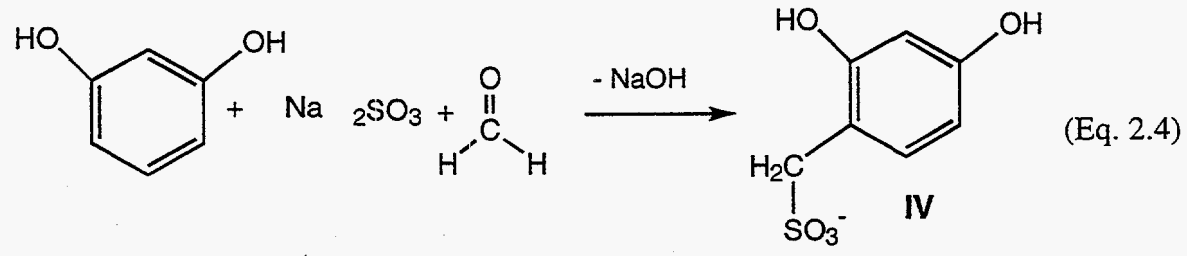

(Eq. 2.4)

This group is expected to increase the solubility of both the monomer and the resulting polymer, although its most important function is increasing the salt tolerance of the gel system. The properties of resorcinol gels, like many water soluble and water-swellable polymers are greatly influenced by the presence of salt. Calcium, sodium and potassium salts, which are all potential constituents of water employed in near-bore treatment, dramatically influence the gel time of traditional RF systems. The gel times of SMRF systems are less sensitive to salt concentrations above 1%, providing a potential advantage over the related RF systems.

The objectives of this study have been to determine the structures of components in the sulfomethylated resorcinol monomers, define the nature of reactive species in this mixture, examine alternative routes for the preparation of sulfomethylated resorcinols, and test possible modifications of the SMRF protocol that improve the cost effectiveness of the process, and provide greater control of the gelation characteristics.

Experimental

All reagents including resorcinol, aqueous formaldehyde solutions and sodium sulfite were used as received. Syntheses of sulfomethylated resorcinol and hydroxymethyl sulfate were performed according to previously published procedures.[1,3] Gelation studies were performed in a 41°C isothermal bath. Nanopure water was used in the preparation of samples for gelation studies. gelation studies employing monomers other than sulfonated resorcinol were performed at pH values ranging between 9.5 and 13, and with salt concentrations at a constant 1%. Mass spectrometric studies were performed using the fast atom bombardment (FAB) technique. ^{1}H and ^{13}C NMR spectra of resorcinol, SMRF monomers and sodium hydroxymethyl sulfate were acquired on a 400MHz Brucker FT/ NMR using D_2O as a solvent. Samples were scrupulously dried under high vacuum (10^{-5} torr) prior to data acquisition in order to avoid a water background signal.

Results and Discussion

NMR spectroscopy is a convenient method for analysis of the structure of resorcinol derivatives. The ^1H NMR spectrum of resorcinol, shown in Figure 2.1, exhibits three sets of resonances in the region characteristic of aromatic hydrogen nuclei. This is the expected pattern for the three different aromatic hydrogen environments of resorcinol.

Sulfomethylated resorcinols (SMR) could exist as a range of substitutional isomers. There are three possible SMR isomers that contain a single sulfomethyl group (**V**-**VII**).

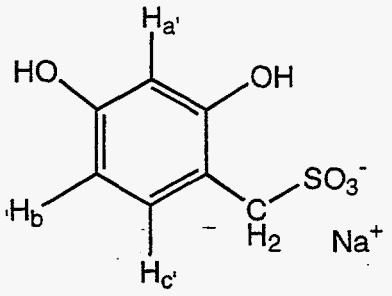

4-sulfomethyl resorcinol

V

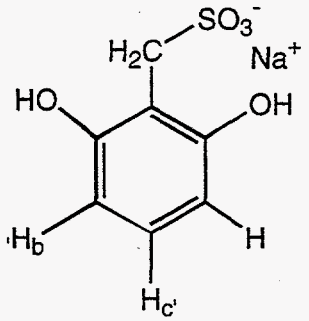

2-sulfomethyl resorcinol

VI

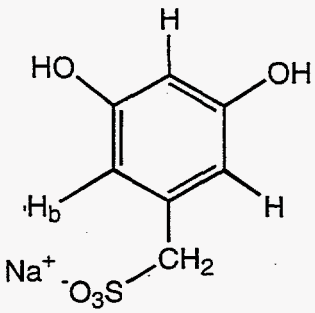

5-sulfomethyl resorcinol

VII

Hydroxyl (OH) groups activate *ortho* and *para* positions on aromatic rings for substitution. Consequently, isomers **V** and **VI** are more likely to be produced than **VII**. Substitution at an aromatic carbon between two substituted carbon centers is disfavored by steric hindrance. As a result, isomer **V** should be the favored SMR product containing a single sulfomethyl group. Based on the same logic, isomer **VIII** is the favored product among SMR isomers containing two sulfomethyl groups (**VIII-XI**).

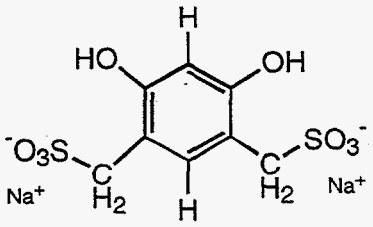

4,6-disulfomethyl resorcinol

VIII

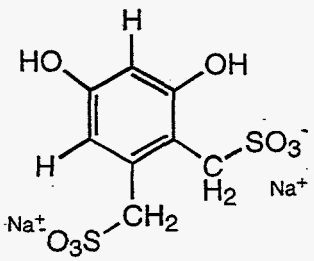

4,5-disulfomethyl resorcinol

IX

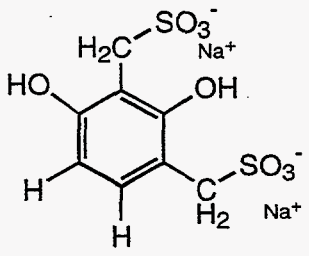

2,4-disulfomethyl resorcinol

X

2,5-disulfomethyl resorcinol

XI

The aromatic hydrogen region of the ^1H NMR spectrum of a sulfomethylated resorcinol is shown in Figure 2.2. It is clear from this spectrum that the SMR monomer is actually a mixture of

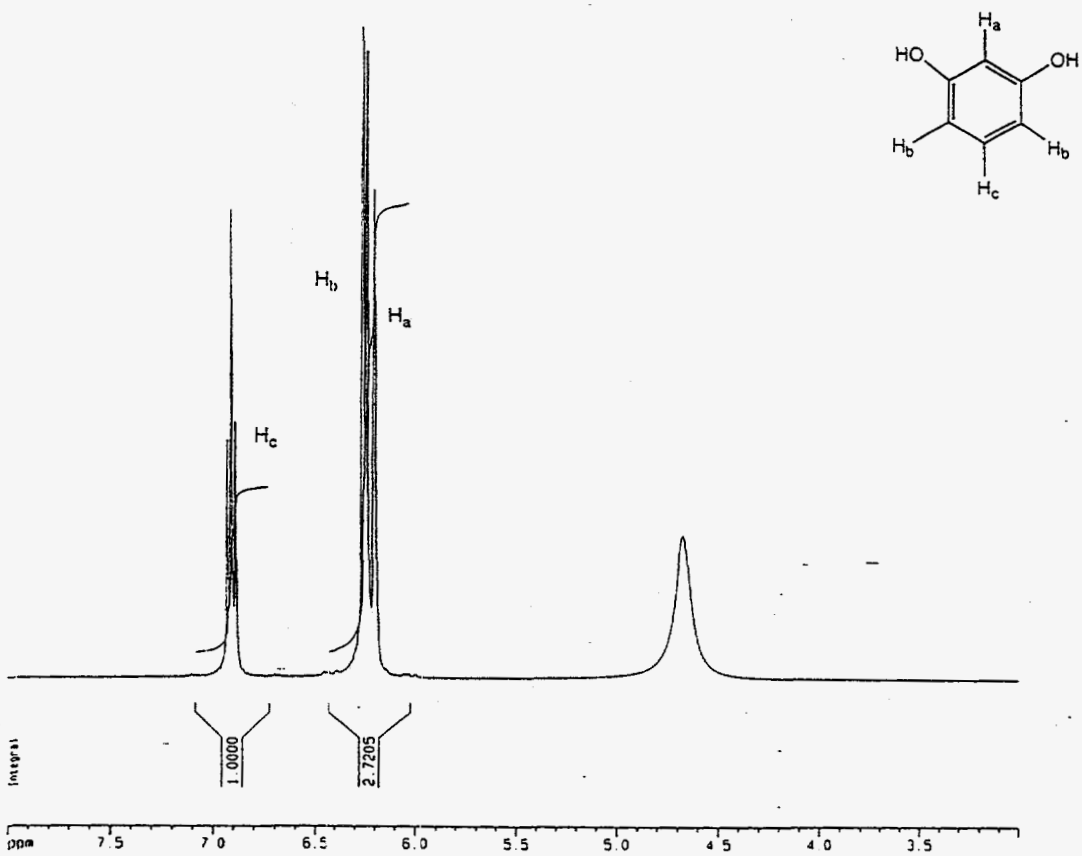

Figure 2.1 : ^{1}H NMR Spectrum of Resorcinol in D_2O.

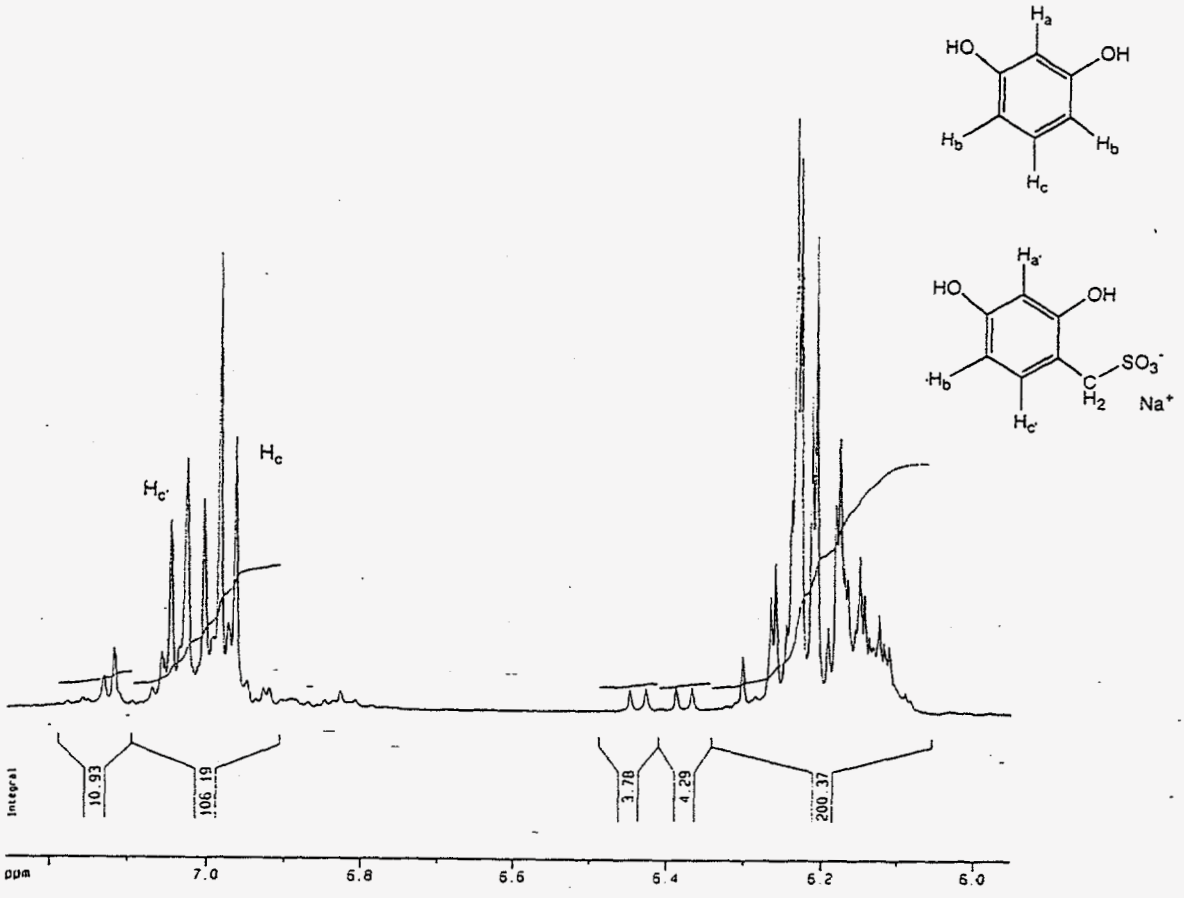

Figure 2.2 : ^1H NMR Spectrum of Sulfomethylated Resorcinol in D_2O

isomers. The largest sets of resonances in the spectrum - composed of the triplet around $\delta = 7.00$ and the three most intense lines around $\delta = 6.22$ - clearly belong to unmodified resorcinol. The intensity of these resonances indicates that resorcinol comprises approximately 60 percent of the SMR monomer. The next most discernible feature, representing the second most abundant species in Figure 2.2 is the doublet centered around $\delta = 7.06$. Based on its chemical shift, this doublet must represent $H_{C'}$ in either **V** or **VI**. Since the doublet character of this resonance limits this hydrogen to only one near neighbor hydrogen, this product can be assigned as **V**. This product comprises about 30 percent of the monomer stream. The residual resonances in the spectrum point to a complicated mixture of additional products, possibly including isomers in which resorcinol bears either one or two hydroxymethyl substituents. These products make up the rest of the monomer mixture.

An analysis of the same mixture by mass spectrometry confirms the presence of both singly and doubly hydroxymethylated resorcinols. Fast atom bombardment (FAB) was used to vaporize the sample, as this is the best method for injecting charged molecules into the gas phase. The mass spectrum shown in Figure 2.3 clearly shows molecular ion envelopes for singly sulfomethylated resorcinols at m/e = 203 and doubly sulfonated resorcinols at m/e = 297. Significant quantities or triply sulfomethylated resorcinols are clearly not formed during the preparation of the SMRs. The higher mass peaks in the spectrum are attributable to hydrogen bond complexes between the observed SMR's and the "matrix" (solvent) used to introduce the sample into the mass spectrometer. For example, the mass envelope at m/e = 389 corresponds to a complex between a doubly sulfomethylated resorcinol and glycerol. The gas-phase association of the SMRs with resorcinol illustrates their strong hydrogen bonding affinity. Unfortunately, FAB mass spectrometry can neither discriminate between various isomers of the SMRs, nor provide more detailed quantitation of the degree of substitution than is provided by NMR spectroscopy.

The monomer distributions determined by NMR spectroscopy are consistent with the stoichiometry of the protocol for preparing SMR monomers. A 1.00:0.75:0.50 ratio of resorcinol to formaldehyde to sodium sulfite is used in these syntheses. This suggests that up to 50 percent of the resorcinol in these mixtures could be sulfomethylated, although this proportion would be reduced by a small percentage of doubly sulfomethylated material. The reactant ratio is statistically likely to favor the formation of singly sulfomethylated monomer, as was observed by NMR spectroscopy. Significantly, adjustments of this mole ratio would produce SMR monomer streams with greatly differing ratios of resorcinol, monosulfomethylated resorcinol and disulfomethylated resorcinol. Such variations should have a dramatic influence on the gelation kinetics of the system in the presence of salt and on the physical properties of the resulting materials. Furthermore, by independently synthesizing mono- and and disulfomethylated resorcinols, it should be possible to probe the role of these materials in the gellation reaction and in interactions with metal cations.

Stoichiometric reactions between resorcinol and sodium hydroxymethyl sulfate hold promise for the synthesis and isolation of both mono- and disulfomethylated resorcinols. Sodium hydroxymethyl sulfate (**XII**) is prepared in 86 percent yield as a freely flowing white solid through reaction of formaldehyde with sodium sulfite (Eq. 2.5).

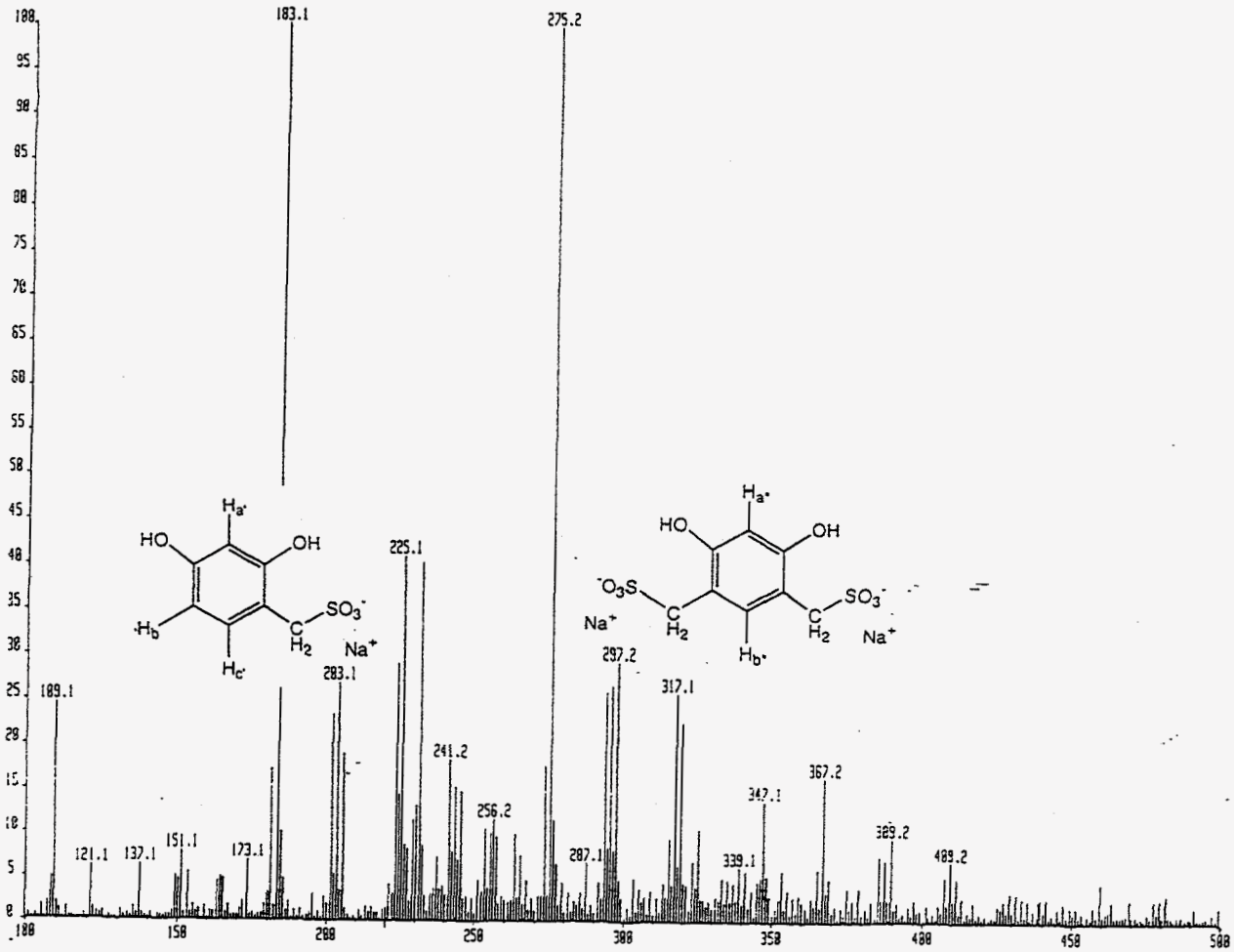

Figure 2.3 : FAB Mass Spectrum of the SMR Product Mixture

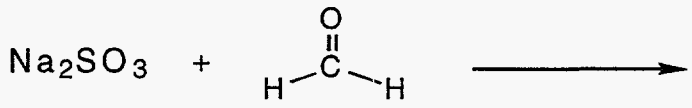

(Eq. 2.5)

XII

The reaction of two equivalents of **XII** with resorcinol in ultra pure water at pH 9 produces a red product similar in appearance to SMR monomers prepared through the standard protocol. NMR spectra of this product (Figure 2.4), while indicative of substitution, appear far more complicated that those obtained for sulfomethylation under the standard conditions described above. Additional studies are underway to determine the viability of this synthetic route.

These studies are important because the ability of the mono- and disulfomethylated products to participate in oligomerization reactions is expected to differ greatly. Oligomerization of SMRs relies on the formation of at least one free hydroxymethyl substituent as the SMR reacts with formaldehyde. This hydroxymethyl group then acts as a site for forming an ether linkage with another resorcinol monomer (see Eq. 2.3 for an example). While a site for hydroxymethylation is open in the monosulfomethylated resorcinol (**V**), both such sites are blocked by sulfomethyl groups in **VIII**. Consequently, it is expected that unless the sulfite (SO_3^{2-}) groups themselves act as leaving groups, the disulfomethylated resorcinols will not participate in oligomer formation.

The red color developed during the synthesis of SMR monomers and during gelation with additional formaldehyde is not characteristic of simple phenoxide anion, but rather suggests the presence of one or more highly conjugated organic intermediates. One such quinone like molecule (**XIII**) could be formed through the loss of hydroxide from a hydroxymethyl resorcinol intermediate (Eq. 2.6).

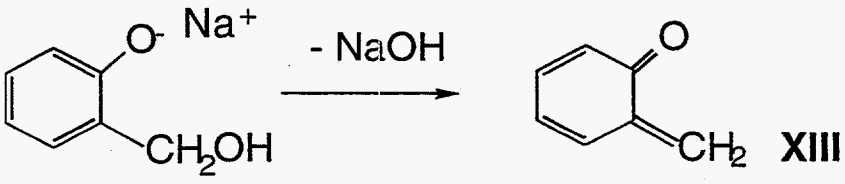

(Eq. 2.6)

XIII

Formation of **XIII** is thought to be a crucial step in the oligomerization of SMRs (Eq. 2.7).

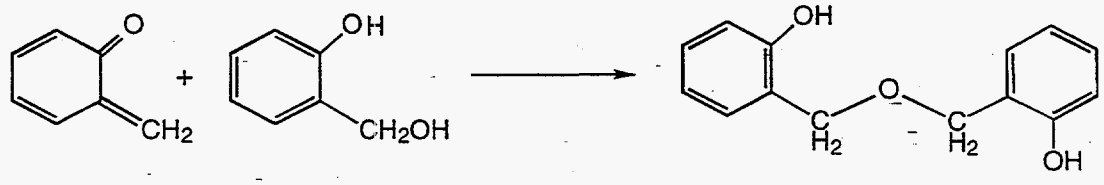

(Eq. 2.7)

Consequently, the development of intensely colored monomer mixtures may be characteristic of the ability of SMR replacements to participate in the gelation process.

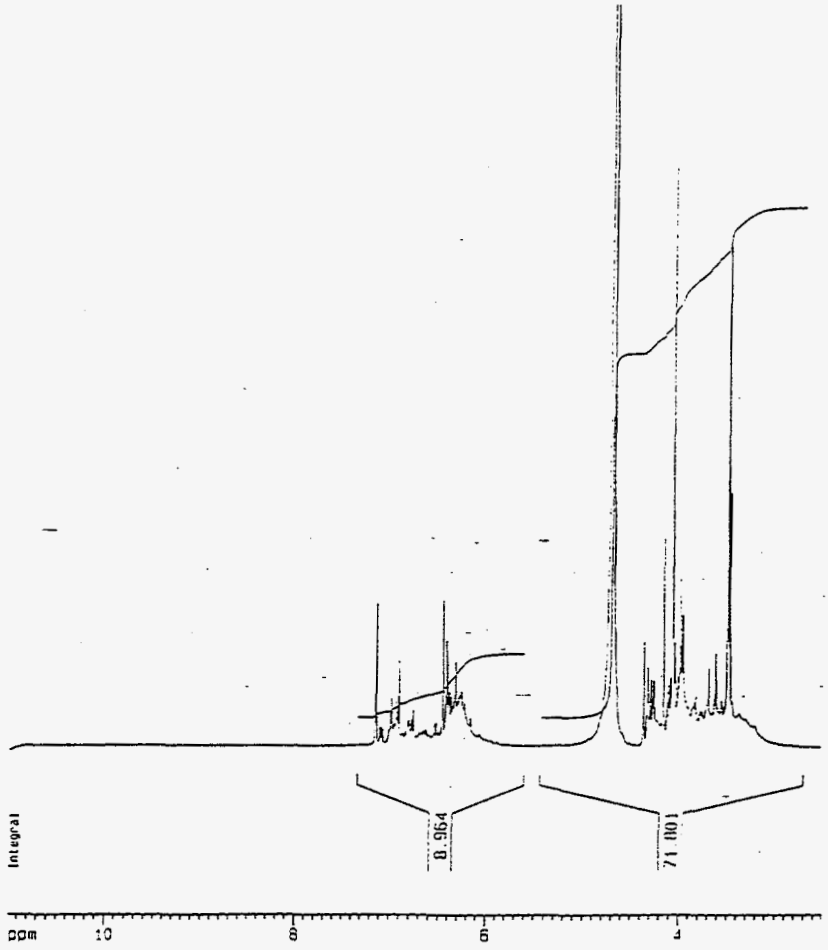

Figure 2.4 : ^{1}H NMR Spectrum of Sulfomethylated Resorcinol in D_2O Produced through a Reaction between Resorcinol and Sodium Hydroxymethyl Sulfite.

Reports outlined in the patent literature indicate that other phenol derivatives form hydrogels with properties similar to those produced with resorcinol.[4] Gelation studies at 41°C under conditions similar to those employed for resorcinol failed to produce hydrogels for a range of alternative phenol monomers (**XIV-XVII**).

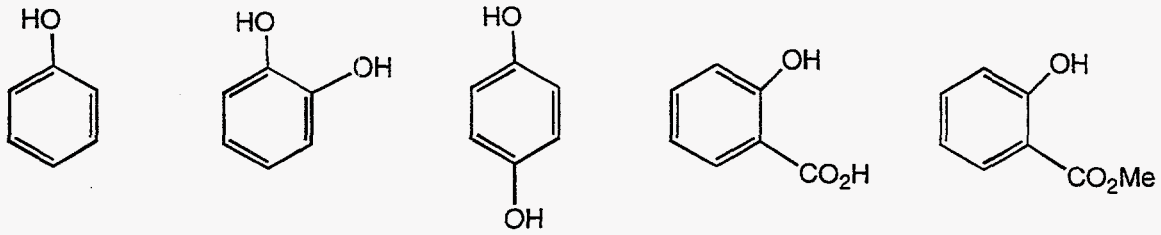

XIV **XV** **XVI** **XVII** **XVIII**

Samples in several of these studies turned the dark red color characteristic of pre-gelation behavior. Such monomers may gel at substantially higher temperatures. These conditions are similar to those observed in certain oil bearing formations, such as those found in the North Sea. Analogs of SMRF that possess higher cure temperatures may be useful in such formations.

Conclusions

1. Current SMRF formulations employ monomer streams containing approximately 60 percent resorcinol, 30 percent monosulfomethylated resorcinol and minor quantities of disulfomethylated materials. The performance and properties of SMRF gels might be greatly influenced by varying the ratios of these constituents.
2. Sodium hydroxymethyl sulfate, which is readily isolated as a free-flowing white solid, may provide be an alternative precursor for the preparation of SMR from resorcinol.
3. While many inexpensive phenol derivatives failed to gel under conditions observed for resorcinol, physical changes in the solutions suggest that these materials may gel at higher temperature. Such materials may prove more suitable than the SMRF system for oil reservoirs whose temperatures exceed 50°C.

References

1. McCool, C.S.; Green, D.W.; Wilhite, G.P.; Zuang, Y.; Pandey, S.N. "Gelation and Permeability Reduction of Resorcinol-Formaldehyde Gel Systems," in *Improving Reservoir Conformance Using Gelled Polymer Systems,* Green, D.W. and Willhite, G.P., Eds., DOE/BC/14881-18, Chapter 2.
2. Seright, R.S.; Martin, F.D. "Impact of Gelation pH, Rock Permeability and Lithology on the Performance of a Monomer-based Gel," paper SPE 20999 persented at the SPE International Symposium on Oilfield Chemistry, Anaheim, CA, Fev. 20-22, 199 1.
3. Falk, R.A.; Gerecht, J.F.; Krems, I.J. *J. Am. Oil Chem. Soc.* **1958**, *35*, 171.
4. (a) Chang, P.W.; Meltz, C.N.; Gruetzmacher, G.D.; Totino, R.A.; European Patent #0177324, 30.09.85. (b) Albonico, P.; Bartosek, M.; Malandrino, A.; Bryant, S.; Lockhart, T.P. *SPE* 28983, 403. (c) Shu, P.; Windsor, W.; Shu, W.R. U.S. Patent #5071890, Dec. 10, 1991.

Chapter 3

Gel Behavior in Fractured Media

Principal Investigators: D.W. Green, G.P. Willhite and C.S. McCool
Graduate Research Assistant: Somenath Ganguly

Introduction

Hydraulic fracturing of production wells to improve production at the primary recovery stage is quite common in petroleum industry. Fracturing of water injection wells often occurs due to over pressure. Also thermal stresses developed due to cold water injection in the formation leads to unintentional fracturing. Over and above all these types of artificial fractures, natural fractures are found in many oil bearing reservoirs. These fractures can constitute a severe water channeling problem at some point of enhanced oil recovery stage. One of the available remedies for water control is a gelled polymer treatment.

Research on the application of gelled polymer treatments in fractured systems is comparatively recent, with most of the effort put forward by Seright.[1,2] Seright studied the performance of different types of immatured, preformed, and mechanically degraded gels by displacing them through fractured cores. In this kind of flow cell, leak off from fracture face into the adjacent matrix is insignificant. In a fractured well, this type of linear flow in the fracture takes place near the well bore. But in the major portion of the fracture, bilinear flow (i.e., two simultaneous flows one along the fracture and the other from fracture into the matrix) should take place, particularly when the gelling solution is of low viscosity. Well testing data and numerical simulation support the bilinear flow mechanism.

The objective of this investigation is to create the bilinear flow environment (as it exists in a fracture) in a physical flow model and study the behavior and effectiveness of a gel system under this condition.

Bilinear Flow and Design of the Flow Cell

Bilinear flow was first attempted in our laboratory by opening the sides of a fractured core slab to atmospheric pressure and controlling the back pressure at the fracture exit. It was found that, when the back pressure exceeds an upper bound, all the influent into the fracture exits through the matrix. A mathematical model was developed to simulate the fluid flow down a fracture with leak off into the adjoining matrix under a specified back pressure, as shown in Figure 3.1. The model had the following assumptions:

1. The model accounts for two mutually perpendicular linear flows; one along the fracture and the other through matrix.
2. Flow process is in steady state.
3. Injected and the resident fluids are of same viscosity.
4. Fracture and matrix permeabilities are space invariant.
5. Matrix outlets are open to atmospheric pressure.

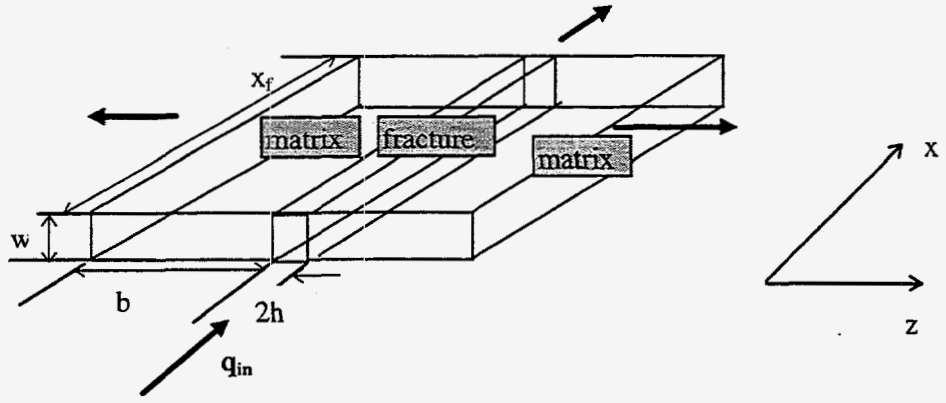

Figure 3.1 : Bilinear flow model.

The flow equations for fracture and matrix are

Matrix:
$$v_m(x) = \frac{k_m}{\mu}\frac{(p_f(x) - p_{atm})}{b} \qquad \text{(Eq. 3.1)}$$

Fracture:
$$\frac{d}{dx}\left(v_f(x)\right) = \frac{1}{h}v_m(x) \qquad \text{(Eq. 3.2)}$$

Darcy's law was used for flow through fracture

$$v_f(x) = \left(\frac{k_f}{\mu}\frac{dp_f(x)}{dx}\right) \qquad \text{(Eq. 3.3)}$$

Combining Equations 3.1, 3.2 and 3.3 :

$$\frac{d^2p_f(x)}{dx^2} = \frac{k_m}{k_f h}\frac{(p_f(x) - p_{atm})}{b} \qquad \text{(Eq. 3.4)}$$

Boundary conditions:

Constant flow at fracture inlet:
$$\frac{dp_f}{dx}\Big|_{x=0} = -\frac{q_{in}\mu}{2wk_f h} \qquad \text{(Eq. 3.5)}$$

Fracture outlet : Two outlet boundary conditions were studied.

Case 1: Constant pressure outlet, $p_f|_{x=xf} = p_b$ (Eq. 3.6)

Case 2: No flow, $\frac{dp_f}{dx}|_{x=xf} = 0$ (Eq. 3.7)

Solution:

The following dimensionless variables are introduced:

$$z' = \frac{z}{b}; \qquad x' = \frac{x}{x_f}; \qquad p' = \frac{p - p_{atm}}{\frac{q_{in}\mu x_f}{2wk_f h}}; \tag{Eq. 3.8}$$

Solution of Equation 3.4, for Case1 boundary condition gives the dimensionless fracture pressure at x' as follows:

$$p_f'\Big|_{x'} = \frac{\{p_b' - \frac{\exp(-\sqrt{A})}{\sqrt{A}}\}\exp(\sqrt{A}x') + \{p_b' + \frac{\exp(\sqrt{A})}{\sqrt{A}}\}\exp(-\sqrt{A}x')}{\exp(\sqrt{A}) + \exp(-\sqrt{A})} \tag{Eq. 3.9}$$

where A is bilinear flow coefficient (a dimensionless constant which characterizes the flow cell) and is expressed as:

$$A = \frac{k_m}{k_f}\frac{x_f^2}{bh} \tag{Eq. 3.10}$$

The solution for Case 2 boundary condition is

$$p_f'\Big|_{x'} = \frac{\{\exp(\sqrt{A}x') + \exp(\sqrt{A}(2 - x')\}}{\sqrt{A}(\exp(2\sqrt{A}) - 1)} \tag{Eq. 3.11}$$

Pressure profile in matrix is linear for both for Case1 & 2 and is given by

$$p_m'\Big|_{x',z'} = p_f'\Big|_{x'}\{1 - z'\} \tag{Eq. 3.12}$$

Typical pressure profile of one symmetric half of the flow cell is shown in Figure 3.2

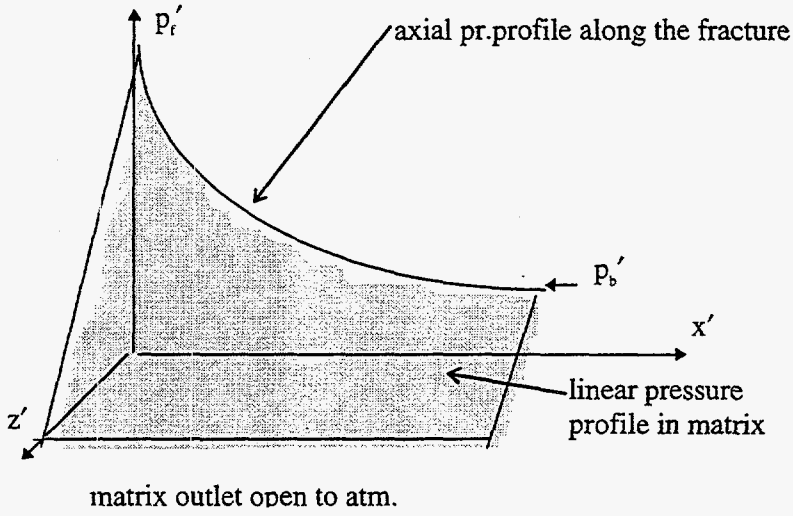

Figure 3.2 : Simulated pressure profiles.

The pressure profile in the fracture, p_f', for the two cases, is plotted in Figure 3.3.

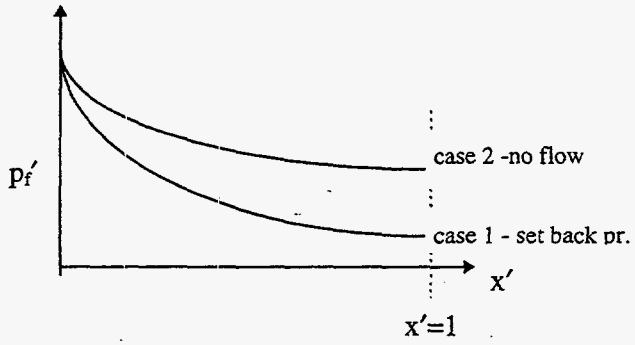

Figure 3.3 : Fracture pressure profile for Cases 1 and 2.

There is an upper bound for the fracture outlet pressure, p_b', which corresponds to "no flow" boundary condition. The back pressure can not be set higher than this upper bound using a back pressure regulator. Experimental difficulties were encountered in controlling a low back pressure. Consequently, flow cell dimension and properties were designed to maximize the upper bound in back pressure. This upper bound is given by Equation 3.11 at $x = x_f$, and can be expressed, using dimensional variables, in the following functional form.

$$p_{upperbound}x_f = \left(\frac{q_w\mu}{2w}\right)\varphi\left(\frac{x_f^2}{k_f h}, \frac{k_m}{b}\right) \qquad \text{(Eq. 3.13)}$$

Viscosity, μ, is defined by the choice of gel system. (q_w/w) was estimated from the flow rate used for gel injection in a reservoir application. $p_{upper\text{-}bound}$ will be maximum when b, h are maximum and x_f, k_m are minimum.

Details and Characterization of the Physical Model

A schematic of the flow cell is shown in Figure 3.4. A Berea slab was fractured into two halves by a hydraulically-operated fracturing blade. The two pieces were held together and the entire assembly was coated with epoxy. The flow goes into the fracture through a small compartment and exits the fracture through a similar compartment. The rest of the inlet and outlet faces were sealed with epoxy. The two sides of the assembly form the matrix outlets. Each of these sides is divided into two compartments. Pressure ports were drilled at different positions on the top of the assembly, and their locations are shown by squares on the top view. The assembly was saturated with 1% NaCl solution. The flow cell was characterized in terms of fracture permeability, fracture aperture width, matrix permeability and matrix porosity.

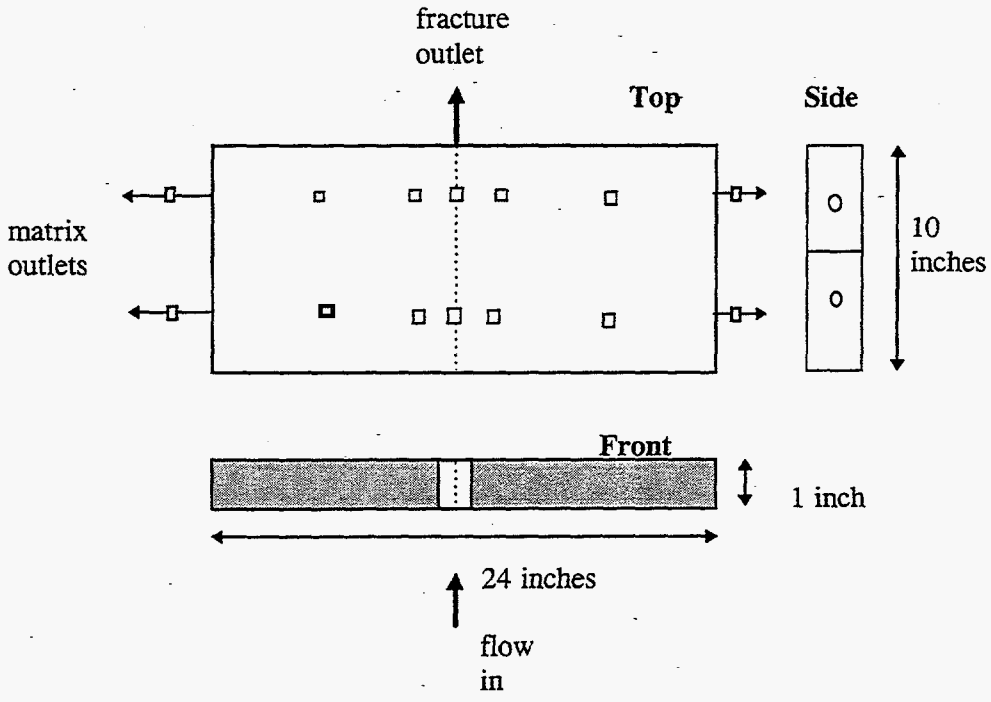

Figure 3.4 : Schematic of physical model.

Fracture permeability. Permeability of the fracture was determined by closing the matrix outlets and flowing brine through the fracture. Darcy's law (Equation 3.14) and theory of flow between two parallel plates[3] (Equation 3.15) were used to compute the aperture width of the fracture.

$$\frac{Q}{(2h)w} = \frac{k_f}{\mu}\frac{\Delta p}{L} \qquad \text{(Eq. 3.14)}$$

$$k_f = \frac{(2h)^2}{12} \qquad \text{(Eq. 3.15)}$$

Results obtained were: $k_f = 8.048\ E\text{-}04\ cm^2 = 8.154\ E\ 04$ Darcy

$(2h) = 0.098$ cm

Fracture tracer test. Brine was displaced through the fracture with the matrix ports closed and the fracture outlet open for flow. A step change in concentration (1% NaCl to 5% NaCl) was introduced in the influent, and the effluent concentration was monitored by a refractometer. The reduced concentration (C/C_0) of the effluent was plotted as a function of time in Figure 3.5. The plot is as expected, i.e. a sharp rise because of fracture breakthrough followed by a long tail because of diffusion into the matrix. Fracture aperture width was determined from this plot using the theory of flow between two parallel plates.[4] The aperture width computed from tracer test was 0.11 cm. This value compared well with the value determined from the fracture permeability.

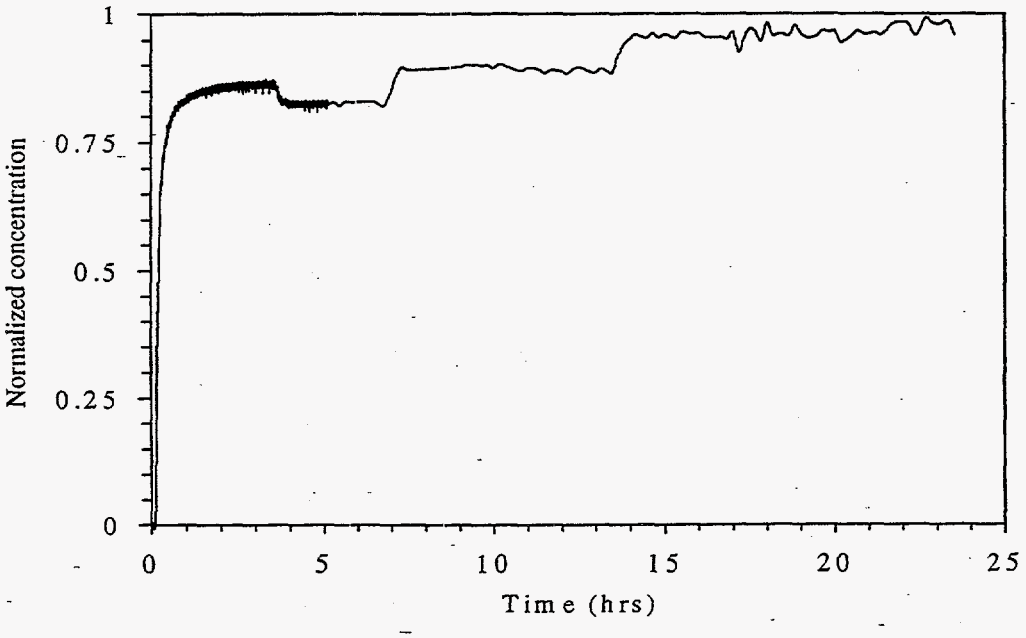

Figure 3.5: Tracer concentration in effluent from fracture as a function of time.

Matrix permeability. Matrix permeability was determined by injecting brine in the fracture and collecting it through each side by closing outlets on the opposite side. Pressure drops were measured between the ports which divide the matrix into sections. Permeabilities of the sections are given in Figure 3.6.

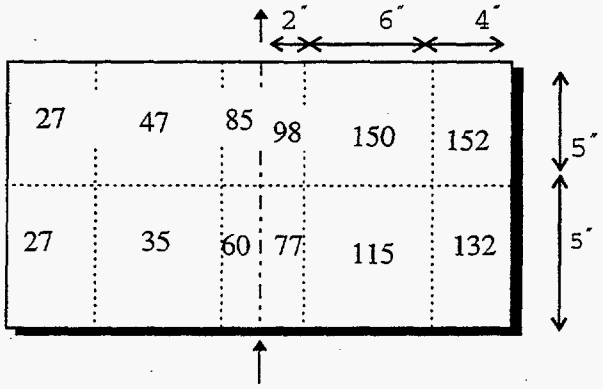

Figure 3.6 : Permeability of individual matrix sections in millidarcies.

Matrix tracer test. Brine displacement experiments were conducted in each half of the cell assembly. A step change in influent concentration was introduced and the effluent concentrations of the two matrix segments (front and back) were monitored with time. The matrix outlets were held at the same hydrostatic head to reduce the crossflow between the front and the rear sections. Analysis of the reduced concentration vs. volume collected, gave an estimate of the matrix pore volume of the front and back sections of each side of the assembly. Pore volume of individual segments are given in Figure 3.7.

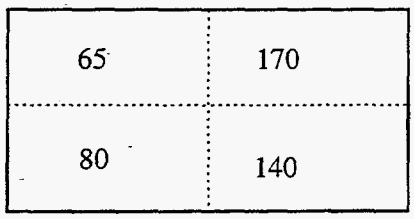

Figure 3.7 : Pore volumes of individual segments in milliliters.

Glycerol Displacements

Experiments were conducted to study the flow behavior when a viscous solution displaces brine through the flow cell. These experiments simulated the more viscous gel/gelant displacing brine without the added complication of *in situ* gelation. These experiments were accomplished using a glycerol-brine solution as the displacing fluid.

A schematic of the equipment for the flow experiment is shown in Figure 3.8. A glycerol-brine solution was injected by an oil pump and a transfer cylinder. The injected solution had a viscosity of 20 cp, which corresponds to the initial viscosity of a Cr(III) - polyacrylamide gelant, that is planned to be used later. The matrix outlets were open to atmospheric pressure. Effluent from the matrix outlets and fracture outlet were collected in graduated cylinders. Volume in the cylinders were recorded as a function of time to determine flow rates. A small drop of effluent was drawn from each port at selected times. Refractive indices of the drops were measured to determine glycerol concentrations in the effluent.

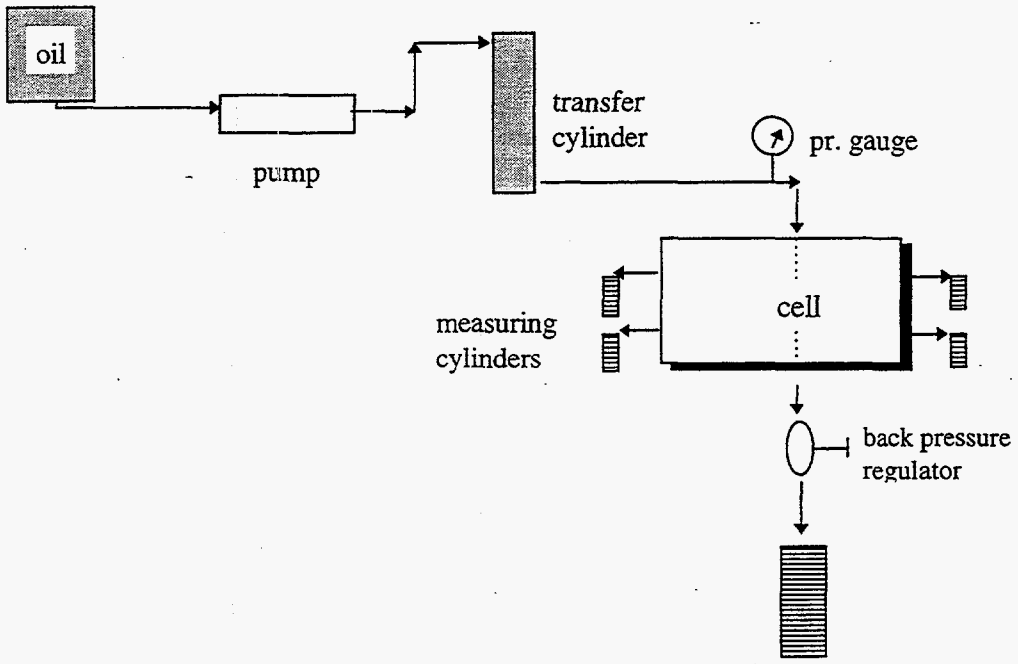

Figure 3.8 : Flow schematic for glycerol displacements.

Three sets of boundary conditions were investigated.

BC-1 Constant injection flow rate and constant back pressure at fracture outlet.
BC-2 Constant injection pressure and constant back pressure at fracture outlet.
BC-3 Constant injection flow rate and constant differential pressure along fracture.

The general observations for glycerol displacements using BC-1 are summarized as follows.

1. After the flow injection started, it took some time for the fracture pressure to develop to the selected back pressure. Flow at the fracture outlet started after this time period. The "no fracture flow period" becomes shorter as the injection flow rate increased or the set back pressure decreased.

2. The matrix flow rates declined rapidly after flow started from the fracture outlet.

3. Pressure profiles in the four matrix quadrants of the cell were similar indicating insignificant crossflow between quadrants.

4. Glycerol broke through at the matrix outlet ports at similar volumes injected that were observed during the tracer tests.

Results of one of the typical BC-1 experiment is elaborated here. A flow rate of 15 ml/min and a fracture end back pressure of 25 psi were used for this flow experiment. The fracture was preflushed with glycerol before the run. Once the fracture flow started, the pressure drop along the fracture remained practically constant at around 0.1 psi. Figure 3.9 describes typical pressure drop data in matrix section. The position of the pressure sensors are as indicated by circles in the rectangular cell diagram. All the three sections register an immediate pressure rise as the flow starts. This is followed by a drop for a short duration because of the decline in matrix flow rate. However the first rise in pressure for the section adjacent to the fracture is significantly higher than the other sections, because this is contributed by the viscous fluid, flowing through this section. As glycerol penetrates more and more, the break point in the pressure profile (due to the viscous front) moves down the matrix sections, changing the pressure drops across them. Flowrates at the fracture outlet and one of the matrix outlets are shown in Figure 3.10, as a function of time.

BC-2 and BC-3 could not be established successfully for the initial period. Beyond this period all three conditions led to similar fracture and matrix flow rates. BC-1 was selected for further experimentation.

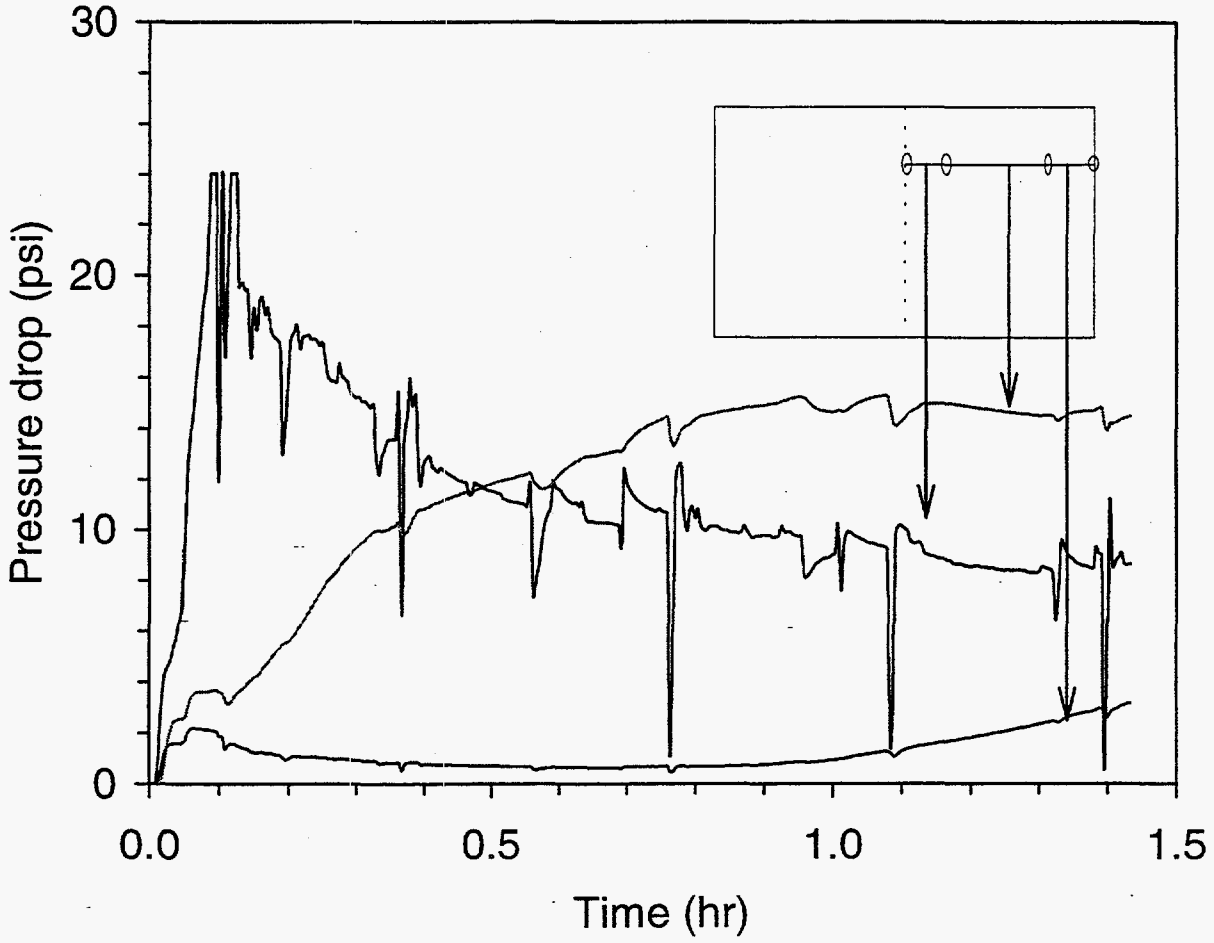

Figure 3.9 : Pressure drops across matrix sections as a function of time.

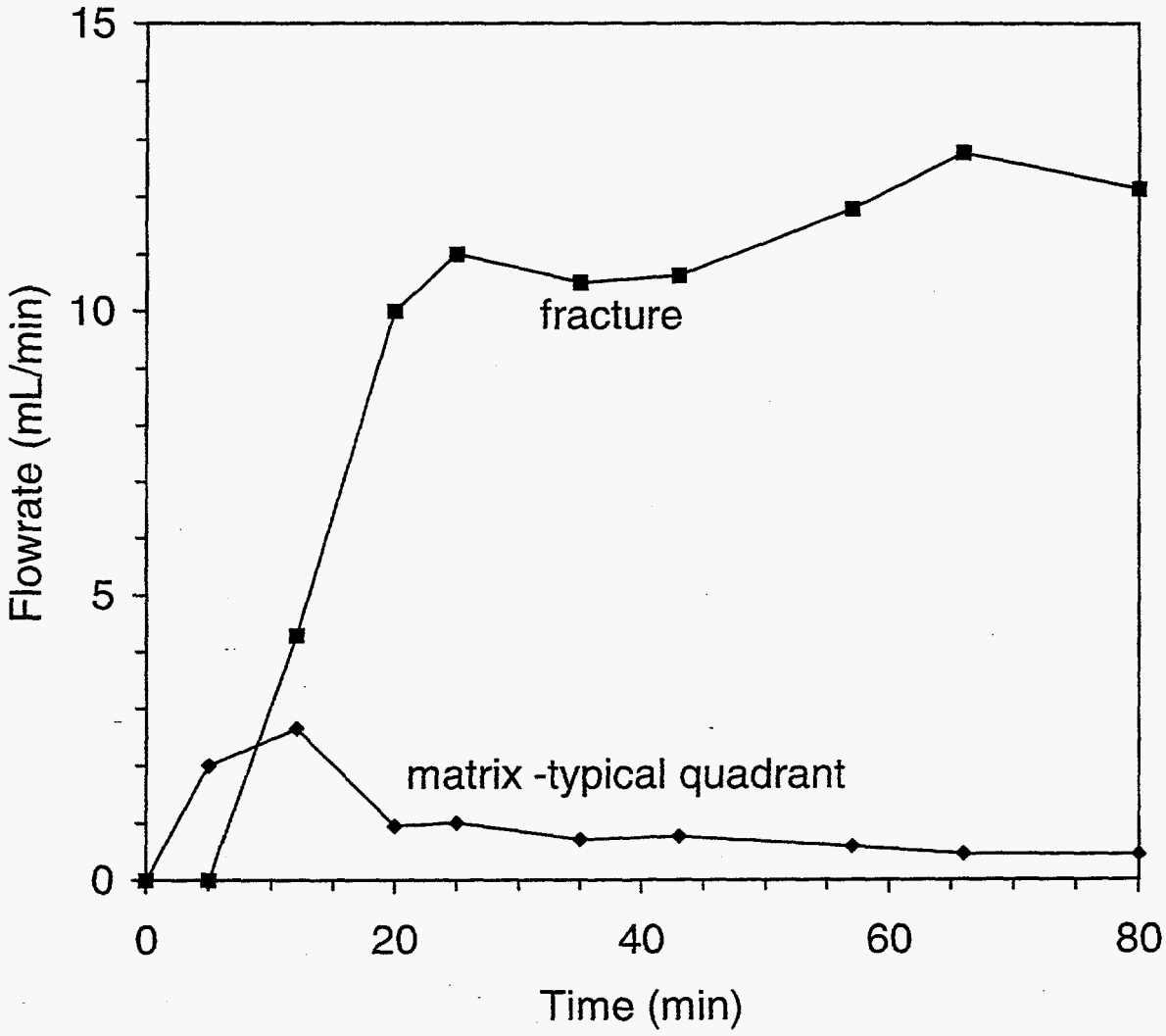

Figure 3.10 : Flow rates of effluent from fracture and matrix.

Summary

1. Performance of a gel system may strongly depend on the flow environment, and accordingly, the behavior of a gel system should be studied in a bilinear flow cell.

2. A physical bilinear flow cell was developed. Flow cell properties were designed using a theoretical bilinear flow model, to simulate reservoir flow environment and to reduce experimental problems.

3. The characteristics of the flow cell during displacement of viscous solution was studied under several boundary conditions. The boundary conditions selected for future experiments were:

    a) Constant flow rate at fracture inlet.
    b) Constant back pressure at fracture outlet.
    c) Atmospheric pressure at matrix outlets.

Future Plan

Glycerol displacements will be simulated by a mathematical model. Gel placement and performance in the fractured flow cell will be investigated.

Nomenclature

A	dimensionless constant of the flow cell
q	flow rate, L^3T^{-1}
w	height of the cell, L
2h	fracture aperture width, L
k	permeability, L^2
p	pressure, $ML^{-1}T^{-2}$
p′	dimensionless pressure
x	length along fracture axis, L
x′	dimensionless length along fracture axis
z	length along matrix axis, L
z′	dimensionless length along matrix axis
v	Darcy velocity, LT^{-1}
2b	flow cell width, L
p_b	set back pressure, $ML^{-1}T^{-2}$

Greek Symbols

μ	viscosity, $ML^{-1}T^{-1}$

Subscripts

f	fracture
m	matrix
atm	atmosphere
in	inlet

References

1. Seright R.S., "Use of Preformed Gel for Conformance Control in Fractured Systems," paper no. SPE/DOE 35351, SPE/DOE Tenth Symposium on Improved Oil Recovery, Tulsa, OK, (April 1996).
2. Seright R.S., "Gel Placement in Fractured Systems," paper no. SPE/DOE 27740, SPE/DOE Ninth Symposium on Improved Oil Recovery, Tulsa, OK (April 1994).
3. Iwai, K., *Fundamental Studies of Fluid Flow Through a Single Fracture*, PhD dissertation, University of California - Berkeley (1976).
4. Bird, R.B, Stewart, W.E., Lightfoot, E.N., *Transport Phenomena*, John Wiley and Sons Inc. (1960).

Chapter 4

Chemical Interaction Between Injected Brine Solutions and Dolomite Core Material

Principal Investigators: G.P. Willhite, D.W. Green and C.S. McCool
Graduate Research Assistant: Bin Zou

Introduction

Injecting gelant into an oil reservoir to change the flow characteristics of the reservoir is a viable improved oil recovery technique. Many gel systems are affected by the pH of the solution. The treatment of carbonate reservoir rock is of particular concern because of the fluid-rock interaction which can alter the pH of the injected solution. In this study, the interaction between injected potassium chloride brine and dolomite core material was investigated. The effects of injected pH and injection rate on composition and pH of the effluent solution were studied. The common-ion effect of calcium and magnesium in the injected solution on the effluent pH and composition was also investigated. A mathematical model based on equilibrium chemistry was used to predict the effluent pH and composition.

A three-stage pH behavior was found when the injected pH varied from 1 to 13. When common ions were present in the injected solution, the dissolution of dolomite was depressed, and the effluent pH was less than that when calcium and magnesium ions were absent. For the same total divalent ion concentration, both calcium and magnesium present in the injected solution had a larger effect on the effluent pH than either individually. The measured pressure difference along the core in a series of runs showed that dissolution of dolomite had no measurable effect on the permeability of the core during the study period.

Background

A few studies have been conducted on the change of pH of the injected solution as it flows through porous rock. Seright[1] injected Cr(III) solutions (as either chromium acetate or chromium chloride) through Indiana limestone cores to assess the propagation of chromium through porous rock. Cr(III) concentration in the effluent never reached the injected concentration after injecting 10 pore volumes of chromium solution for any case studied. Chromium propagated more rapidly when the counterion was acetate as opposed to chloride. No chromium was detected in the effluent after injecting 10 pore volumes of chromium chloride solution through a limestone core.

Stavland et al.[2] studied the retention of chromium(III) in Brent and Berea sandstone cores (with about 2% carbonate content). The authors found precipitation was the most important reason for chromium retention in cores. Precipitation was caused by the dissolution of carbonate minerals that increased the pH of the injected solution. Their experiments also revealed that the retention rate of Cr(III) was lower with less carbonate present in the cores. McCool et al.[3] studied the interaction between a dolomite core

and xanthan-Cr(III) gel system. Significant amounts of Cr(III) precipitated because the pH in the injected solution increased due to the dissolution of dolomite.

Equilibrium relations and the dissolution kinetics in dolomite-carbonic acid-water systems have been studied for such purposes as soil science, the study of secondary changes in sedimentary deposits, the neutralization of acid mine drainage, and the acidizing of petroleum wells.[4] Most previous studies were conducted in agitated batch reactors, rotating disk, or fluidized bed reactor systems in laboratory by using relatively pure dolomitic rock or synthetic dolomite. A few investigators have studied the dissolution reaction using flow through packed bed reactors or consolidated rock cores.[5,6]

The kinetic equations and mechanisms proposed by different investigators are quite different. Those equations and mechanisms might be suitable to explain the corresponding experimental phenomena, but they are not easily generalized. The rate equations derived by Plummer et al.[7] and those from Chou et al.[8] are often used to predict the dolomite dissolution rates within a 2- to 100-fold difference, depending on the reaction conditions. Moreover, the hydrogen ion concentration power indices in their rate equations were different, which means different mechanisms were used to explain their experimental data.

It is believed that the dissolution rate is controlled by surface reaction, reactants or products diffusion, or a mix of both depending on reaction conditions. Also, the dissolution of dolomite reaches equilibrium much faster in a closed-to-atmosphere condition than in an open system in which the transport of carbon dioxide is involved in the reactions. The dissolution rate is affected by the rock lithology such as impurity content, crystal size, rock texture and CaO/MgO ratio in the rock and the injected solution chemistry such as the pH and composition. In most previous investigations, the effect of the rock formation on dolomite dissolution was the dominant interest. Rauch and White[5] investigated the effect of lithology on carbonate dissolution rate. The authors found that the dissolution rate decreased as percentage of dolomite and disseminated insolubles increased.

The general chemistry of dolomite dissolution has been studied extensively though some dissolution mechanisms are still under debate. Because it is a salt of a weak acid, dolomite dissolves in strong acid, carbonated water, and water by different mechanisms.[4] In water, the general chemistry is:

$$CaMg(CO_3)_2 = Ca^{2+} + Mg^{2+} + 2\,CO_3^{2-} \qquad \text{(Eq. 4.1)}$$

When carbon dioxide is present, the dissolution has the reaction:

$$CaMg(CO_3)_2 + 2\,H_2CO_3 = Ca^{2+} + Mg^{2+} + 4\,HCO_3^- \qquad \text{(Eq. 4.2)}$$

When in strong acidic solution, the following reaction occurs:

$$CaMg(CO_3)_2 + 4\,H^+ = Ca^{2+} + Mg^{2+} + 2\,CO_{2(aq)} + 2\,H_2O \qquad \text{(Eq. 4.3)}$$

For an open system or a closed system with reaction product CO_2, CO_2 may participate as in the following reactions:

$$H_2CO_3 = CO_{2(aq)} + H_2O \qquad \text{(Eq. 4.4)}$$

and

$$H_2CO_3 = H^+ + HCO_3^- = 2H^+ + CO_3^{2-} \qquad \text{(Eq. 4.5)}$$

The specific reaction rates for the hydration of CO_2 and the dehydration of H_2CO_3 (Eq. 4.4) are known (Lasaga[9]) and are relatively small when compared with the specific rates for the ionic dissociation of carbonic acid (Eq. 4.5) and other complexation reactions. Consequently, the rate of ionic partition reactions can be considered infinitely fast with respect to the two possible controlling steps, namely, the heterogeneous dissolution reaction of dolomite (Eqs. 4.1- 4.3) and hydration/dehydration reaction (Eq. 4.4). Therefore, equilibrium chemistry can be partly or fully used in the simulation. It serves as the basis for most numerical modeling for this system.

The heterogeneous dissolution of dolomite is limited both by the kinetics of the reaction at the solid-liquid interface and by the mass transfer of reactant and/or products through the fluid boundary layer. When dolomite is dissolved, the products and/or the reactants form a buffer system in the reactive boundary and sequentially in the solution, which regulates the dissolution behavior and dominates the pH history of the solution.

Common-ion effects on the carbonate dissolution rate have been studied. Sjoberg and Richard[10] investigated the kinetics of carbonates dissolution in solution containing dissolved calcium. The results indicate that the presence of dissolved Ca^{2+} decreases the rate of the reaction, making the dissolution process more transport-controlled. Berner[11] studied the comparative dissolution characteristic of carbonate minerals in the presence and absence of aqueous magnesium ion. It was found that added magnesium ions depressed the dissolution of carbonates and caused a depression in the steady-state pH below values predicted from distilled water at the same P_{CO2} from both theoretical and experimental evidence.

In this study, core-flooding experiments were conducted by injecting KCl brine solutions at selected pH values to understand the effect of pH on the chemical speciation of the solution. The effects of flow rate on the pH and concentrations in the effluent solution were investigated. The effects of added calcium and magnesium in the injected brine were also studied.

Experimental

The rock material studied was Baker dolomite which contains calcium carbonate and magnesium carbonate at mole percentages of 57 and 43, respectively. Insoluble residue in concentrated hydrochloride acid is less than 0.05% by weight. Baker dolomite is no longer available due to the abandonment of the quarry.

KCl, $CaCl_2$ and $MgCl_2$ were used to prepare the injected solutions. 1M hydrochloride acid or 1M sodium hydroxide solution was used to adjust pH. Brines were stored in collapsible containers to eliminate carbon dioxide exchange with the atmosphere.

The core flooding apparatus is shown in Figure 4.1. The effluent pH was monitored immediately when the sample was collected under a nitrogen blanket device to minimize the invasion or the degassing of carbon dioxide. The pH was also measured by an in-line pH electrode. The calcium and magnesium concentrations were measured by Perkin-Elmer atomic absorption spectrophotometer. Four pressure transducers were used to monitor the pressure difference along the core during core flooding. The permeability of the core was calculated from pressure and flow rate data using Darcy's Law. The effluent samples were collected by an automatic fraction collector. The injection rate was controlled by the pumps and calibrated by frequently weighing the collected sample at a specific time intervals. In some experiments, a Fisher Titrimeter II automatic FEP system was used for carbonate analysis.

A single core was used in the experiments. The core had a length of 15 cm and a diameter of 3.7 cm. The core material was dried at 100 °C for 2 days before it was coated with epoxy. Two pressure ports are placed at equal intervals along the core which divide the core into three equal length sections. The porosity of the core was 25% and 26.5% measured by gravimetric and dispersion methods, respectively. The permeability of the core was 70 md after the preliminary core floods. A water bath was used to keep the core at a constant temperature of 25 °C. Tracer experiments were conducted using a step change of injected potassium chloride concentration to evaluate flow characteristics of the core.

Results and Discussions

Eight flow experiments were conducted using a single Baker dolomite core. The first two runs were preliminary runs and are not discussed here. The injected brine pH and composition as well as the injection strategies for Runs 3 through 8 are summarized in Table 4.1.

Table 4.1 : Brine composition and injection rates

Experiment	Injected solution	Injection rates (flow rates injected in the order as indicated, mL/min)
Run 3	pH 4.3, 2% KCl	0.11, 1.1, 5
Run 4	pH 3.1, 0.5% KCl	0.1,1.1,5.56,11.1,21
Run 5	pH 2.58, 0.5%	0.075, 0.11, 0.855, 1.15, 4.24, 8.30, 16.50
Run 6	pH 10.87, 0.5%	0.125, 0.234, 0.597, 1.165, 5.79, 11.14
Run 7	pH 5.7, 0.5% KCl	0.11, 0.55, 1.1, 5.5, 11
Run 8	pH 5, 0.5% KCl with various Ca, Mg concentrations	1.1 (see Table 4.2)

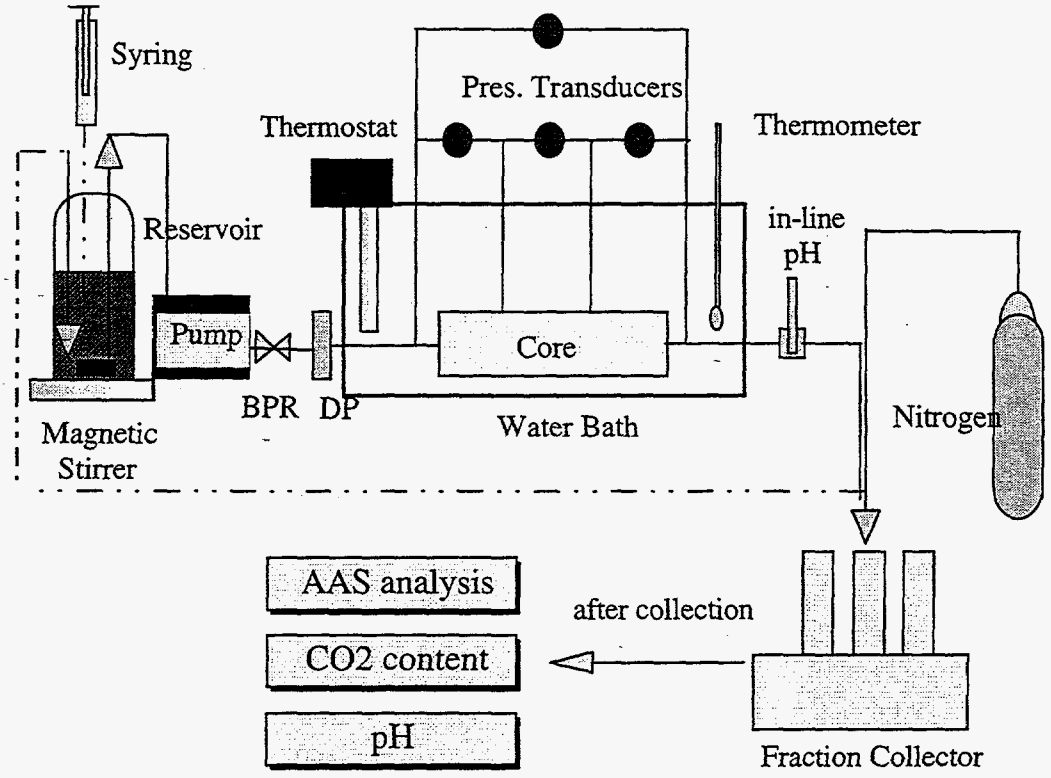

Figure 4.1 : Schematic of experimental apparatus.

Figure 4.2 is the data from Run 5 and shows the effect of injection rate on the effluent pH, and concentrations of calcium and magnesium. The injected solution was 0.5% KCl at a pH of 2.58. The core had been saturated with pH 3.1, 0.5% KCl brine for more than 5 days before Run 5. The effluent solution at the beginning is the resulting solution from the pH 3.1 brine being in contacted with the Baker dolomite core. The first injection rate was 1.15 mL/min, and after several pore volume injection, the effluent pH stabilized at 7.5. (Flow rates are indicated in Figure 4.2 by the value between vertical dashed lines.) When the injection rate was reduced to 0.075 mL/min, the effluent pH stabilized at 7.75. A stable pH was reached in a relatively short time after every change in flow rate. For the experimental injection rates ranging from 0.075 mL/min (about 9.5 hours residence time) to 16.50 mL/min (about 2.6 minutes residence time), effluent pH decreased as injection rate increased. During the run, the same injection rate, 1.15 mL/min, was applied three times, and the effluent pH stabilized at similar values. Effluent concentrations of calcium and magnesium were higher at lower injection rates. The molar ratio of the effluent Ca/Mg concentration was close to 1 which indicated that the dissolution was stoichiometric.

Effluent pH is shown in Figure 4.3 for Runs 3 to 7 as a function of the residence time in the core. The injected pH values were varied from 2.58 to 10.87 and are indicated in Figure 4.3 as the symbols at zero residence time. The effluent pH was a function of the injected pH and residence time. Except for Run 6 (pH 10.87), the effluent pH values are much higher than the injected pH. In the other runs, dissolution of dolomite increased the pH of the injected brine and the effluent pH increased as the residence time increased. Effluent pH stabilized for residence times greater than 40 minutes. The lower the injected pH, the longer the time to reach a constant value.

Magnesium concentrations in the effluent are shown in Figure 4.4 as function of residence time for several runs. For each injected pH value, the Mg concentration became stable at residence times longer than 40 minutes. Effluent measurements (Figures 4.3 and 4.4) indicated that the injected solution approached equilibrium at residence times longer than 40 minutes (injection rates less than 1 mL/min). The stabilized effluent pH and Mg concentrations suggests that the fluid-rock interactions occurred in the vicinity of the inlet end. For Run 6 (pH 10.87), the decrease in effluent pH as the residence time increased may be caused by the slow dissolution of quartz or clay minerals in high pH solution or dissolution of carbon dioxide from the atmosphere.

The effect of the injected pH on the effluent pH and effluent magnesium concentrations are shown in Figure 4.5 at the lowest injection rate (highest residence time) for each run. When the pH of the injected brine was less than 4, the effluent pH increased and the effluent magnesium concentration decreased rapidly as the injected pH increased. As the value of pH of the injected brine was increased from a value of 4.3 to 5.7, the effluent pH values were similar.

The results suggested that an equilibrium model can be used to simulate the effluent pH and concentrations for flow of brines in dolomite in which the contact times are on the order of hours or more. Based on this fact, an equilibrium model was developed and used to model the effluent pH and concentrations. The simulation results are described later.

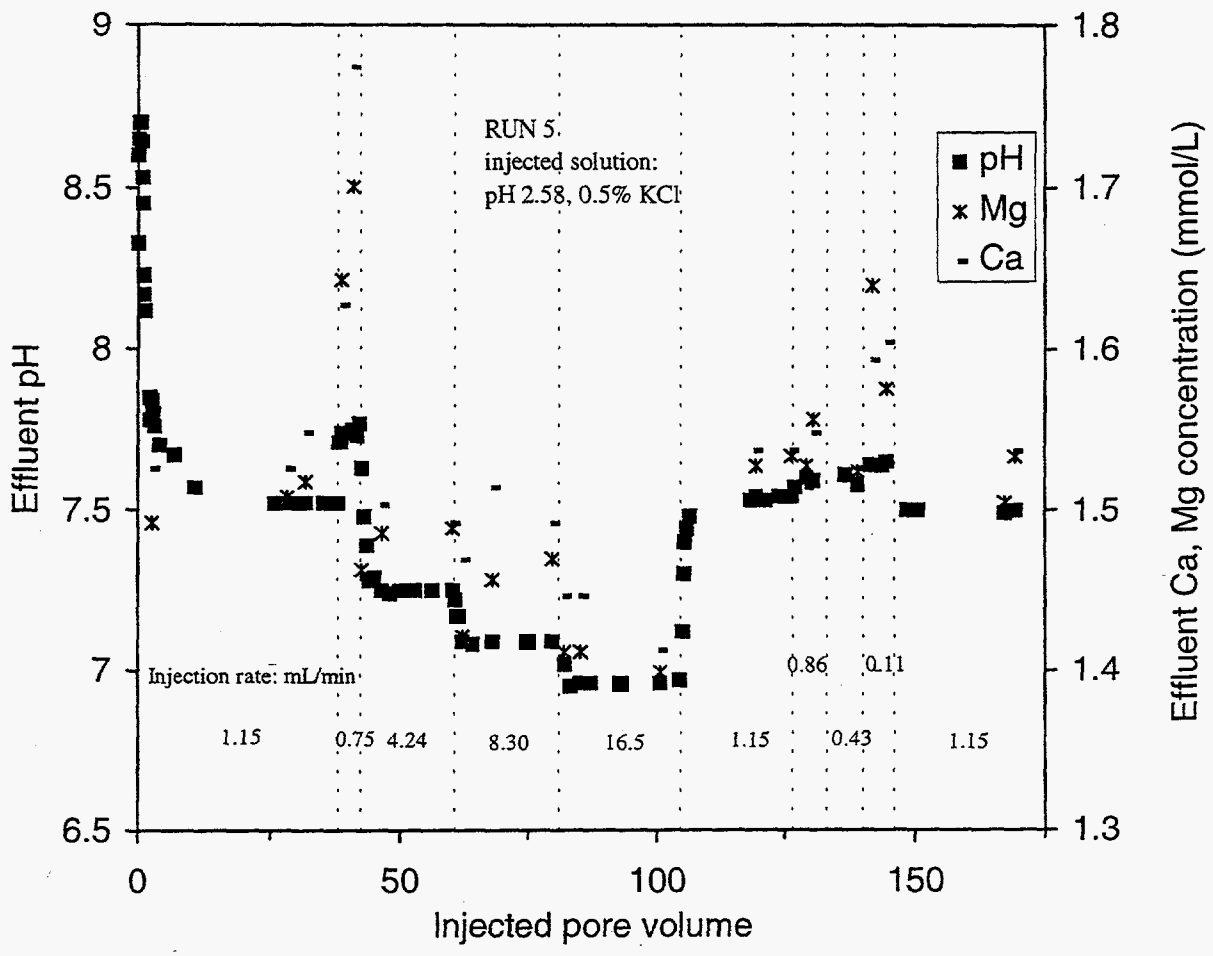

Figure 4.2 : Effect of injection rate on effluent pH and calcium and magnesium concentrations at injected pH value of 2.58.

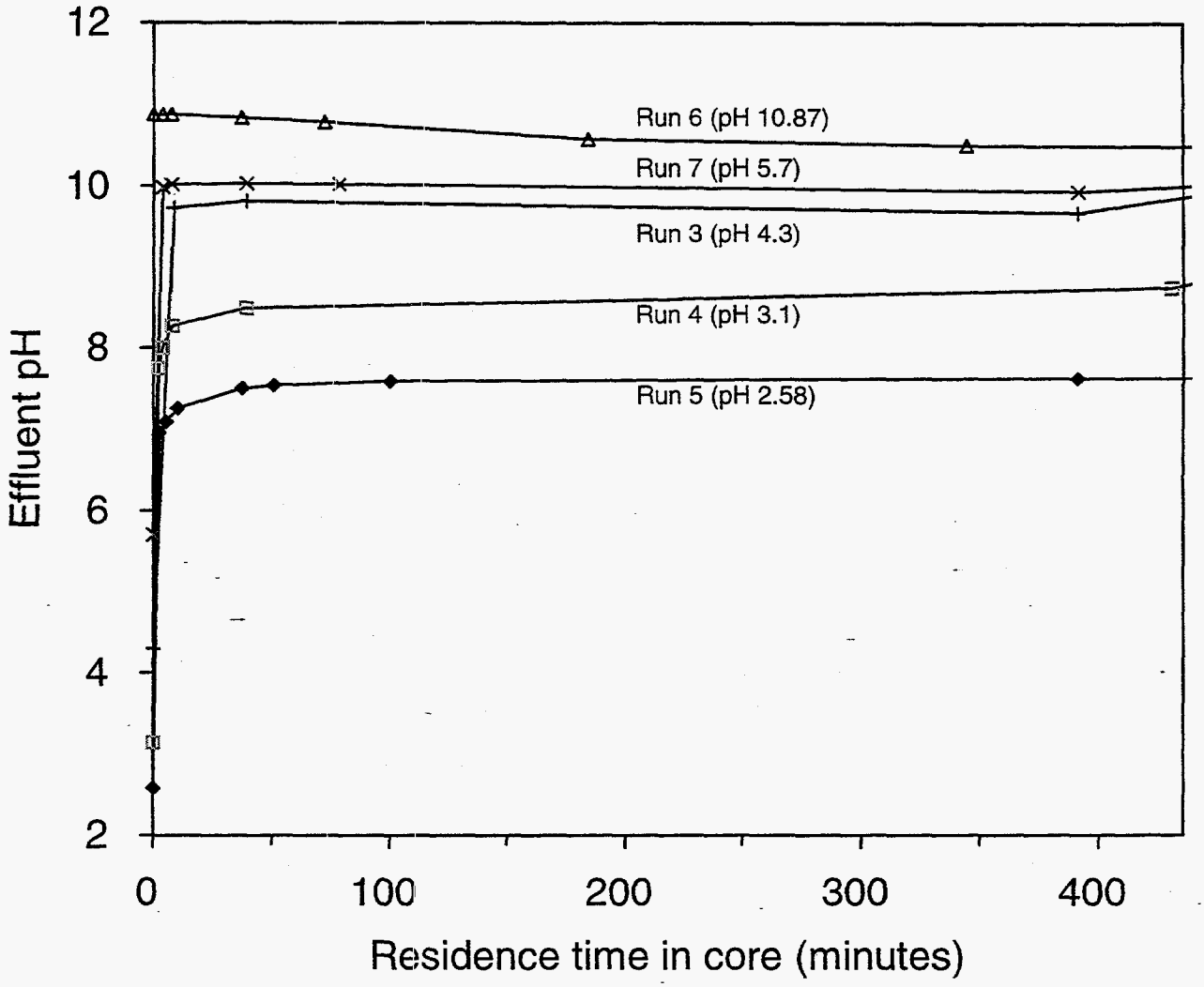

Figure 4.3 : Effect of injection rate on effluent pH for different injected pH values.

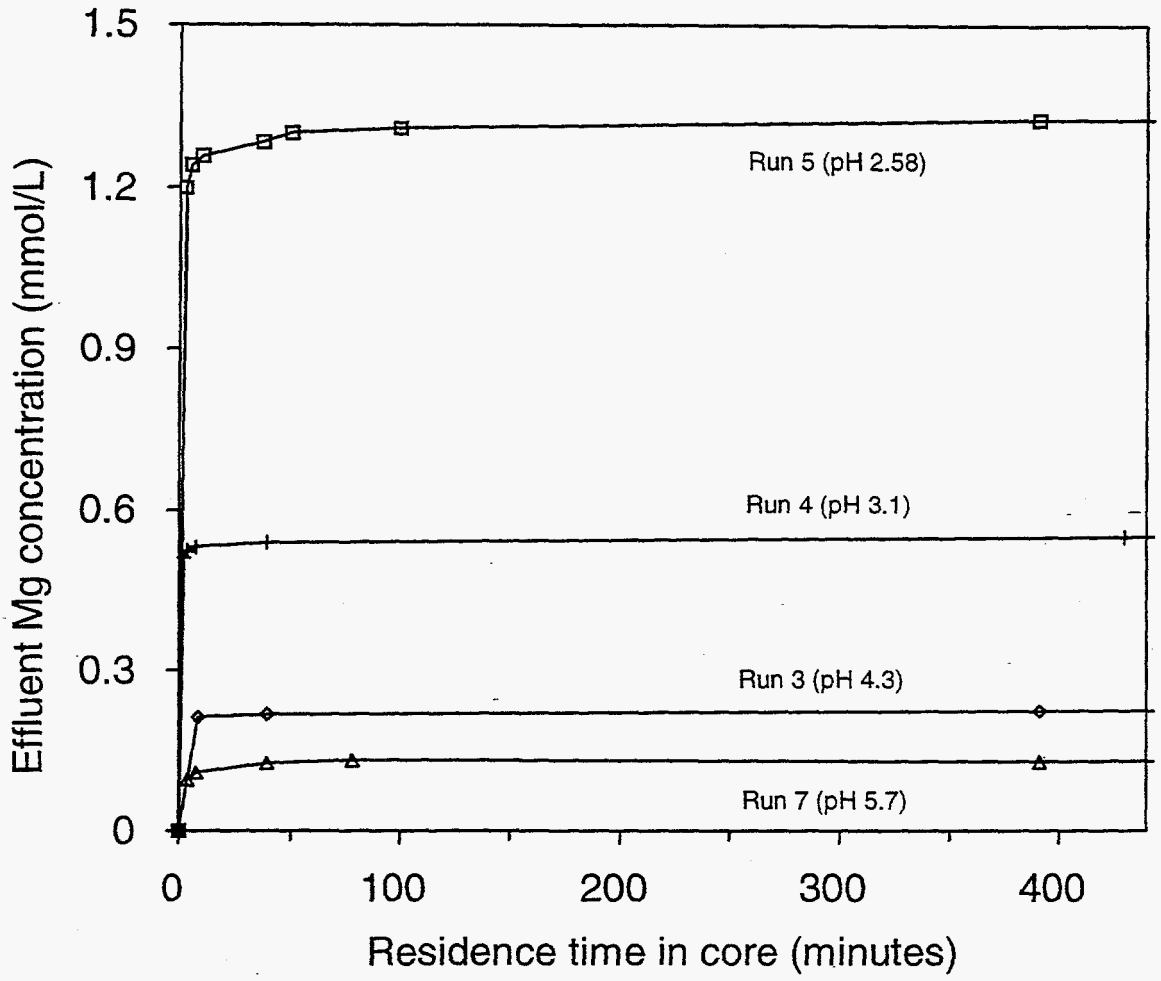

Figure 4.4 : Effect of injection rate on effluent magnesium concentration for different injected pH values.

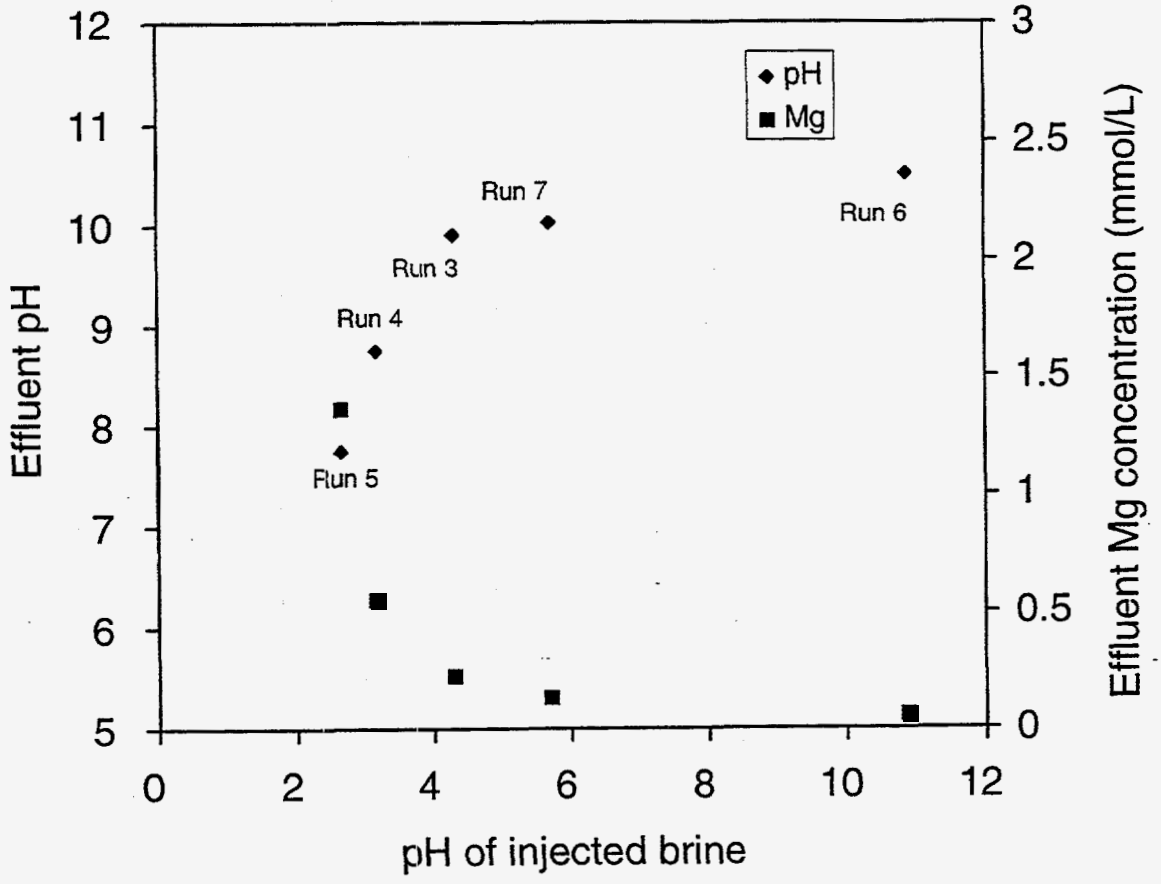

Figure 4.5 : Effect of injected pH on effluent pH and Mg concentration.

Figure 4.6 shows the permeability history of the Baker dolomite core. Approximately 1000 pore volumes of brine were pumped through the core with no apparent permeability change for measurements on the entire core length. The permeability of the first section increased slightly during the low-pH flooding. Mass balance calculations by estimating the amount of dissolved magnesium content also indicated that the porosity change was negligible (less than 0.3%).

Run 8 was conducted to investigate the effect of the calcium and magnesium concentration in the injected fluid on the effluent pH and the dissolution of dolomite in the Baker dolomite core. The injection rate was 1.1 mL/min for the entire run. Two series of injected solutions were used. All solutions contained 0.5% KCl at a pH of 5. The injected solution in Series A contained selected calcium concentrations. The injected solution of Series B contained a series of selected calcium and magnesium concentrations. The total divalent ion molar concentration in Series B was equal to the molar calcium concentration in the corresponding solution of Series A. For example, the calcium and magnesium concentrations in B3 are both 0.0125 mol/L. The sum is equal to the calcium concentration in A3.

The injected concentrations for Run 8 are shown in Table 4.2. The effect of total injected calcium and magnesium concentrations on effluent pH is shown in Figure 4.7. The effluent pH decreased as the injected divalent concentration increased. Comparing Series A with Series B, the presence of both calcium and magnesium in the injected solution had a larger effect on the effluent pH than when only calcium was present at the same divalent ion concentration. This showed that the common ions depressed the dissolution of the dolomite, shifted the equilibrium state of the system and hence prevented further increase of the pH in the effluent solution from dissolution of dolomite. This process may be visualized by examining the dolomite equilibrium in Eq. 4.6.

$$CaMg(CO_3)_2 \Leftrightarrow Ca^{2+} + Mg^{2+} + 2\,CO_3^{2-} \qquad \text{(Eq. 4.6)}$$

Adding Ca^{2+} and/or Mg^{2+} to the injected brine will shift the equilibrium to the left side of Eq. 4.6, suppressing dissolution.

Table 4.2 : The composition of the injected solution of Run 8

Solution number in Series A or B	1	2	3	4
Series A	pH 5, 0.5% KCl	pH 5, 0.5% KCl with 0.0025 mol/L Ca^{2+}	pH 5, 0.5% KCl with 0.025 mol/L Ca^{2+}	pH 5, 0.5% KCl with 0.25 mol/L Ca^{2+}
Series B	pH 5, 0.5% KCl	pH 5, 0.5% KCl with 0.00125 mol/L Ca^{2+}, 0.00125 mol/L Mg^{2+}	pH 5, 0.5% KCl with 0.0125 mol/L Ca^{2+}, 0.0125 mol/L Mg^{2+}	pH 5, 0.5% KCl with 0.125 mol/L Ca^{2+}, 0.125 mol/L Mg^{2+}

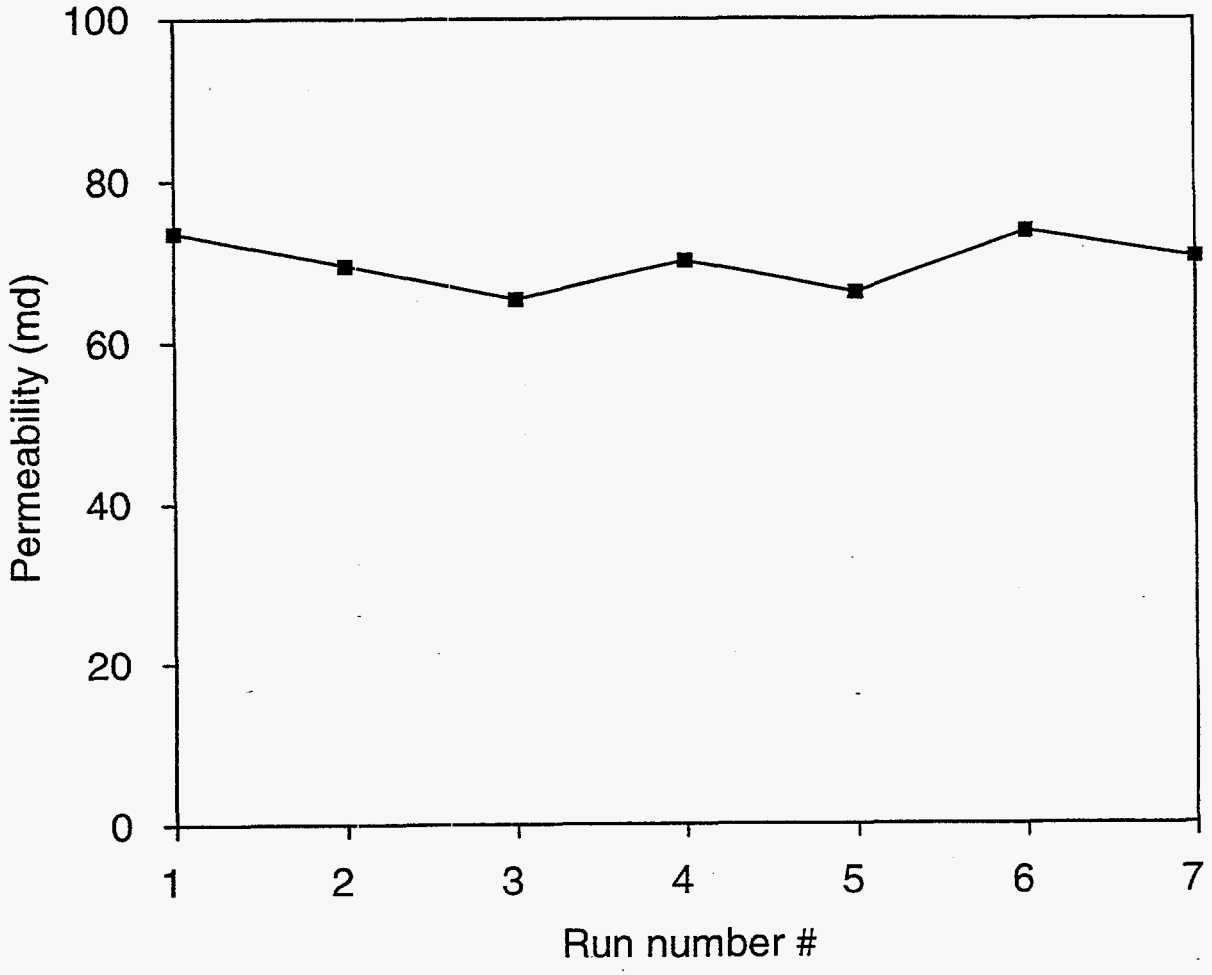

Figure 4.6 : Overall permeability history of the Baker dolomite core.

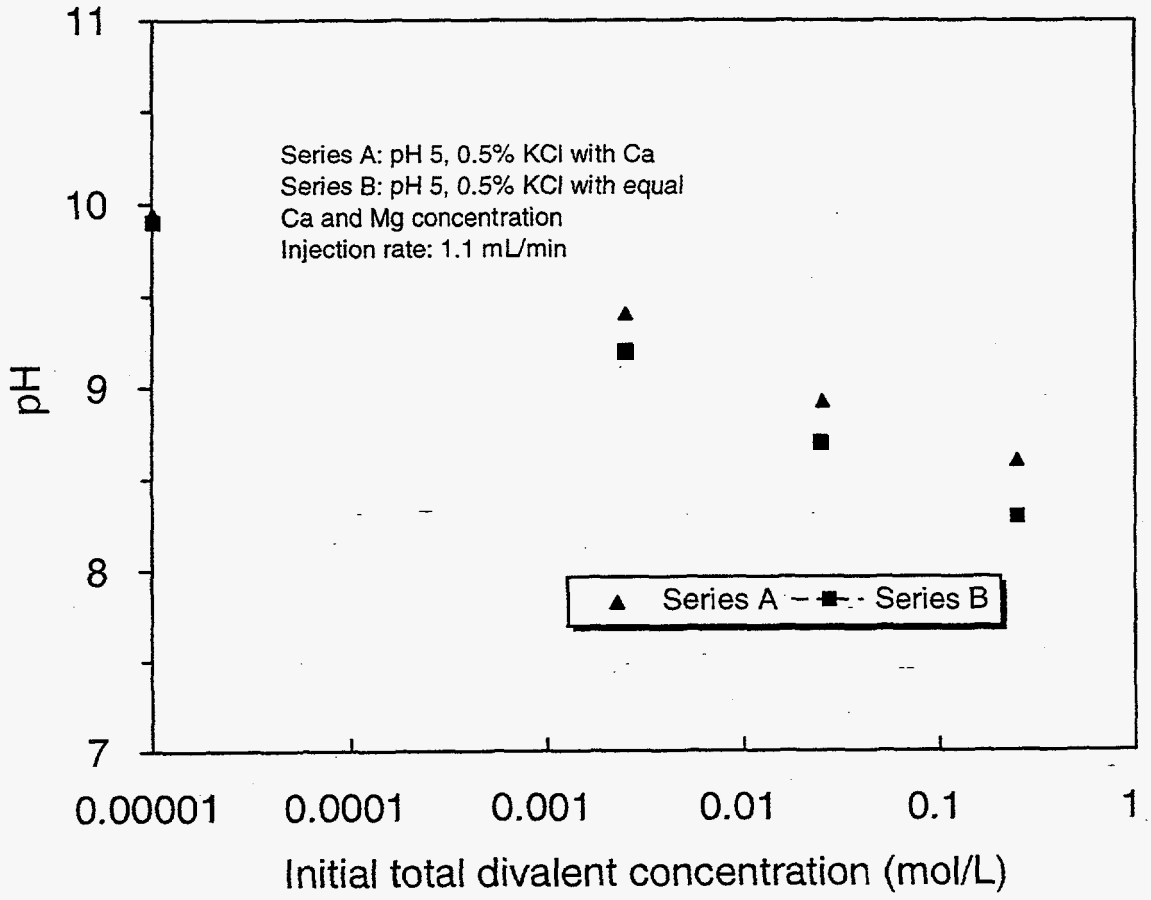

Figure 4.7 : Effect of calcium or magnesium ions in the injected solution on effluent pH.

Simulation

The interaction between injected solutions and the dolomite core was simulated using PHREEQE. PHREEQE is a FORTRAN program that assumes thermodynamic equilibrium of geochemical reactions and is based on a comprehensive thermodynamic data base. Details of program are described by Parkhurst et al.[12]

In the simulations, equilibrium was assumed for all liquid-phase reactions. The partitioning of ions was calculated by numerical iteration to satisfy equilibrium constants under the constraints of solubility products. The Debye-Huckel equation was used to calculated activity coefficients for the charged species. Mass balance equations for calcium, magnesium and carbonate for the total system (liquid and solid) were used. Oxygen and carbon were combined in the "element" carbonate. Hydrogen ion concentration was calculated by an electrical neutrality equation to alleviate data input problems. Potassium and chloride ions were considered as tracers with constant concentrations. The assemblage of all the relationships produced a set of non-linear algebraic equations. Newtonian iteration was used in the solution. A summary of the reaction chemistry used in the simulation system given in Table 4.3.

Table 4.3 : Summary of the reaction chemistry used in simulation

1. ELEMENTS

Hydrogen, Potassium, Calcium, Magnesium, Chlorine, Carbonate

2. REACTIVE CHEMICAL SPECIES

Fluid species:

H^+, K^+, Ca^{2+}, Mg^{2+}, Cl^-, CO_3^{2-}, HCO_3^-, OH^-, $CaHCO_3^+$, $MgHCO_3^+$, $CaCO_3^0$, $MgCO_3^0$, $CaOH^+$, $MgOH^+$, H_2O

Solid species:

$CaMg(CO_3)_2$ (dolomite), $CaCO_3$ (calcite, possible product), $MgCO_3$ (possible product)

3. REACTION EQUILIBRIUM

Solid phase dissolution, and other possible solubility constrains: ([X]: activity of X)

$CaMg(CO_3)_2 = Ca^{2+}+Mg^{2+}+2CO_3^{2-}$	$K_{sp} = [Ca^{2+}]\,[Mg^{2+}]\,[CO_3^{2-}]^2$	$-\log K_{sp} = 17.02$
$CaCO_3 = Ca^{2+} + CO_3^{2-}$	$K_{sp} \geq [Ca^{2+}]\,[CO_3^{2-}]$	$-\log K_{sp} = 8.31$
$MgCO_3 = Mg^{2+} + CO_3^{2-}$	$K_{sp} \geq [Mg^{2+}]\,[CO_3^{2-}]$	$-\log K_{sp} = 8.2115$
Equilibrium Reactions :		
$H_2O = H^+ + OH^-$	$K_w = [H^+]\,[OH^-]$	$-\log K_w = 13.996$
$H^+ + CO_3^{2-} = HCO_3^-$	$K_{eq} = [HCO_3^-]/([H^+][CO_3^{2-}])$	$-\log K_{eq} = -10.33$
$2H^+ + CO_3^{2-} = H_2CO_3$	$K_{eq} = [H_2CO_3]/([H^+]^2[CO_3^{2-}])$	$-\log K_{eq} = -16.706$
$Ca^{2+} + H_2O = CaOH^+ + H^+$	$K_{eq} = [CaOH^+]\,[H^+]/([Ca^{2+}])$	$-\log K_{eq} = 12.919$
$Mg^{2+} + H_2O = MgOH^+ + H^+$	$K_{eq} = [MgOH^+]\,[H^+]/([Mg^{2+}])$	$-\log K_{eq} = 11.41$
$Ca^{2+} + CO_3^{2-} = CaCO_3^0$	$K_{eq} = [CaCO_3^0]/[Ca^{2+}]\,[CO_3^{2-}]$	$-\log K_{eq} = 3.224$
$Mg^{2+} + CO_3^{2-} = MgCO_3^0$	$K_{eq} = [MgCO_3^0]/[Mg^{2+}]\,[CO_3^{2-}]$	$-\log K_{eq} = 2.98$
$Ca^{2+} + H^+ + CO_3^{2-} = CaHCO_3^+$	$K_{eq} = [CaHCO_3^+]/([Ca^{2+}][H^+][CO_3^{2-}])$	$-\log K_{eq} = -11.55$
$Mg^{2+} + H^+ + CO_3^{2-} = MgHCO_3^+$	$K_{eq} = [MgHCO_3^+]/([Mg^{2+}][H^+][CO_3^{2-}])$	$-\log K_{eq} = -11.77$

Equilibrium concentrations for the Ca-Mg-K-Cl-CO_2-H_2O system were calculated over the range of injected pH values from 1 to 13. Solid dolomite was assumed to be in excess and dissolved to satisfy the solubility product. Brine concentrations were those used in the flow experiments. The solid curve in Figure 4.8 is the calculated equilibrium pH and the dashed curve is the calculated equilibrium magnesium concentration. The equilibrium calcium concentration was essentially the same as that of magnesium. Experimental data of Figure 4.5 are also plotted in Figure 4.8. Good agreement is observed between the model prediction and measured effluent pH and magnesium concentration.

According to both experimental data and simulation curve, the effluent pH exhibited a three-stage behavior as a function of the injected pH. When the injected pH was less than 4, the effluent pH was much higher than the injected pH and increased as the injected pH increased. In this lower-pH range, the equilibrium magnesium concentration decreased exponentially as the pH increased. When the injected pH was between 4 and 10, the effluent pH was almost a constant value of 10, and the Mg concentration showed little variation with the increase of the injected pH. When the injected pH was higher than 10, the effluent pH was almost equal to the injected pH. Interactions between the injected brine and the high-pH injected solution caused little change in the pH of the solution as it flowed through the core. The dissolution of dolomite in a high-pH brine was slightly greater than that in the middle-pH range.

The PHREEQE model was used to simulate the experimental results obtained for Run 8 where magnesium and/or calcium were contained in the injected brine. Analysis of calcium, magnesium and carbonate in the effluent solutions for Series A experiments in Run 8 showed that the effluent was supersaturated when compared to the calcite solubility product. Two types of simulations for these runs were conducted. Case 1 was run without the constraint of the calcite solubility product which allowed for the supersaturation of calcium. Case 2 was run with the constraint of the calcite solubility product.

The measured effluent Ca and Mg concentrations and the two simulation cases are shown in Figure 4.9 for Series A experiments. Case 1 simulations were in much better agreement with the experimental data than Case 2 simulations.

The measured and simulated pH for RUN 8 - Series A and B experiments are shown in Figure 4.10. The effluent pH decreased as the injected divalent ion concentrations increased. For comparison, the effluent pH was 9.9 when the injected solution contained no calcium or magnesium (injected pH of 5 and at a flow rate of 1.1 mL/min). The experimental data and the simulated results both showed that the presence of both calcium and/or magnesium suppressed the increase of pH of a solution that has come in to contact with dolomite. The combination of calcium and magnesium suppressed the pH increase more than calcium alone. A supplemental experiment and a series of simulation runs of the common-ion effect of magnesium in the injected solution showed that the individual presence of magnesium had a similar effect as that of calcium.

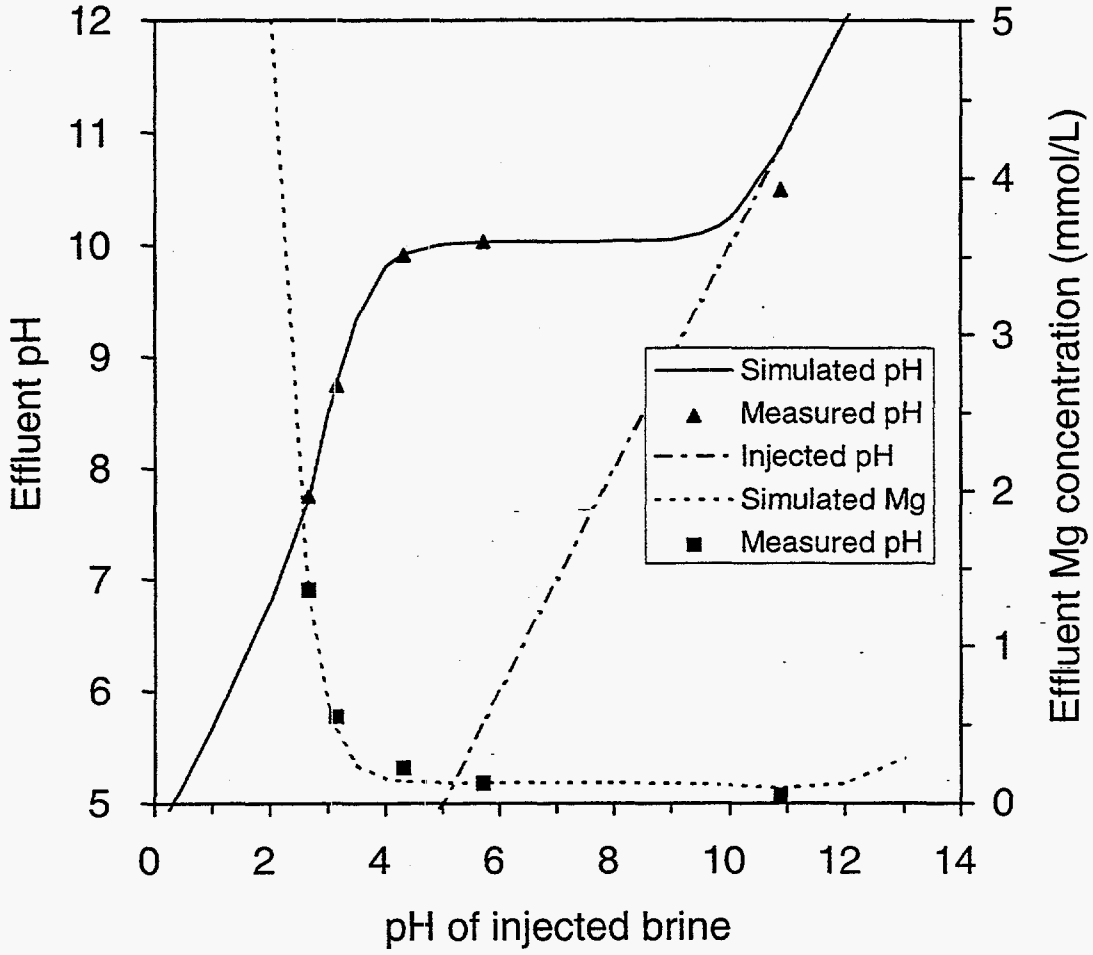

Figure 4.8 : Comparison of pH and magnesium concentration between experimental data and simulated equilibrium results.

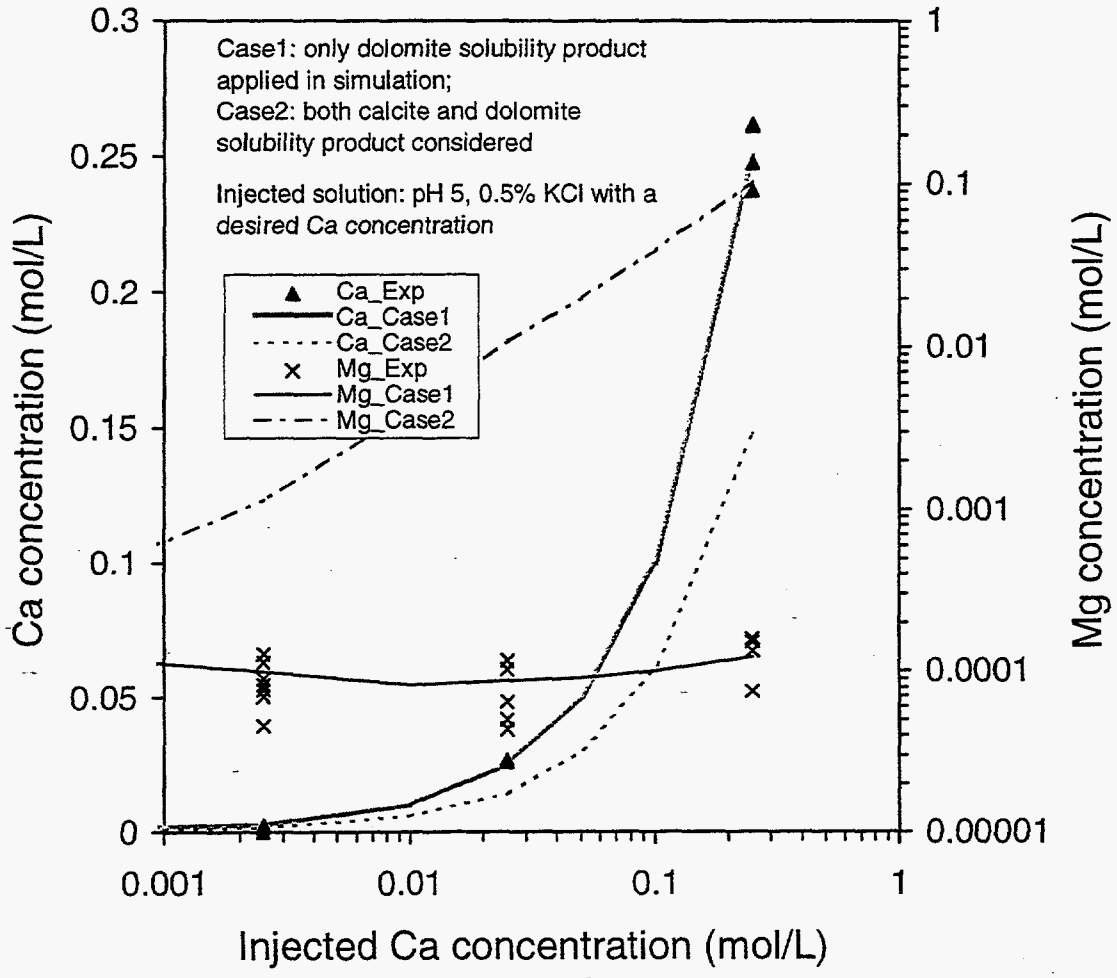

Figure 4.9 : Comparison between simulated results and experimental data for calcium and magnesium concentrations.

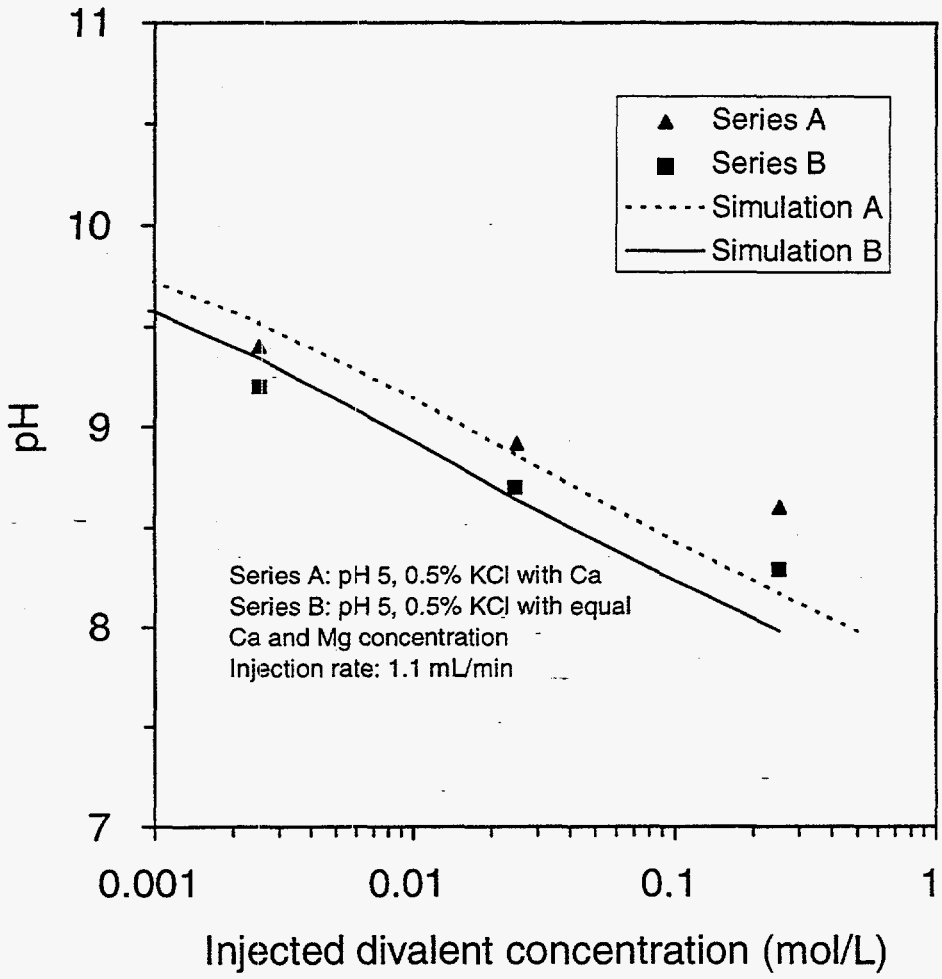

Figure 4.10 : Effect of injected calcium and magnesium concentrations on effluent pH - experimental data and simulated equilibrium results.

Conclusions

The following was concluded from the experimental investigation and the simulations for the Ca-Mg-K-Cl-CO_2 system.

1. The effluent pH and composition is a function of both injected pH and injection rate. The effluent pH demonstrates a three-stage behavior when the injected pH increases from 1 to 13. When the injected pH is less than 4, with the increase of the injected pH, the effluent pH increases, the dissolution of dolomite decreases exponentially. When the injected pH between 4 to 10, the change of the injected pH has little effect on the effluent pH which is always around 10. Within this pH range, reducing the injected pH does not help achieving a lower effluent pH. When the injected pH is above 10, the effluent pH increases linearly with the increase of the injected pH, which is essentially the same as the injected pH.
2. The kinetic dissolution characteristics are observed by applying different injection rates during core flooding. However, the major change in both concentration and pH happens at the immediate vicinity of the inlet end of the core.
3. Dissolution of dolomite during core flooding up to 1000 pvi had little effect on porosity and permeability of the Baker dolomite core.
4. The pH and concentrations in the effluent solution with a residence time longer than 40 minutes can be simulated by equilibrium model.
5. Added Ca^{++} and Mg^{++} ions in the injected brine suppresses the dissolution of dolomite and produces a lower equilibrium pH as compared to the case of with no added ions.
6. The presence of both calcium and magnesium ions in the injected brine has the larger effect on the effluent pH than either Ca^{2+} or Mg^{2+} present individually.

References

1. Seright, R.S., "Impact of permeability and lithology on gel performance," SPE/DOE 24190, presented on Eighth Symposium on Enhanced Oil Recovery, Tulsa (April 22-24, 1992).
2. Stavland, A., Ersdal, T., Kvanik, B., Lohne, A., Lund, T. and Vikane, O., "Evaluation of Xanthan-Cr Gels for Deep Emplacement: Retention of Cr(III) in North Sea Sandstone Reservoir," Seventh European Symposium on Improved Oil Recovery, Moscow, Russia (Oct. 27-29, 1993).
3. McCool, C.S.,Green, D.W. and Willhite, G.P., "Fluid-rock interactions between Xanthan-Cr3+ gel systems and dolomite core material," SPE 28987, presented at SPE Inter. Symp. on Oilfield Chem., San Antonio (Feb. 14-17, 1995).
4. Lund, K., Fogler, H.S. and McCune, C.C., "Acidization-I. The dissolution of dolomite in hydrochloric acid," *Chem. Eng. Sci.*, v. 28, 691-700 (1973).
5. Rauch H.W. and White, W.B., "Dissolution kinetics of carbonate rocks I. Effect of lithology on dissolution rate," *Water Resource Research*, 13(2), 381-394 (1977).
6. Hadad, M., "Modeling of limestone dissolution in packed-bed contactors treating dilute acidic water," Ph.D. thesis, Syracuse University (1986).
7. Busenberg E. and Plummer, L.N., "The kinetics of dissolution of dolomite in CO2-H2O system at 1.5 to 65 and 0 to 1 atm PCO2," *Amer. J. Sci*, 282, 45-78 (1982).
8. Chou, L., Garrels, R.M. and Wollast, R., "Comparative study of the kinetics and mechanisms of dissolution of carbonate minerals," *Chemical Geology*, 78, 269-282 (1989).

9. Lasaga, A.C., "Chemical Kinetics of Water-Rock Interactions," *J. of Geophysical Research*, 89, 4009-4024 (1984).
10. Sjoberg E.L. and Richard, D.T., "The effect of dissolved calcium on calcite dissolution kinetics in aqueous solution at 25 oC," *Chemical Geology*, 49, 405-413 (1985).
11. Berner, R., "Comparative dissolution characteristics of carbonate mineral in the presence and absence of aqueous magnesium ion," *Amer. J Sci.*, 265, 45-70 (1967).
12. Parkhurst D.L., Thorstenson, and Plummer, L.N., "PHREEQE-a computer program for geochemical calculations," US Geol. Survey Water Resource Invest. PB81-167801 (1980).

Chapter 5

Delayed Gelation of a Polyacrylamide - Chromium(III) System

Principal Investigators: D.W. Green, G.P. Willhite and C. S. McCool
Graduate Research Assistant: Dilip Natarajan

Introduction

The polyacrylamide - chromium(III) gel system is a widely used system for the treatment of fractures. Short gel times make this system unfavorable for application to matrix conformance problems. An effective mechanism to delay gelation could make the PAAm - Cr(III) system applicable for in - depth treatment of porous media.

Lockhart and co-workers[1-3] showed that gels prepared from organic salts of chromium had significantly longer gel times than those prepared from inorganic sources. Acetate, malonate and propionate were among the anions studied. McGuire[4] studied the effect of different chromium acetate salts and added sodium salts of the corresponding anions, on the rate of gelation. These studies showed that longer gel times could be obtained with chromium acetate and that the presence of excess sodium acetate further delayed gelation .

The objective of this study was to study the capability of sodium acetate to delay the gelation of PAAm - Chromium(III) acetate gel systems. The performance of this system was studied in bottle tests and in the porous media.

Experimental

Bottle Tests. Figure 5.1 is a schematic of the gel mixing procedure. Stock solutions of the polymer and chromium salt were prepared with the required concentrations. Sodium acetate and/or sodium chloride were placed in the polymer stock. The polymer stock solutions were then stirred for 24 hours (Aldrich lot #9 or Alcoflood 935 was used). Chromium stocks were prepared from 50% solutions provided by McGeane - Rohco or from reagent grade salt by Alfa products. These solutions were stirred for about an hour. They were then used as fresh stock or allowed to hydrate for a month depending upon the experiment.

Samples from the stocks were mixed at a ratio of 3 : 1 (polymer : Cr.(III)) to give the final gel solution with 5000 or 9000 PPM polymer, 100 PPM Cr(III) (0.00192 moles/kg solvent) and desired salt concentration. The pH was adjusted to 5.0 ($\pm$ 0.1) at the time of mixing, using 1 N acetic acid. The amount of acetic acid needed for this purpose was measured and was found to be too small to significantly change the acetate concentration The gel solutions were then maintained at a constant temperature of 25 °C.

Viscosity of the gel solutions was measured as a function of time with a micro - viscometer. The samples were assumed to have gelled when the viscosity went beyond 205.6 cp which is the maximum range of the instrument when operated at a shear rate of 11.25 per second. This gel time agreed well with visual observations of the gel samples.

Sandpack Runs. The gel solution used in the sandpack runs had a composition of 5000 PPM polyacrylamide (Alcoflood 935), 100 PPM Cr(III) (McGeane - Rohco) and an initial pH of 5.0. The parameters studied in these runs was the sodium acetate concentration and the age of the Cr(III) stock.

Figure 5.2 is the schematic of the experimental setup used to conduct displacement experiments in the porous media. The unconsolidated sandpacks were prepared from acid- washed Wedron silica sand with a grain fineness of 144.3. The sand was packed using a pneumatic packer in holders made from acrylic plastic stock. The pack holders had an ID of 1.5 inches and a length of 1 foot. Pressure ports were provided at intervals of two inches, dividing the pack into 6 sections. These ports enabled the measurement of pressure differentials across the sections and the entire length of the pack. Screens were placed at the ends to avoid sand washout.

Physical characteristics of the porous media were evaluated prior to gel injection. The porosity of the pack was estimated by weighing the sandpack dry and completely saturated with water. This was followed by a tracer test where a step change in salt concentration was introduced and effluent samples were measured using a differential refractometer. The results of this test were used to study the homogeneity of the pack and check the porosity estimated from the weight measurements. Water was then injected into the pack at known flow rates and the pressure differentials across the sections and the whole pack were measured. This data was then used to determine permeabilities of the pack and individual sections.

Before the injection of the gel solution, a buffer solution of acetic acid and sodium acetate at a pH of 5.0 , was injected into the sandpack and shut in for 24 hours. The buffer contained the same amount of sodium acetate as the gel solution to be injected. Effluent sample analysis showed that the pH of the buffer did not change significantly during injection and after shut - in period.

The polymer stock solution was loaded in a transfer cylinder and was displaced using oil while the crosslinker solution was directly pumped into the in - line mixer. Gel samples were collected from the in - line mixer prior to injection into the sandpack. The pressure differentials were measured during injection. The displacement experiment was terminated when the pressure differential across the pack was greater than 80 psi or when sufficient quantities of the gel solution were pumped through the pack.

Effluent samples were collected and their pH was measured. If the solution didn't gel during injection, the pack was shut in at 25 °C for a time period greater than the gel time determined from bottle tests. Water or brine was then injected into the pack to determine the post treatment permeabilities.

Samples of gel solution were prepared manually from the stock solutions. Screen factors and viscosities of these and the in - line mixer samples were measured with respect to time.

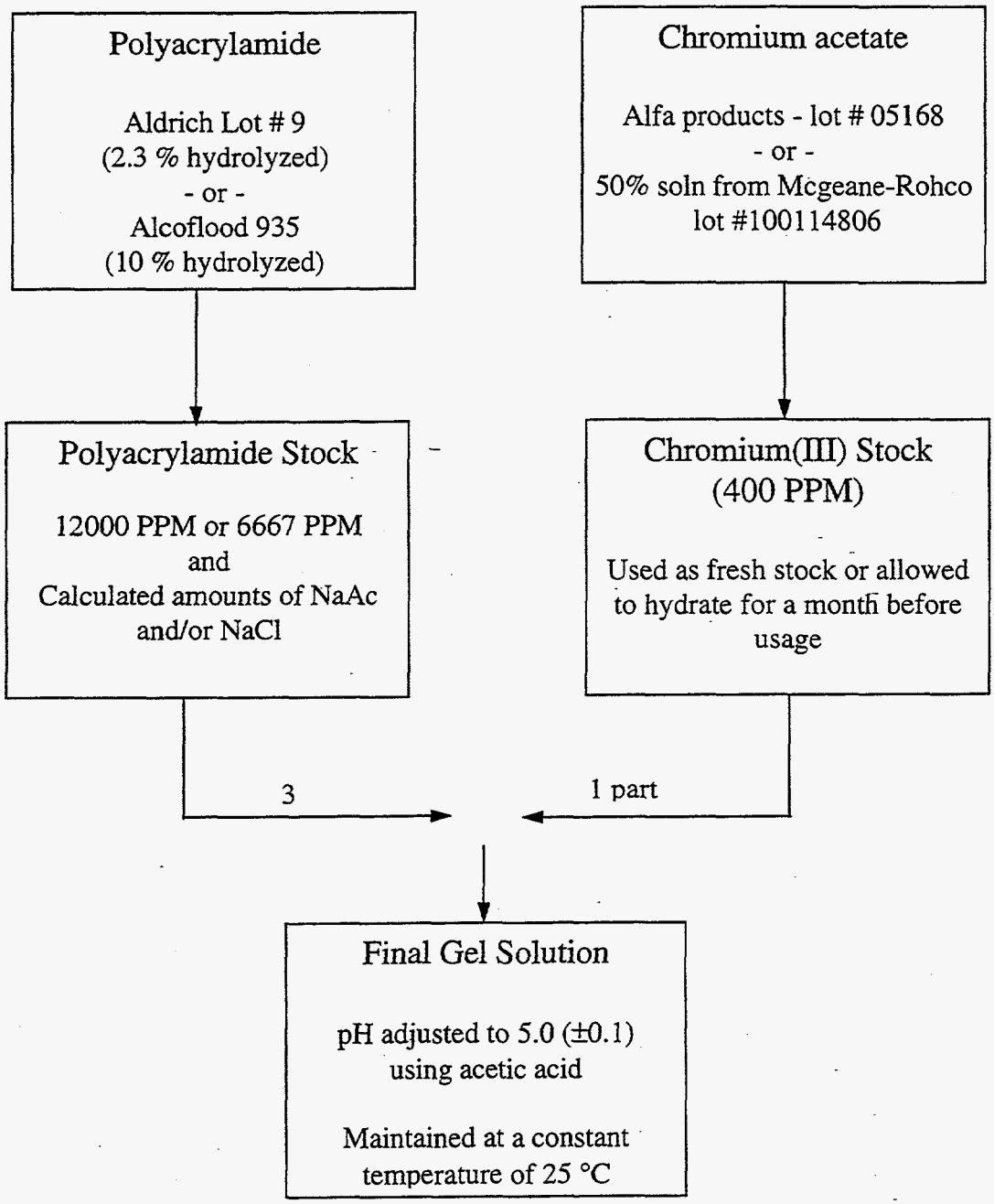

Figure 5.1 : Gel mixing procedure.

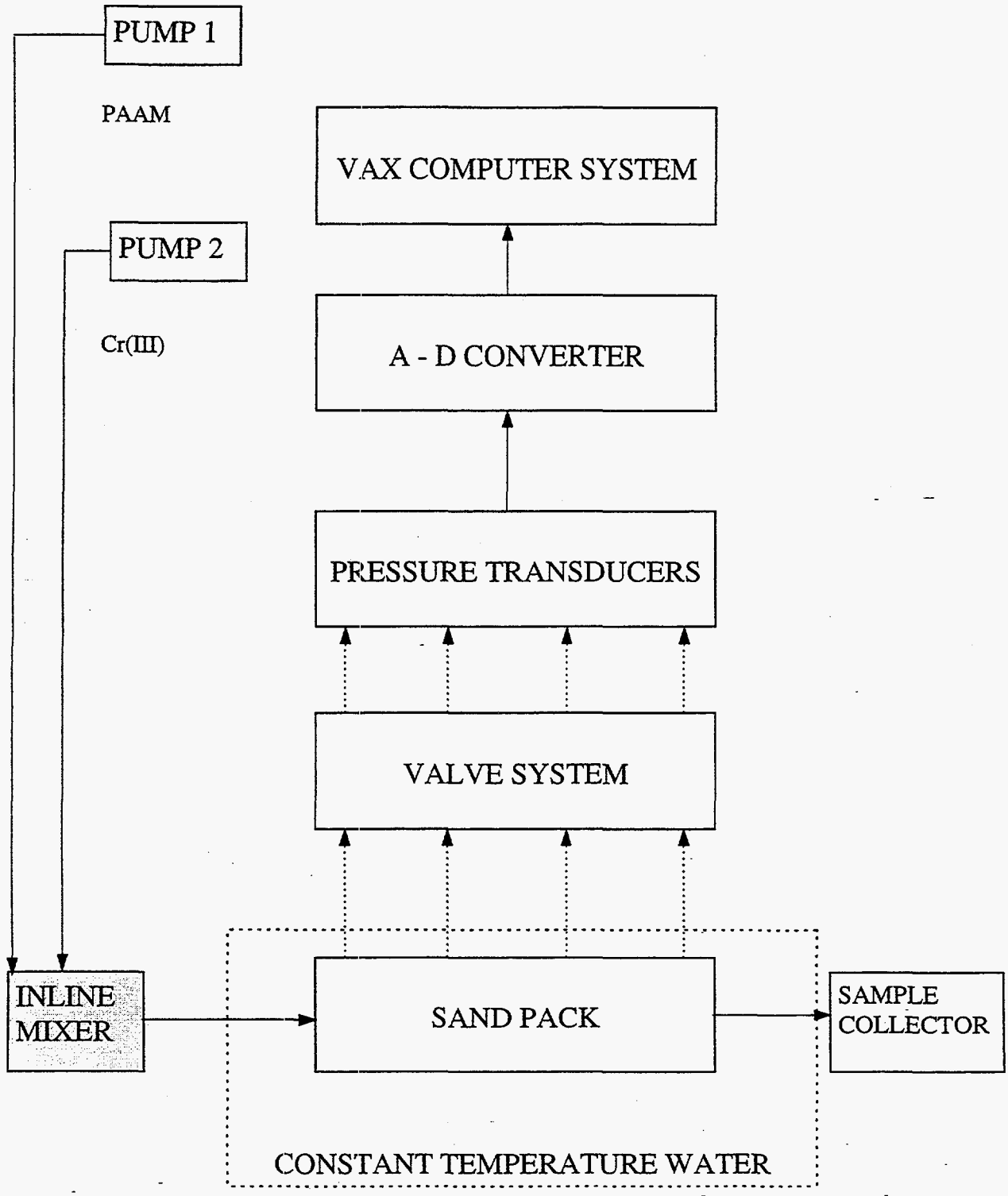

Figure 5.2 : Set up for displacement experiments.

Results and Discussion

Bottle Tests. Table 5.1 gives the details on the bottle tests conducted. Viscosity data were plotted verses time to determine the gel time. Figure 5.3 is a typical viscosity- time plot for a gel sample. The gel times estimated from these bottle tests were plotted against the parameter studied.

Results presented in Figures 5.4 and 5.5 were obtained from gel samples prepared with Aldrich polyacrylamide (lot # 9) and chromium acetate salt obtained from Alfa products. Figure 5.4 is a plot of gel times as a function of sodium acetate concentration for samples prepared with added sodium acetate. The gel times increase sharply beyond a particular critical salt concentration.

Figure 5.5 presents gel times as a function of sodium chloride concentration for samples prepared with sodium acetate concentrations of 0.06m and 0.08m. The presence of sodium chloride reduced the gel times significantly in samples with higher acetate concentration.

Results presented in Figures 5.6 and 5.7 were determined from gel samples prepared with Alcofloōd 935 and 50% chromium acetate solution by McGeane - Rohco. The effects of sodium acetate concentration and the age of the chromium stock solution are shown in Figure 5.6. The gel times were found to reduce with the age of the chromium stock and increase with the acetate concentrations. The results from batches 1 & 3 (see Table 5.1) could not be compared by scaling concentrations based on the degree of hydrolysis. Figure 5.7 is a plot of gel times with respect to sodium chloride. Sodium chloride was found to reduce the gel times up to a concentration of approximately 0.5m.

Sandpack Runs. A description of the displacement experiments is given in Table 5.2. The initial permeabilities of the sandpacks are listed in Table 5.3. Sodium acetate concentration and age of the Cr(III) stock were the parameters studied.

Gel injection data are presented as apparent viscosity as a function of pore volumes injected. Apparent viscosities were calculated from the pressure differentials using the Darcy's law assuming that the permeabilities remain constant (Eq. 5.1). Apparent viscosity is a measure of the flow resistance in the sandpack over which the pressure differential was measured.

$$\mu_{app} = \frac{k \cdot A \cdot \Delta p}{q \cdot L} \qquad \text{(Eq. 5.1)}$$

where,

μ_{app}	=	apparent viscosity
k	=	permeability
A	=	cros- sectional area
Δp	=	pressure differential across a section
q	=	volumetric flow rate
L	=	section length

Table 5.1 : Description of bottle tests

Batch #	Polymer Stock	Cr(III) Stock	Salt Concentration Range (moles /Kg solvent)		Results
			NaAc	NaCl	
1	Aldrich lot # 9 2.3% hydrolyzed 12000 PPM	Alfa pdts -- lot # 05168 400 PPM of Cr(III) (one month old)	0.0 --1.0 m	None	Figure 5.4
2	Aldrich lot # 9 2.3% hydrolyzed 12000 PPM	Alfa pdts -- lot # 05168 400 PPM of Cr(III) (one month old)	0.06 and 0.08m	None, one tenth, equal and ten times the concentration of NaAc	Figure 5.5
3	Alcoflood 935 10 % hydrolyzed 6667 PPM	50% CrAc soln from McGeane - Rohco - 400PPM (fresh and one month old stocks used)	0.0 - 1.0 m	None	Figure 5.6
4	Alcoflood 935 10 % hydrolyzed 6667 PPM	50% CrAc soln from McGeane - Rohco - 400PPM (fresh stock)	0.09 and 0.104 m	None, equal, 2, 3, 5 & 10 times the NaAc concentration	Figure 5.7

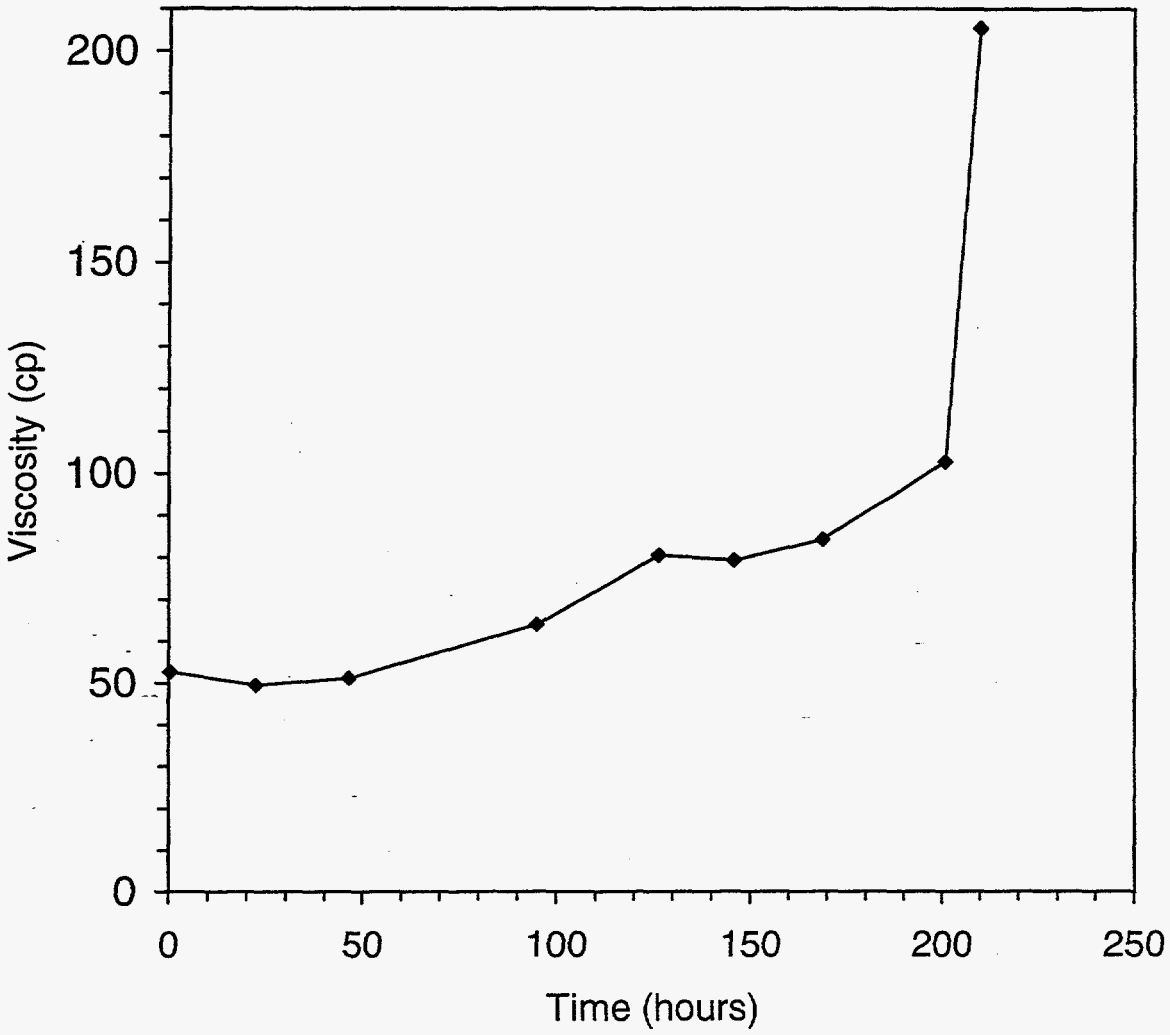

Figure 5.3 : Viscosity as a function of time for gel sample.

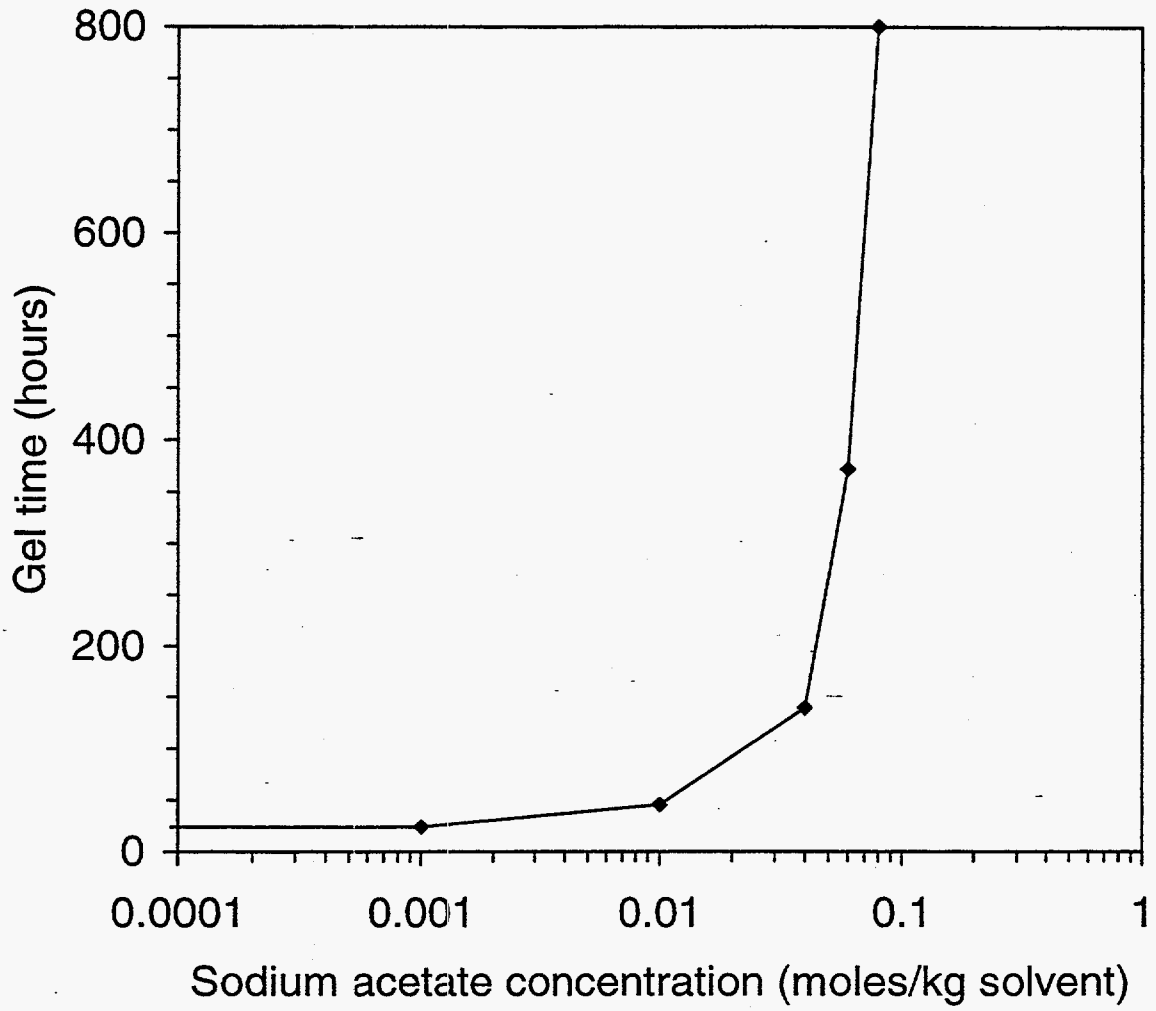

Figure 5.4 : Effect of sodium acetate concentration on gel time; Aldrich polymer, Cr(III) - Alfa Products.

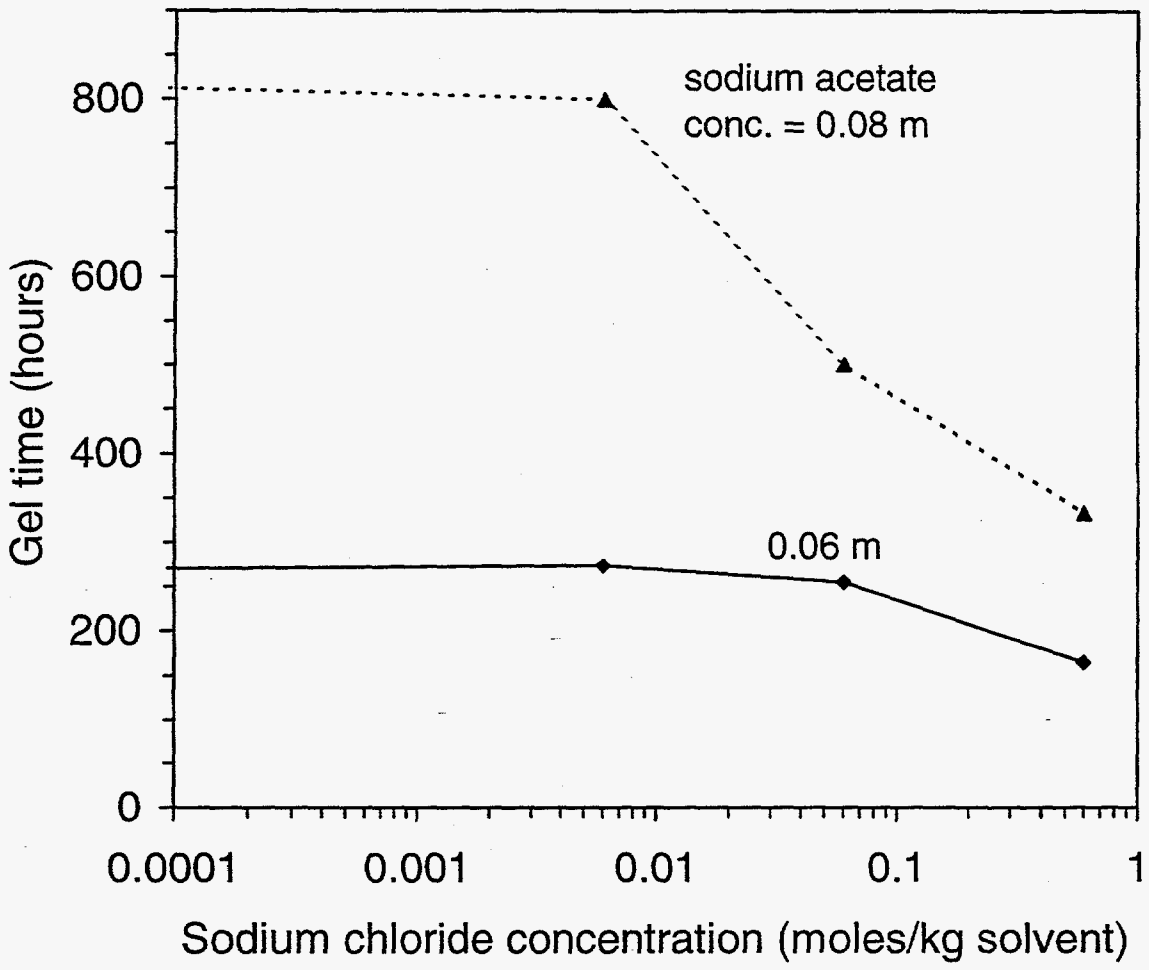

Figure 5.5 : Effect of sodium chloride concentration on gel time; Aldrich polymer, Cr(III) - Alfa Products.

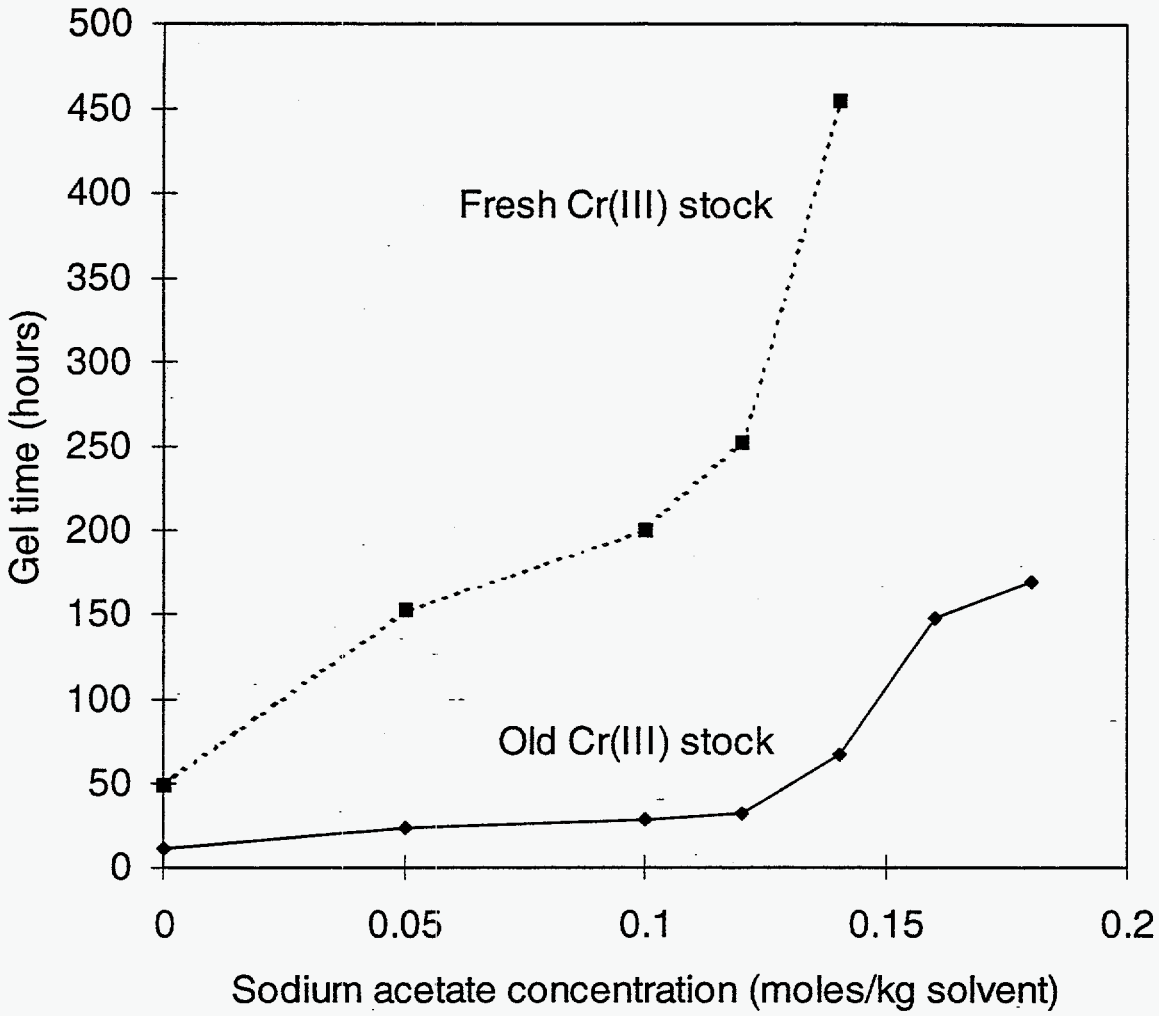

Figure 5.6 : Effect of sodium acetate concentration and age of Cr(III) Stock on gel time; Alcoflood 935 polymer, Cr(III) - McGeane - Rohco.

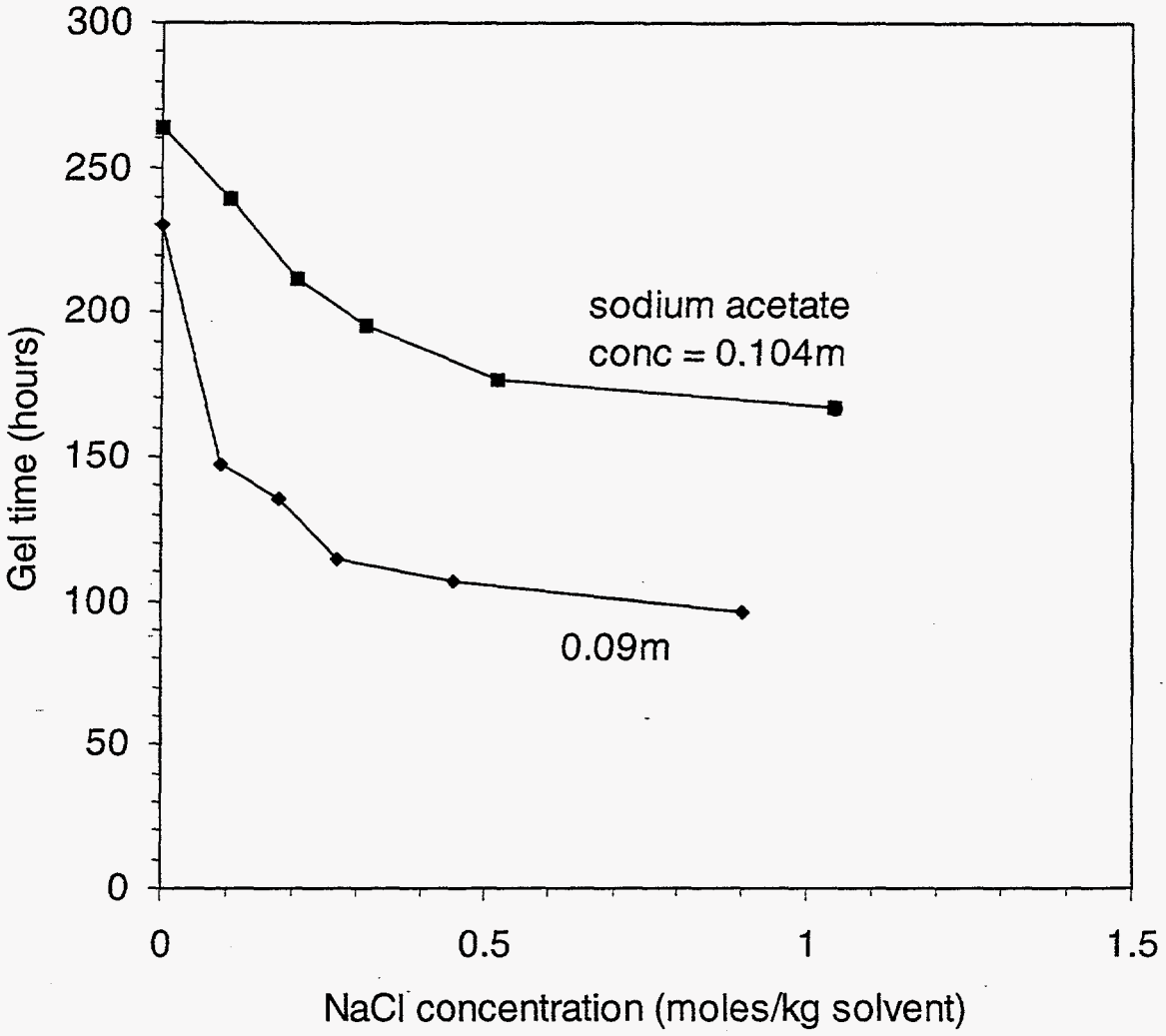

Figure 5.7 : Effect of sodium acetate concentration on gel time; Alcoflood 935 polymer; Cr(III) -McGeane - Rohco.

Table 5.2 : Description of Sandpack Runs

Run #	Porosity & Pore volume	Average overall Permeability (md)	Sodium acetate concentration & Age of Cr(III) stock	Gel time in bottles	Volume injected (PV)
Flow rate = 0.6 mL/mini --- (polymer = 0.45 mL/min & Cr(III) = 0.15 mL/mini) *Dimensions : Length = 30.48 cm, Diameter = 3.81 cm & Section length = 5.08 cm*					
SP2	ϕ = 0.36 PV = 125.4 mL	2406	0.12 m & a month old Cr(III) stock	20 hours	1.17
SP3	ϕ = 0.34 PV = 117.9 mL	2894	1.0 m & a month old Cr(III) stock	> 4 months	4.3
SP4	ϕ = 0.347 PV = 120.6 mL	3529	0.2 m & fresh Cr(III) stock	1 month	1.37
SP5	ϕ = 0.28 PV = 97.6 mL	3152	0.088 m & fresh Cr(III) stock	148 hours	7

Table 5.3 : Initial Permeabilities of Sandpack Sections in Millidarcies

	Overall	Sections					
		1st	2nd	3rd	4th	5th	6th
SP2	2406	2143	2586	2195	2780	3089	2735
SP3	2894	3620	2930	2969	3132	2630	3184
SP4	3529	2825	3526	4807	3244	2410	3362
SP5	3152	5526	3289	2953	2276	2498	6294

GEL SOLUTION INJECTION IN SP2

The gel solution injected in SP2 had a composition of 5000 PPM polymer, 100 PPM Cr(III) (aged for a month) and 0.12m sodium acetate at a pH of 5.0. The gel time determined for this sample from bottle tests was 20 hours.

Flow resistance in the sandpack and in each section of the sandpack are shown in Figure 5.8 as apparent viscosities as a function of pore volumes of gelant injected. The apparent viscosities increased as the gel solution front displaces the resident buffer solution and continued to rise rapidly. The injection had to be stopped after 1.17 pore volumes (3.5 hours) to avoid damaging the sandpack. The apparent viscosity should have been in the range of the viscosity of the gel solution (50 cp) if the permeabilities were constant and gelation had occurred. The data show that significant flow resistance develops in the pack with injection of gel solution much earlier than anticipated from gel time measurements in bottle tests.

From the figure it is seen that the rate of increase of the apparent viscosity is maximum in the fourth section. The plateaus for the first four sections were caused by over ranging of the transducers. The screen viscometer and microviscometer measurements conducted on batch samples are presented in Figure 5.9. The data didn't show any significant increase in the screen factor or the viscosity for the first 3.5 hours which corresponds to the injection of 1 PV. Thus this run showed that bottle tests weren't indicative of the behavior in the porous media.

The pack was allowed to sit in a water bath for 24 hours and attempts were made to inject water. Flow through the pack couldn't be established even at flow rates as low as 0.01 mL/min.

GEL INJECTION IN SP3

Based on the results from SP2, it was decided to see if higher sodium acetate concentration could increase the gel time in the porous media to allow injection without significant development of flow resistance. A gel solution similar to that injected in SP2, but with significantly higher sodium acetate concentration of 1.0m was injected in SP3.

Flow resistance in the sandpack during gelant injection are shown in Figure 5.10. The apparent viscosities increased as the polymer front displaced the resident brine solution and stabilized around 80 cp after 1 pore volume was injected. About 4 pore volumes were injected. The initial viscosity of this gel solution determined from bottle tests was around 50 cp at a shear rate of 11.25 per second. The bumps in the plots were due to minor malfunctions of the Cr(III) pump.

The pack was maintained at 25 °C in a water bath for about four months. Water was injected in the sandpack and the injected water fingered through at minimal pressure differentials indicating absence of any flow resistance due to gelation. Viscosity and screen factor measurements made on the bottle samples during this time are shown in Figure 5.11. No gelation of the bottle samples was observed during the 4 month period.

It was concluded that sodium acetate concentration used in this run delayed gelation in both bottle tests and the porous media.

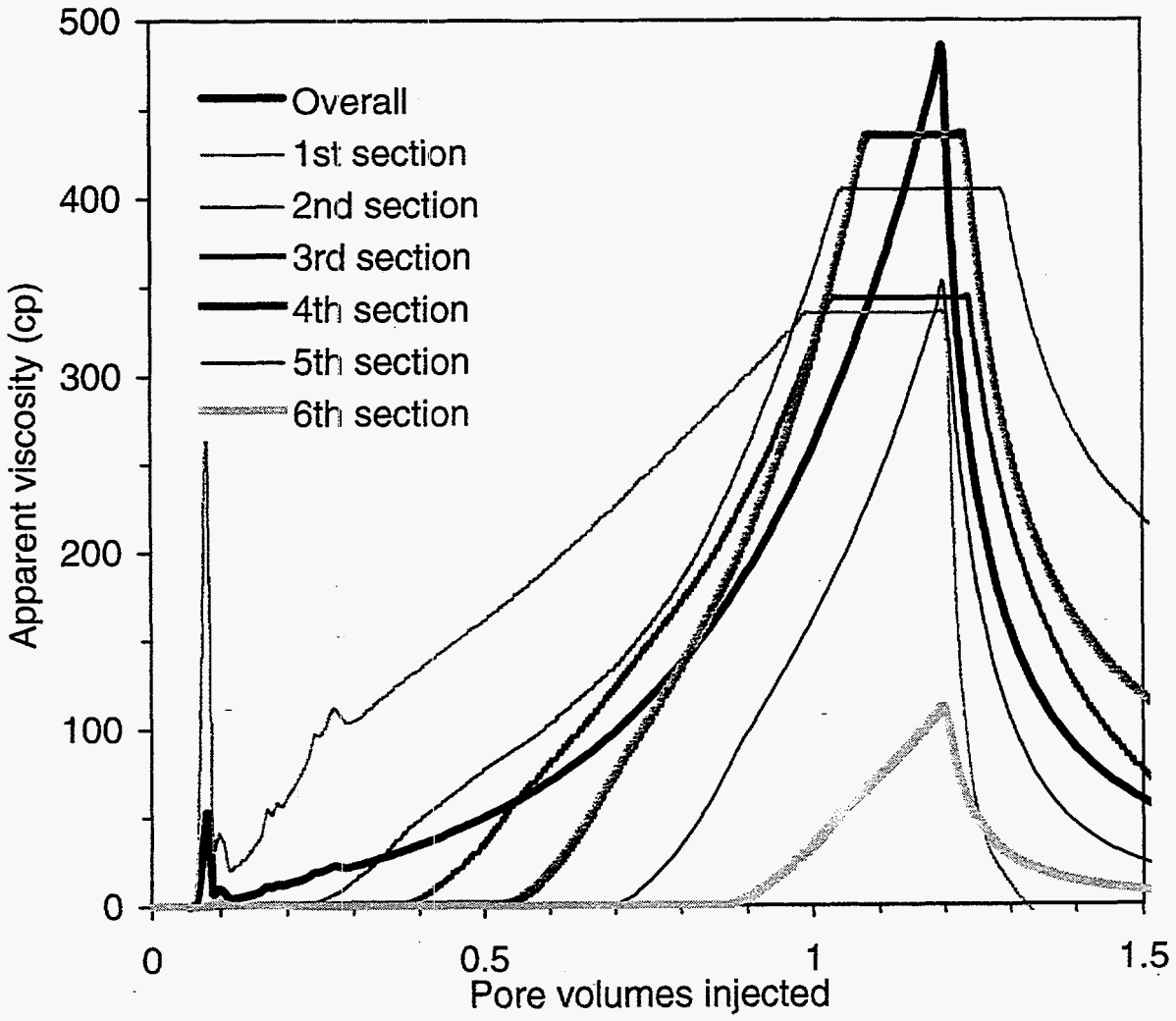

Figure 5.8 : Flow resistance during gel injection in SP2; Aged Cr(III) stock and sodium acetate conc. of 0.12 m.

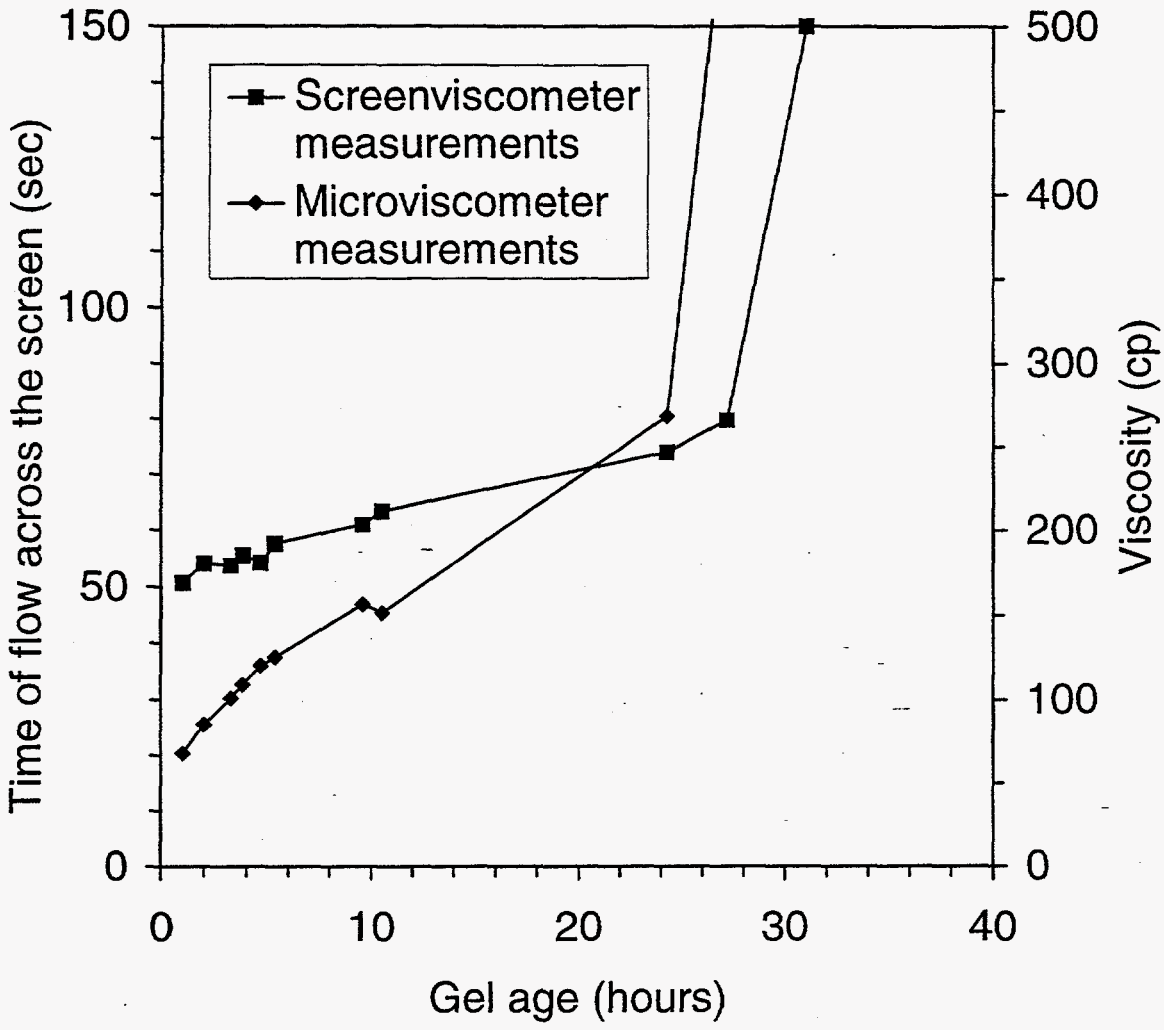

Figure 5.9: Screen viscometer data and viscosity for gel solution injected in SP2.

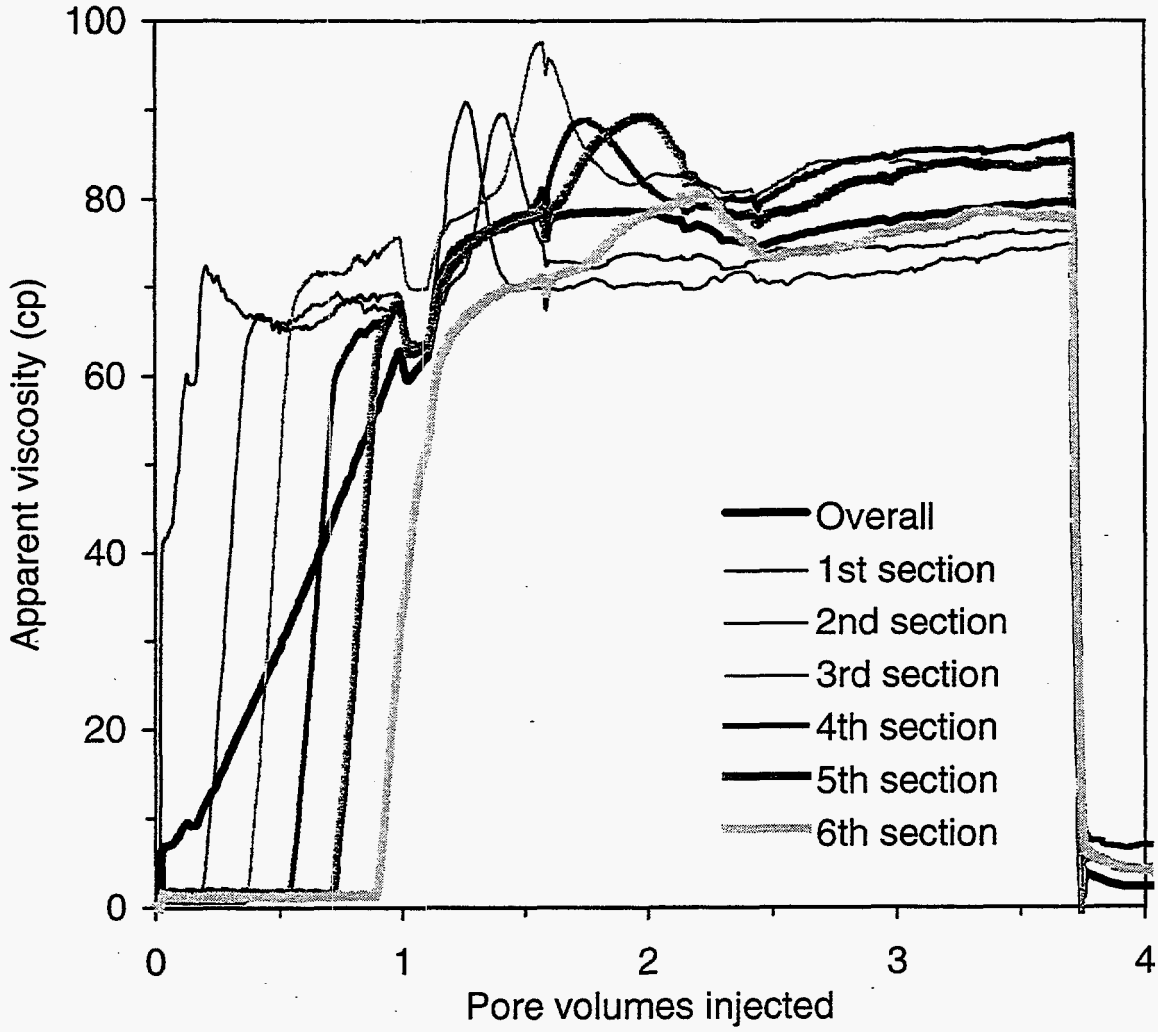

Figure 5.10: Flow resistance during gel injection in SP3; Aged Cr(III) stock and sodium acetate conc. of 1.0 m.

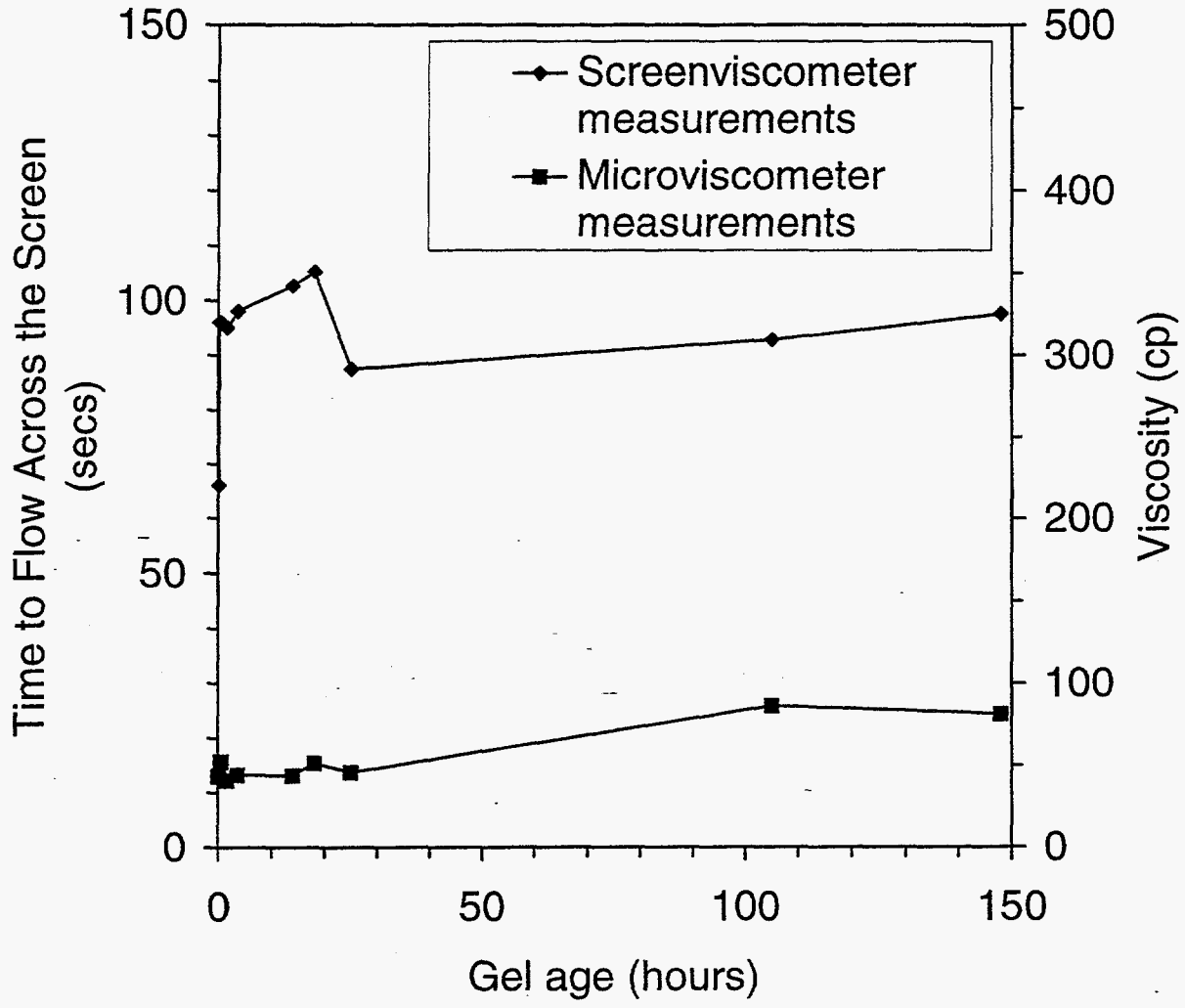

Figure 5.11: Screen viscometer data and viscosity for gel solution injected in SP3.

GEL SOLUTION INJECTION IN SP4

The crosslinker solution was aged approximately a month before injection in SP2 & SP3. The stock solution underwent a color change from green to purple. Literature[5] indicated that this was due to the hydration of the coordinated chromium ion. Aged crosslinker solutions were found to give lower gel times. Fresh chromium stock was used in SP3 and SP4.

A gel solution having containing 5000 PPM polymer, 100 PPM Cr(III) and 0.2 m sodium acetate was injected into SP4. The pH of the solution was maintained at approximately 5.0. The gel time of this sample was approximately 45 days.

Flow resistance in the sandpack during gelant injection are shown in Figure 5.12. The viscosity increased as the more viscous gel solution displaced the resident buffer. When about one pore volume was injected, sand was detected in the effluent solution. As more gel solution was injected, the sand washout became significant and the experiment had to be stopped. The pack was not disturbed and was left in the water bath for 45 days. Water was then injected to estimate the post gelation permeability. Water flowed easily at low pressure differentials due to the channels formed by the sand washout. After the pack was tapped and re packed, the post gelation injection behavior was similar to SP2, indicating the presence of a persistent gel in place.

GEL INJECTION IN SP5

A gel solution with 5000 PPM polymer, 100 PPM of fresh Cr(III) stock and 0.088 m sodium acetate was injected in SP5. The gel time of this sample in bottles was approximately 150 hours. Coarse sand was placed at the ends of the pack to avoid sand washout. This resulted in higher permeabilities in the first and last sections.

Flow resistance in the sandpack and its sections during gelant injection are shown in Figure 5.13. During the first pore volume of injection, a typical viscous displacement behavior was exhibited. As more gel solution was injected, the viscosities rose steady though not as rapidly as in SP2. As injection was continued, significant flow resistance developed in the last section. The apparent viscosities in this section are quite high despite the high permeability of this section. About 7 PVs were injected before shut-in. The screen viscometer and microviscometer measurements on the bottle samples of this gel are presented in Figure 5.14.

Attempts to inject brine into the sandpack after 8 days of shut-in were unsuccessful at a pressure drop 0f 100 psi. Thus complete reduction of the permeability was obtained.

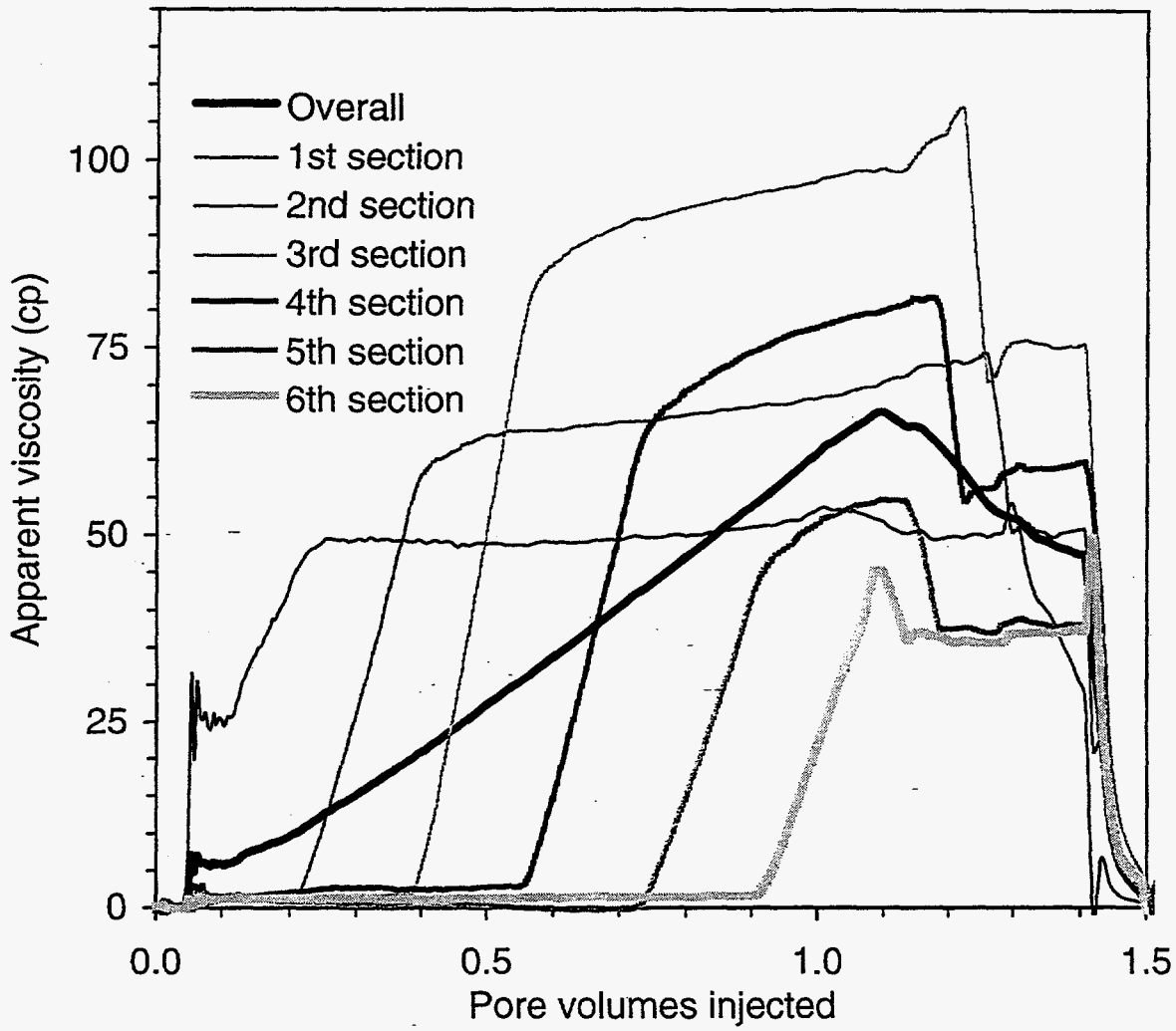

Figure 5.12 : Flow resistance during gel injection in SP4; Fresh Cr(III) stock and sodium acetate conc. of 0.2 m.

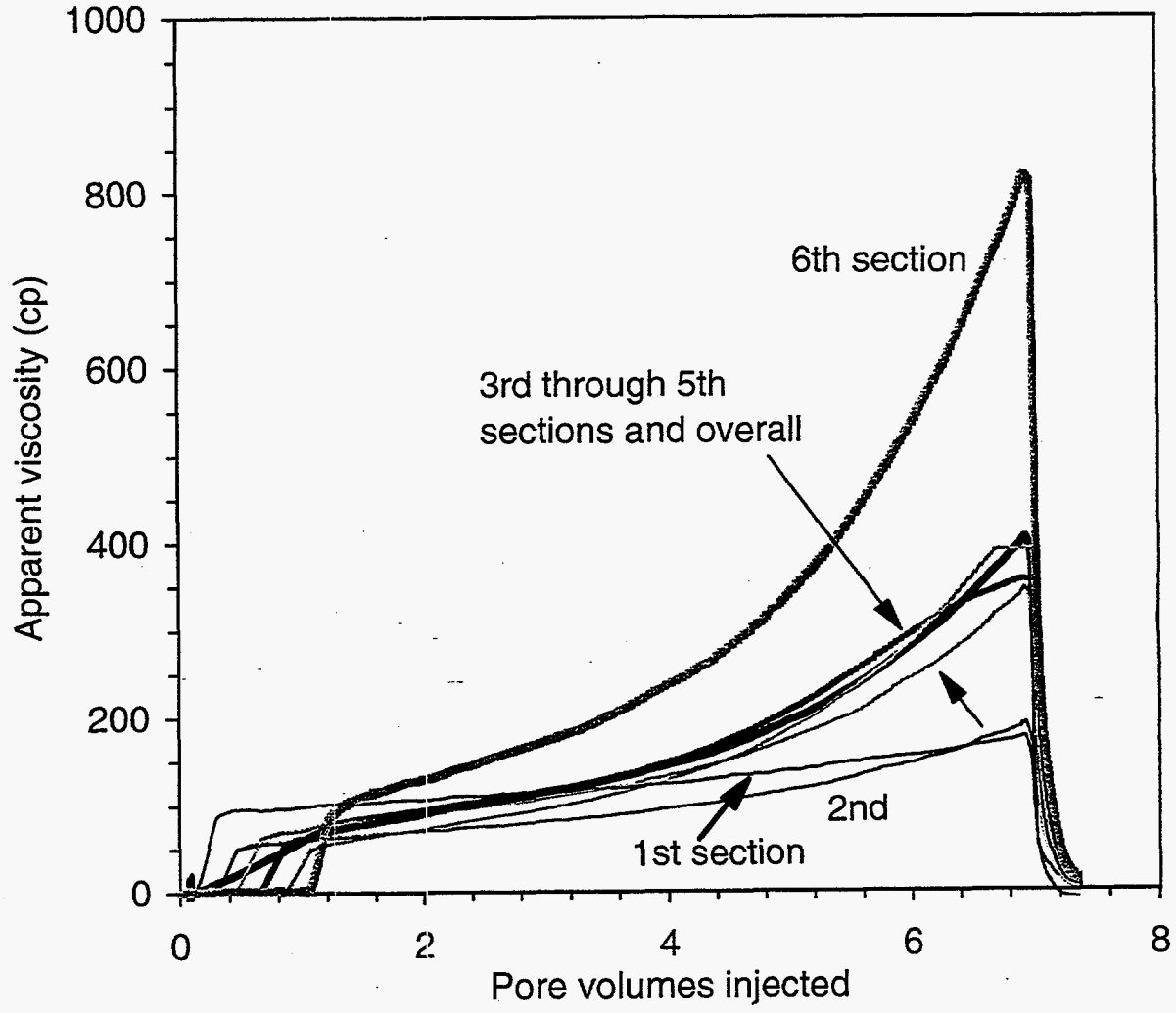

Figure 5.13 : Flow resistance during gel injection in SP5; Fresh Cr(III) stock and sodium acetate conc. of 0.088 m.

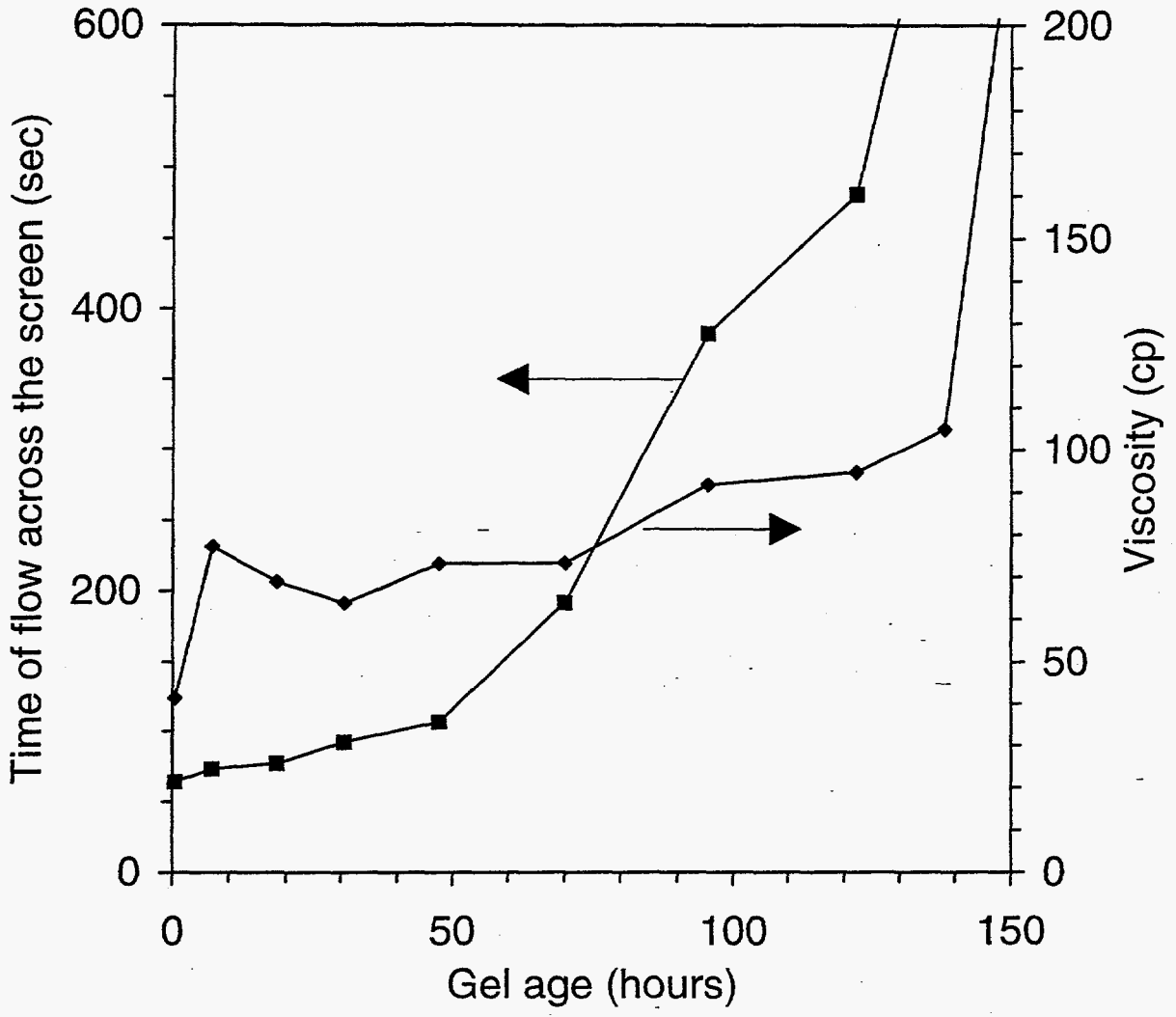

Figure 5.14: Screen viscometer data and viscosity for gel solution injected in SP5.

Summary

Bottle Tests.

1. Sodium acetate is effective in delaying gelation. Sufficiently high concentrations were found to delay gelation for more than 6 months at 25°C.
2. Depending upon the polymer used, there is a critical concentration of sodium acetate at which there is a significant increase in the gelation delay.
3. Degree of hydrolysis of the polymer, could not be used for scaling the concentrations of other reactants in the gel solution.
4. Aged chromium(III) acetate resulted in reduction of gel times.
5. Presence of sodium chloride in the PAAm - Cr(III) - sodium acetate system, reduced the gel times.

Sandpack Runs.

1. Sodium acetate delayed gelation in sandpacks were fresh chromium acetate stock solutions were used.
2. The results from the bottle tests do not correlate with the behavior in the porous medium. The time needed for the development of significant flow resistance in sandpacks was less than one fifth of the corresponding gel time of the solution in the bulk.
3. The gels formed are impermeable and persistent. Significant flow could not be established once gelation was complete.

Future Work

Determine if there exists a sodium acetate concentration that can be injected into the sandpack without the development of significant flow resistance and that will gel following a reasonable shut in period. The effect of sodium chloride on the gel time of the PAAm - Cr(III) - sodium acetate gel system will be studied in the porous media.

References

1. Lockhart, T.P., "Chemical and Structural Studies on Cr(III)/PAAm Gels," Paper SPE 20998 presented at the 1991 SPE International Symposium on Oilfield Chemistry, Anaheim, CA (February 20 -22).
2. Paola Albonico, Giovanni Burrafato, Alberto Di Lullo and T.P Lockhart., "Effective Gelation - Delaying Additives for Cr(III)/Polymer Gels," Paper SPE 25221 presented at the SPE International Symposium on Oilfield Chemistry, New Orleans, LA (March 2 - 5, 1993).
3. Lockhart, T.P, Paola Albonico., "A New Gelation Technology for In - Depth Placement of Cr(III) - Polymer Gels in High - Temperature Reservoirs," Paper SPE/DOE 24194 presented at the SPE/DOE Symposium for Enhanced Oil Recovery, Tulsa, OK (April 22 - 24, 1992).
4. Green D.W, Willhite G.P and Mark McGuire., "Improving Reservoir Conformance Using Gelled Polymer Systems," Annual Report, U.S. Department of Energy report # DOE/BC/14881-5, Chapter 5 (August 1994).
5. Hunt, J.A., "An Experimental Study of the Kinetics of the Crosslinking Reaction Between Chromium(III) and Polyacrylamide," Doctoral Dissertation, University of Kansas (1987).

Chapter 6

The Performance of the KUSP1-Boric Acid Gel System for Controlling Carbon Dioxide Mobility

Principal Investigators: S. Vossoughi, G.P. Willhite, and D.W.Green
Graduate Research Assistant: Koorosh Asghari

Introduction

Carbon dioxide miscible flooding is a proven method for improved oil recovery. However, there are major problems during the field applications of this technique. Because of the heterogeneity in the reservoir and the low viscosity of injected carbon dioxide, carbon dioxide tends to finger through the high permeability zones of reservoir. Consequently, that portion of the oil which is in low permeability zones of reservoir will not be recovered when applying carbon dioxide flooding.

Research has been conducted to develop methods to increase the overall efficiency of the carbon dioxide flooding processes by decreasing the unfavorable mobility ratio between carbon dioxide and oil. Examples of these methods are: (1) water-alternating-gas (WAG) process[1], (2)carbon dioxide-foam process[2], and (3)viscosified carbon dioxide process[3].

In-depth gel placement has been studied for years as a method for blocking the high-permeability thief zones in waterflooding processes. In this method, a gelant solution containing of polymer and crosslinker is injected into the reservoir. When the gelant is placed in the high permeable zones of reservoir and forms a rigid three dimensional gel structure, the permeability is reduced by factors of 100 or more. Injected water will flow through the lower permeability zones of reservoir and displace mobile oil.

In depth gels have been studied for carbon dioxide flooding process.[4,5] Xanthan gum polymer with Cr(III) as the crosslinker, a phenolic-based gel system, a vinyl-based gel, and polyacrylamide-Cr(III) gel systems have been tested for carbon dioxide applications. Results showed that gel systems based on polyacrylamide and xanthan were not as effective as phenol and vinyl-based gels.

Gel systems using alkaline solutions (pH=12) of KUSP1 biopolymer have been studied for applications to waterflooding.[6,7] In situ gelation was achieved by methods which reduce the pH of the polymer solution below 10.8. Direct CO_2 injection into the polymer solution and using an ester as a pH reducing agent were reported.[8] KUSP1 was also gelled by adding orthoboric acid. The mechanism by which orthoboric acid gels KUSP1 is different than by pH reduction. The gelation behavior of KUSP1-boric acid system was characterized.[9] By selection of boric acid concentration, and the solution pH, it is possible to obtain gelation times from several minutes to several days.

The objective of this study is to assess the performance of the KUSP1-boric acid gel system for application to the carbon dioxide flooding process. Work was conducted on the syneresis behavior of the KUSP1-boric acid gel system, the performance of the system in sandpack at low pressures, and in Berea cores using super critical carbon dioxide.

Syneresis Behavior of KUSP1-Boric acid Gel

Polymeric gels commonly used for profile modification of petroleum reservoirs are known to swell or to synerese when in contact with brine for a sufficient period of time.[10,11] Both swelling and syneresis can substantially change the volume and properties of a gel placed in formation and therefore affect the long term performance of a gel treatment.

The effect of temperature, pH of the gel-polymer solution, the type of aqueous environment, and the pH of the aqueous environment on the syneresis of KUSP1-boric acid gel was studied. The composition of the gel system was:

KUSP1 biopolymer	1% by weight
Sodium chloride	1% by weight
Orthoboric acid	0.5 mol/kg gel solution
Sodium hydroxide	1 N Solvent
pH of gel-polymer solution	9.8-10.5
Gelation time at 41 °C	~ 48 hours

To study the effect of temperature on the syneresis of this system, samples of the KUSP1-boric acid gel were prepared at a pH of 10.7 and maintained at temperatures of 27, 41, and 63 °C. Gel samples initially contained all the solvent and conformed to the shape of the bottle. As syneresis occurred, the gel shrank but retained the geometric shape of the bottle. Two sets of experiment were conducted.

1. ***Syneresis of original gel***: As a result of syneresis, the gels expelled brine. The expelled brine was removed from the bottles daily and the gel was weighed.
2. ***Syneresis in the presence of fresh brine***: About 20 mL of fresh 1% NaCl brine was added to each sample soon after the gel formed and before the onset of syneresis. The brine solution was removed, and the gel was weighed. Fresh 1% NaCl brine was added to the gel sample on a daily basis.

The syneresis of the KUSP1-boric acid gel system is shown in Figures 6.1, 6.2, and 6.3 for the temperatures of 27, 41, and 63 °C, respectively. These data show that the rate of syneresis and the final value of the gel syneresis increased with temperature and when the gel sample was brought into contact with fresh brine solution. The effect of contacting the gel sample with fresh brine diminshed with increasing temperature.

The large syneresis due to the contact with fresh brine solution raised the question that the introduction of fresh brine might have caused removal of boric ions from the gel. Therefore , an experiment was conducted to study the effect of three solutions on the syneresis of the gel. Gel samples were prepared at a pH of 10.7 and kept at 41 °C. The solutions studied were distilled water, 1.0 % NaCl brine and a 1.0 % NaCl brine containing 0.5 mol boric acid/kg solution. These

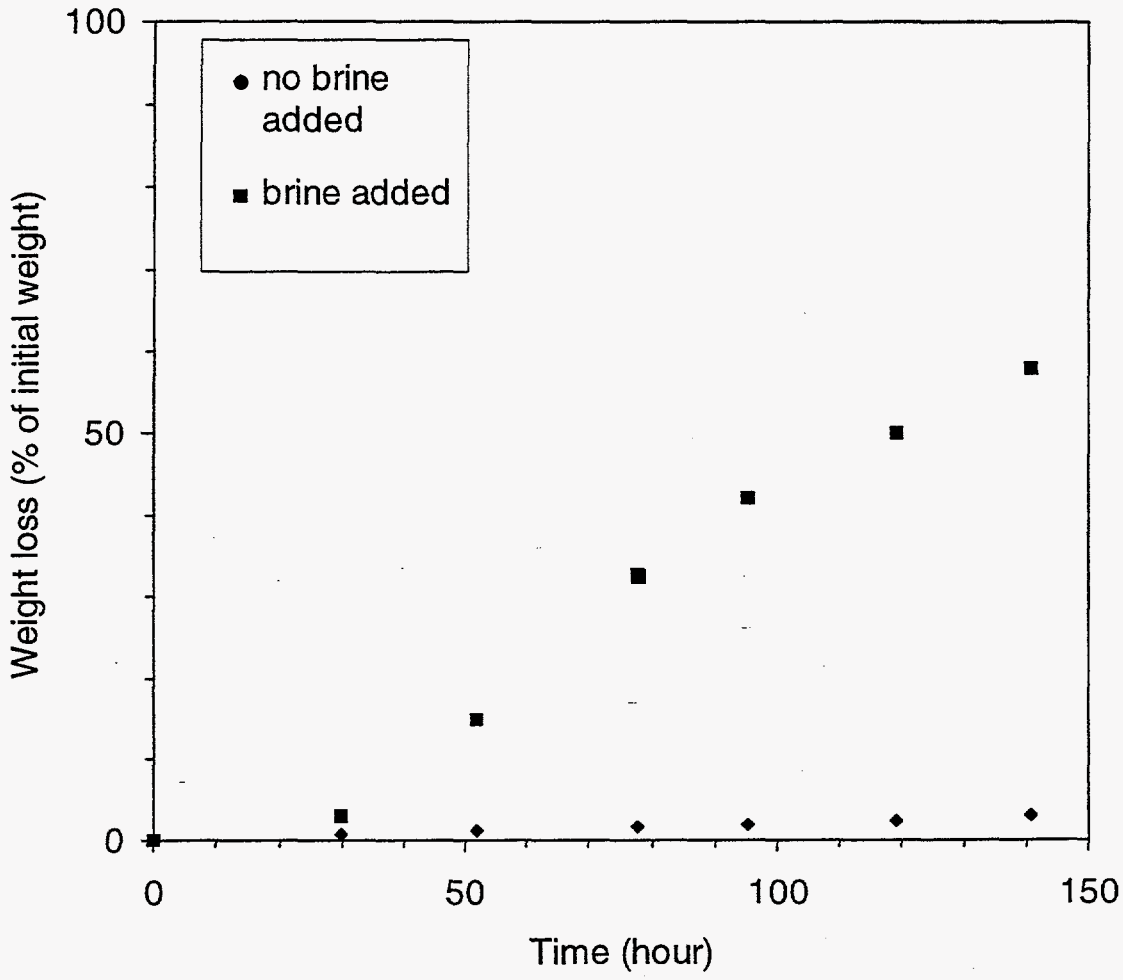

Figure 6.1 : KUSP1-boric acid syneresis at 27 °C

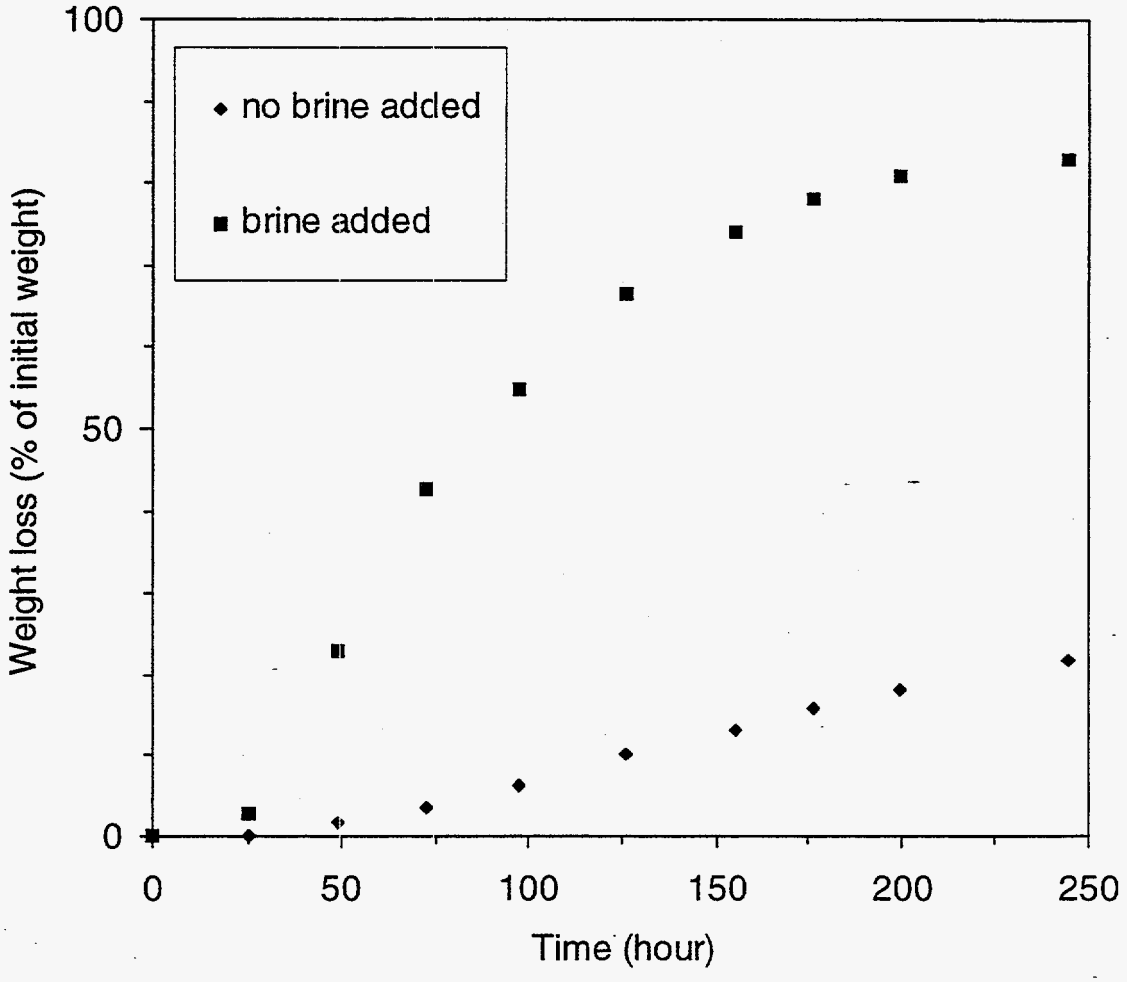

Figure 6.2 : KUSP1-boric acid syneresis at 41 °C

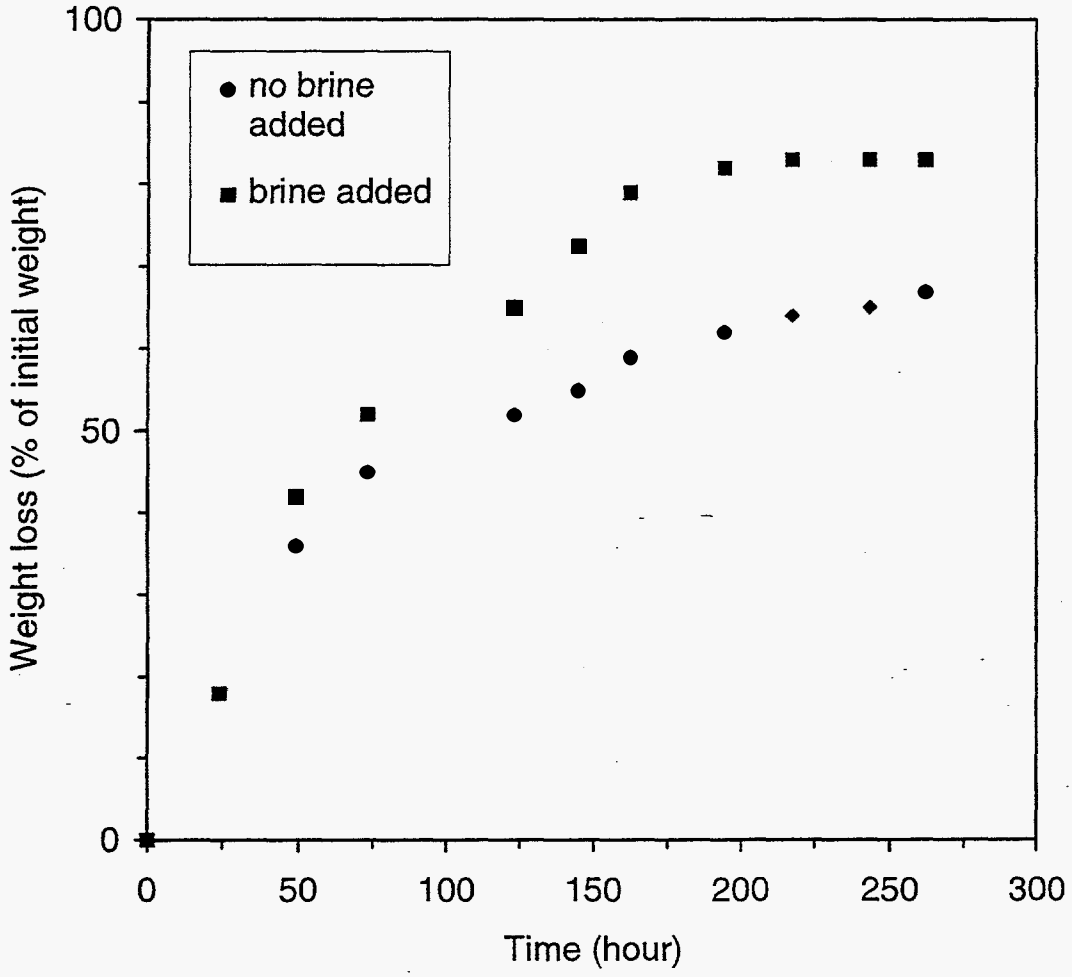

Figure 6.3 : KUSP1-boric acid syneresis at 63 °C

solutions were added to the formed gel and replaced daily with fresh solutions. The gels were weighed daily. The results of this experiment are shown in Figure 6.4 and show that the rate of syneresis for this gel was not dependent on the aqueous environment surrounding the gel.

Effect of the pH of gel solution on the rate of syneresis of KUSP1-boric acid gel was studied at 41 °C. The pH values of gelant samples were adjusted at 10.4, 10.02, and 9.69. Syneresis was measured by the method used for the brine-added experiments as discussed earlier. The pH of the added brine was about 7. The results of this experiment are presented in Figure 6.5, which shows that the gel sample made from gelants with pH=9.69 exhibit about 20% less syneresis than the sample made from gelant with pH=10.4.

The following conclusions were made From the above syneresis experiments:

1. KUSP1-boric acid gel systems synerese and lose up to 85% of initial weight of the gel.
2. Higher temperature increased the rate and final value of syneresis.
3. Subjecting the gel to an aqueous environment increased the rate of syneresis and the amount of syneresis.
4. The major effect of pH was observed after 100 hours at 41 °C, when The higher the pH of the gelant, the higher the rate of syneresis.
5. Syneresis of the KUSP1-boric acid gel was not significantly affected by the composition of the aqueous environment.

Flow Experiment in a Sandpack at Low Pressures

The objective of the sandpack flow experiments was to study the effect of syneresis on the permeability of a porous media treated with a KUSP1-boric acid gel system. A sandpack with a diameter of 3.5 cm and length of 23 cm was used for this experiment. The experiment was conducted at 41 °C and atmospheric pressure. Pressure differences along the sandpack were measured and used for the determination of permeability. A schematic diagram of experimental apparatus is shown in Figure 6.6.

The initial permeability and pore volume of the sandpack were about 4000 md and 85 mL, respectively. About 3 pore volumes of gelant (pH = 10.7) were injected into the sand pack. The sandpack was shut-in for about 72 hours. The gel time for samples of the effluent collected during gelant injection was about 36 hours.

After gel formed inside the sand pack, a 1% NaCl brine solution (at 0.1 mL/min) was injected into the gelled sand pack. Tracer tests were conducted in the gelled sandpack while continuously injecting brine at 0.1 mL/min, by changing the injected NaCl concentration from 1% to 1.5%. Effluent concentrations were determined by an in-line refractometer. The effective pore volume available for flow was calculated by integrating the effluent concentration data. Figure 6.7 shows the available volume for flow and the sandpack permeability changed as a function of the pore volumes of brine injected. The volume available for flow increased from about 6% to about 50% of the original pore volume by injecting about 35 pore volume of brine through the gelled sandpack. The increase in effective pore volume was indicative of the syneresis of KUSP1-boric acid gel in the sandpack. The permeability of the sandpack increased with the increase in effective

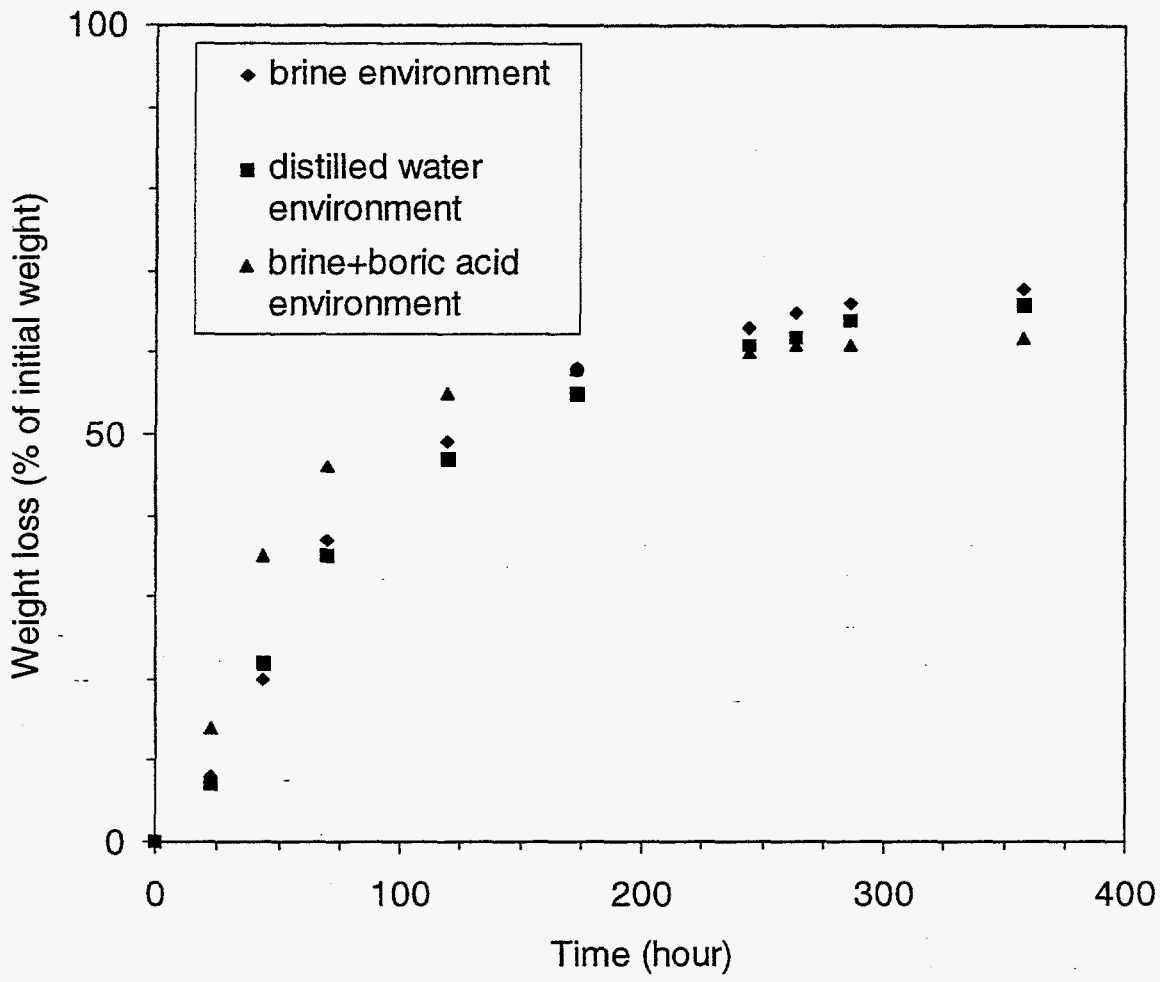

Figure 6.4 : Effect of different environments on the syneresis of KUSP1-boric acid gel, at 41 °C

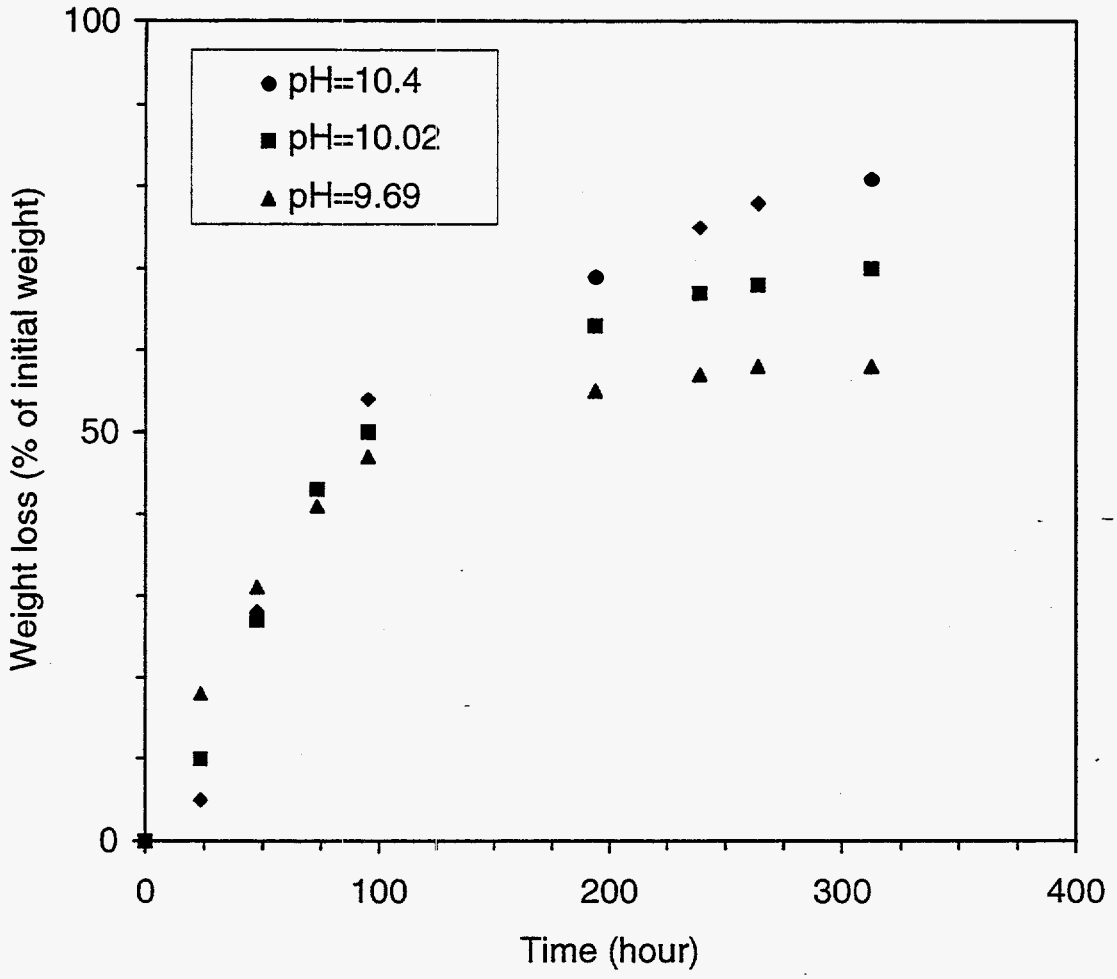

Figure 6.5 : Effect of the pH of the gelant on syneresis behavior of KUSP1-boric acid gel. Experiment conducted at 41 °C

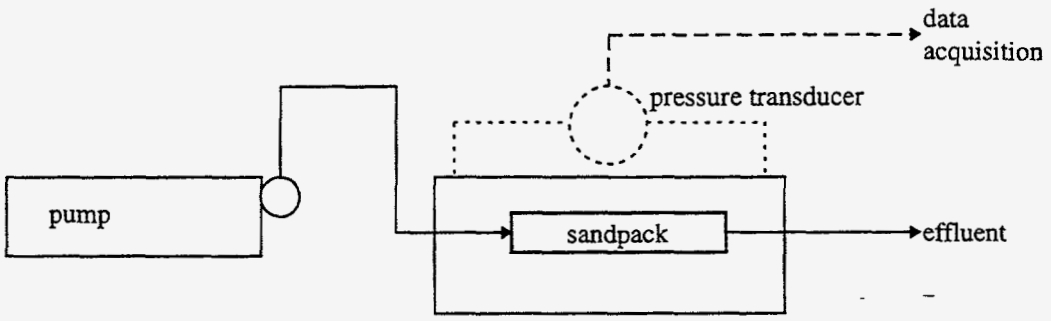

Figure 6.6 : Schematic diagram for the sand pack flow experiment.

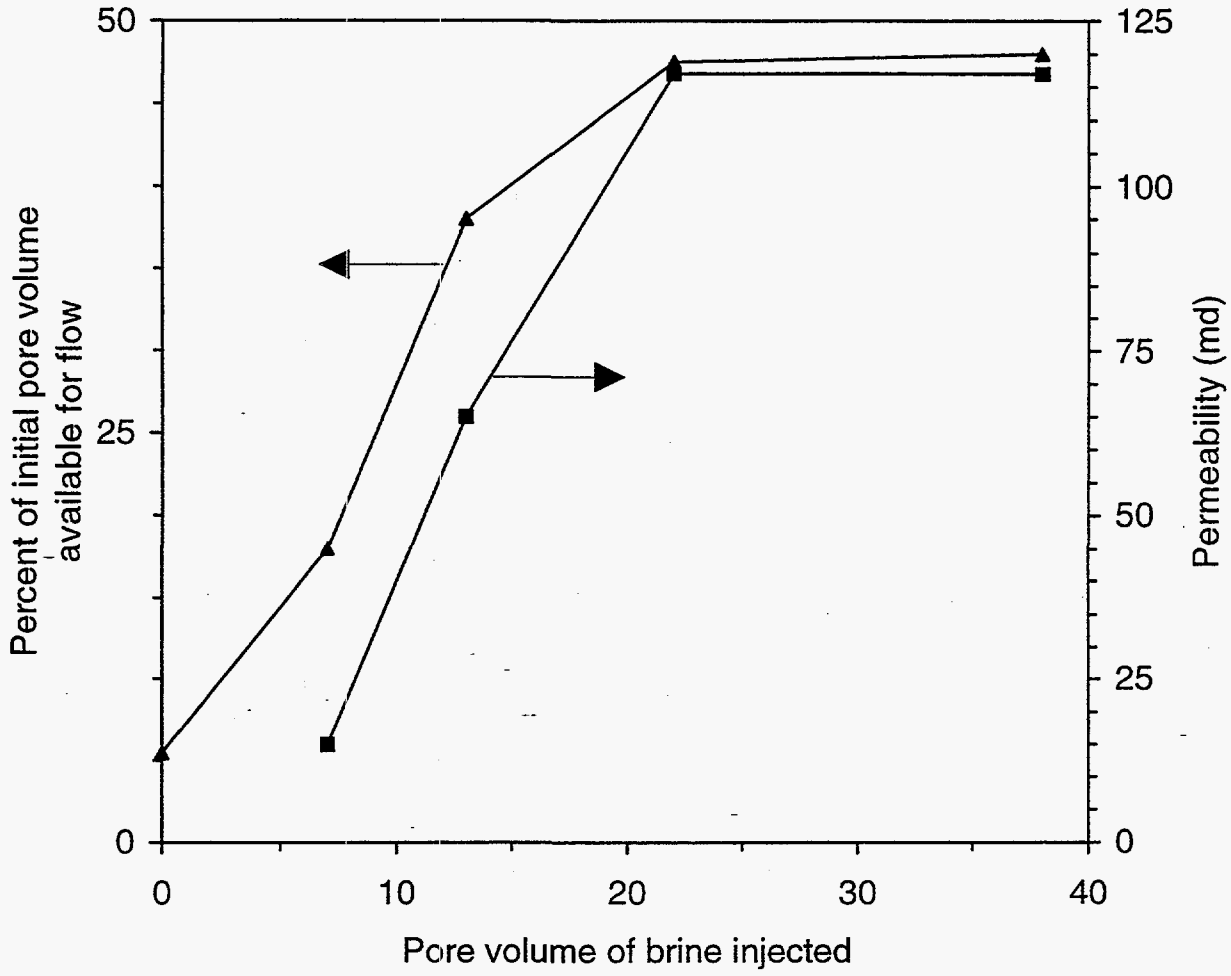

Figure 6.7 : Increase in available pore volume and permeability for flow in the gelled sand pack

pore volume but remained at low values as compared to the pre-treatment permeability. The residual resistance factor after syneresis was about 34.

Flow Experiment in Berea Core at High Pressures

The objective of this experiment was to investigate the performance of a KUSP1-boric acid gel in a Berea sandstone core at conditions similar to reservoirs that are candidates for carbon dioxide flooding. A Berea core with a diameter of 5 cm and a length of 30 cm was used. Experiments were conducted at 41 °C. A schematic diagram of the experimental apparatus is shown in Figure 6.8. A high-pressure core holder with a back-pressure regulator were used to maintain the outlet pressure at 1200 psi. Transducers were connected to the core holder to measure the pressure drops across four sections of the core. The first and fourth sections were 5 cm long, and the second and third sections were 10 cm long.

The flow experiment was conducted in the following sequences:

1. Measure the initial brine permeability in the core.
2. Displace brine with carbon dioxide to a residual saturation and measure the initial permeability of carbon dioxide in the core in presence of the residual brine saturation
3. Displace carbon dioxide with brine and measure the brine permeability in presence of residual carbon dioxide in the core.
4. Inject several pore volumes gelant into the core.
5. Wash the inlet and outlet tubes and shut-in the core for sufficient time for gelation.
6. Inject brine into the core and determine the brine permeability and the residual resistance of the gelled core.
7. Increase the core pressure to 1200 psi.
8. Inject carbon dioxide into the gelled core and determine carbon dioxide permeability and the residual resistance factor for carbon dioxide.
9. Inject brine into the gelled core and determine brine permeability and the residual resistance factor for brine.
10. Repeat steps 8 and 9.

The initial pore volume and porosity of the core were measured gravimetrically as 133.8 mL and 22%, respectively. Initial permeabilities of each section and the total core length are presented in Table 6.1.

Table 6.1 : Initial brine permeability for different sections of the core.

core section	1	2	3	4	overall
brine permeability (md)	395	605	576	475	518
brine permeability (md) at CO_2 residual saturation	370	514	516	440	420

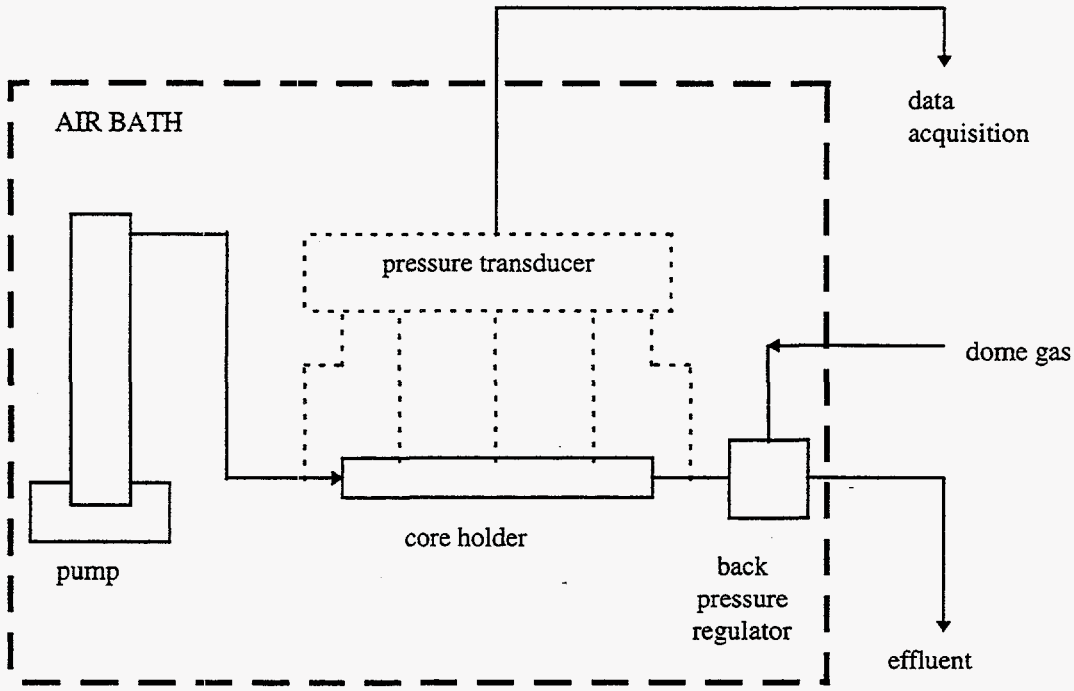

Figure 6.8 : Schematic diagram for the core flow experiment.

Carbon dioxide was injected through the core at a back pressure of 1200 psi and a temperature of 41 °C until no water was produced. The overall permeability to carbon dioxide at residual water saturation was 163 md.

Before injecting the gelant into the core, a filter test was conducted to study the possibility of frontal loading phenomenon during injecting KUSP1-boric acid solution into the core. Three 5-micron filters were connected in series as shown in Figure 6.9. Pressure drops across each filter was measured. A KUSP1-boric acid solution was prepared and injected through the filter apparatus at 6 mL/min. Pressure difference across the second and third filters remained almost constant at 1 psi while the pressure difference across the first filter increased to values as high as 11 psi. This experiment indicated that frontal loading would occur if the gel-polymer solution was not filtered prior to injection into the core.

About 600 mL of gelant (pH adjusted at 11) was prepared and filtered through a 5-micron filter. The viscosity of the polymer solution was 3.72 cp. About 3 pore volumes of the gelant was injected through the core at 10 mL/min. The effluent pH was monitored and is shown in Figure 6.10. The effluent pH was about 6 as the residual brine was displaced from the sandpack. The effluent pH then increased to about 11 as the gelant exited the core.

After injecting 3 pore volumes of gelant into the core, the inlet and outlet tubing of the core were purged and the core was shut in. Samples of the effluent and the injected gelant formed gels after about 48 hours. The core holder was shut-in for four days.

1% NaCl brine at 0.07 mL/min was injected into the gelled core. The pressure behavior of the sections of the core during brine injection are shown in Figure 6.11. For all sections of the core, the pressure differences increase to a maximum and then decrease. The maximum pressure drop for the first section of the core was much less than the other sections. The pressure drop maxima occur first in section one, followed by section two, then section three, and finally section four. Based on this behavior, a hypothesis is made that during injecting brine into the gelled core, channels are formed and the onset of the pressure drop decrease is caused by the formation of these channels. Channels are formed initially in section one where the brine enters the core, then by the continued brine injection, channels are formed in section two, three and so on. Table 6.2 shows the permeability and the residual resistance factor (RRF) of different sections of the gelled core at the maximum pressure difference condition.

Table 6.2 : Permeability and residual resistance factors(RRF) at maximum pressure difference during the initial brine injection into the gelled core.

core sections	1	2	3	4	overall
final k(md)	1.4	0.445	0.249	0.235	0.31
RRF	324.5	1155	2072	1872	1355

Brine injection at 0.07 mL/min was continued until 4.4 pore volume of brine was injected into the core. The permeability of different sections and the residual resistance factor (RRF) of the core at 4.4 pore volumes injected are given in Table 6.3.

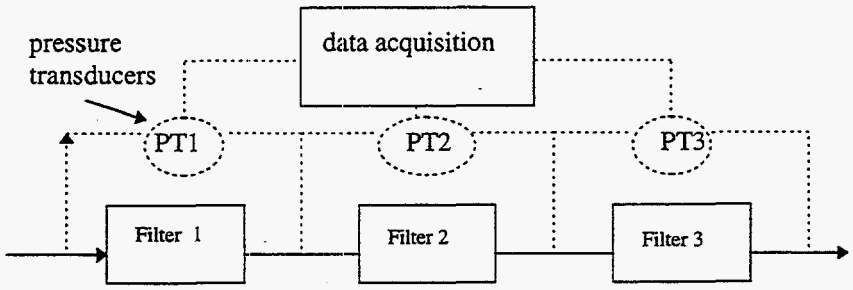

Figure 6.9 : Filter set-up for the filtration test.

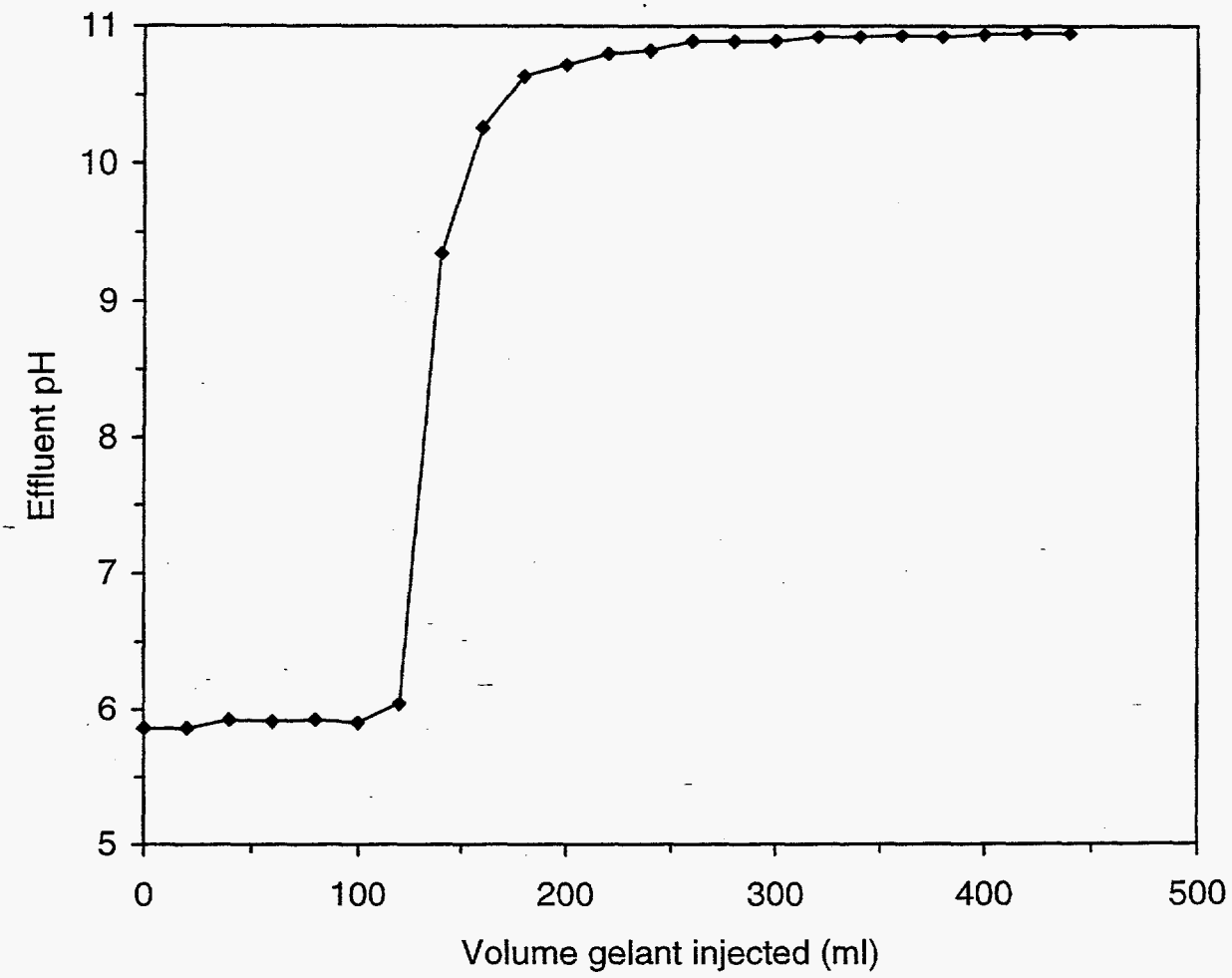

Figure 6.10 : Core effluent pH change during injecting KUSP1-boric acid solution into the core

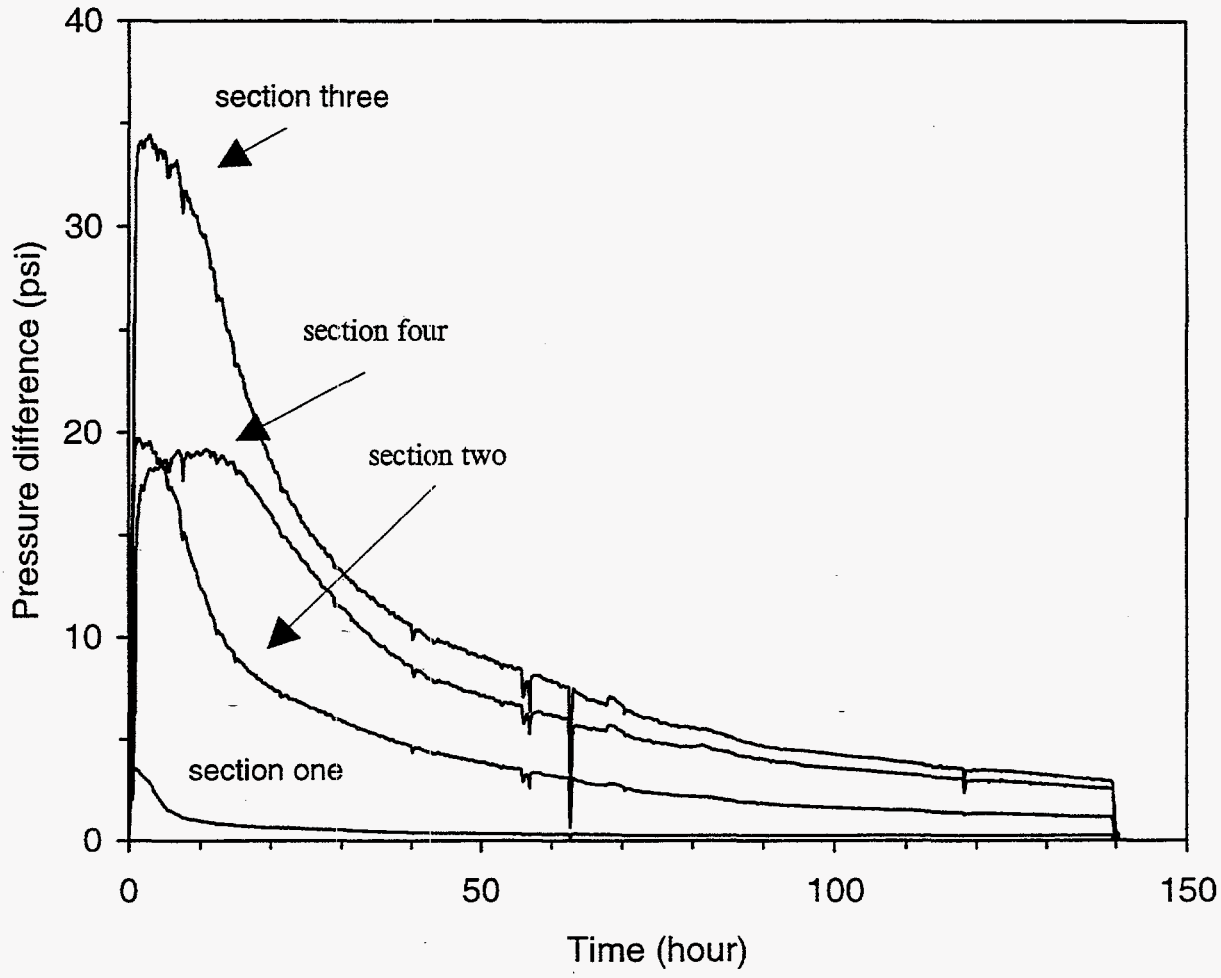

Figure 6.11 : Pressure variations in different sections of the gelled core during brine injection

Table 6.3 : Brine permeability and residual resistance factor (RRF) in the gelled core after injecting 4.4 pore volume brine into the gelled core.

core sections	1	2	3	4	overall
final k(md)	17.5	7.73	3.13	1.76	3.47
RRF	21.1	66.5	164.8	250	121

Brine injection rate was increased to 0.1 mL/min and 5 pore volumes of brine were injected into the gelled core. Permeability of the core sections after the 9.4 pore volumes of brine were injected are given in Table 6.4.

Table 6.4 : Brine permeability and residual resistance factor (RRF) in the gelled core after injecting 9.4 pore volumes of brine.

core sections	1	2	3	4	overall
final k(md)	27.6	11	6.4	4.8	7.14
RRF	13.4	46.3	80.6	91.7	58.8

Comparison of the values given in Tables 6.2 to 6.4 shows that the permeability of core increased with brine injection.

In order to study the effect of high pressure on the permeability of the gelled core, the core pressure was increased to 1200 psi and one pore volume of brine was injected into the core at 0.1 mL/min. The core permeability and the residual resistance factor (RRF) for this case are given in Table 6.5.

Table 6.5 : Brine permeability and residual resistance factor (RRF) in the gelled core at 1200 psi.

core sections	1	2	3	4	overall
final k(md)	11	17	13	17	12.5
RRF	33.6	30.2	39.7	23.5	33.6

The core pressure was reduced to the atmospheric pressure and brine injection was continued until 16.5 pore volumes of brine. The overall permeability of the gelled core was approximately constant at 15 md, much lower than the initial permeability of the core. The overall residual resistance factor was 28 at this time. Therefore, it was concluded that the KUSP1-boric acid gel system significantly reduced the permeability of the Berea sandstone core and was stable under the prolonged injection period of brine.

In order to investigate the performance of the KUSP1-boric acid gel during carbon dioxide flooding, water and carbon dioxide were injected alternately into the gelled core. About 20 pore volumes of carbon dioxide were injected into the core followed by the injection of about 20 pore volumes of brine. This cycle was repeated four times. This experiment was conducted at a back pressure of 1200 psi and a temperature of 41 °C.

The permeability to the injected fluid was determined after the pressure drops across the core became stable. A significant increase in the permeability of the gelled core occurred when carbon dioxide was first introduced into the gelled core. The overall permeability of the gelled core to brine which was about 15 md before carbon dioxide injection and increased to about 70 md after injecting carbon dioxide. Table 6.6 summarizes the permeability to carbon dioxide and brine for the four cycles.

Table 6.6 : Permeability and residual resistance factors of the gelled core to carbon dioxide and brine for different cycles.

INITIAL PERM. (md)		OVERALL CORE PERMEABILITY (md)							
		CYCLE ONE		CYCLE TWO		CYCLE THREE		CYCLE FOUR	
CO2	brine	CO2	Brine	CO2	brine	CO2	brine	CO2	brine
164	420	19	68	18	71	17	85	26	90
		OVERALL CORE RESIDUAL RESISTANCE FACTOR							
		8.6	6	9	6	9.5	5	6.3	4.7

The permeability of the gelled core to carbon dioxide remained almost constant during three WAG cycles where about 80 pore volumes of each fluid were injected but increased during the fourth WAG cycle. Permeability to brine increased continually during each cycle. The residual resistance factors for brine and carbon dioxide are given in Table 6.6. The low residual resistance factors (compared to those reported in Tables 6.2 to 6.4) indicated that the KUSP1-boric acid gel system lost part of its effectiveness as a blocking agent for brine after the core was subjected to carbon dioxide flooding.

Summary

Based on different sets of experiments conducted for characterizing KUSP1-boric acid gel system, the following conclusions are made:

1. This gel system shows a very strong syneresis behavior when exposed to the brine used to prepare the gel. The rate of syneresis is increased with increasing temperature, boric acid content, and decreasing pH.
2. Syneresis of KUSP1-boric acid gel leads to an increase in pore volume available for flow and an increase in the gelled core permeability with continued injection.
3. Prior to injecting carbon dioxide into the core, KUSP1-boric acid showed a large reduction in permeability for brine.
4. The gel reduces the brine permeability in the porous media regardless of the significant level of syneresis that happens to the gel.
5. After injecting carbon dioxide into the gelled core for four WAG cycles, the residual resistance factor was 4.7 for the flow of brine and 6.3 for supercritical carbon dioxide.

References

1. Jenkins, M.K., "An Analytical Model for Water/Gas Miscible Displacement," SPE/DOE paper 12632, presented at the SPE/DOE Forth Symposium on Enhanced Oil Recovery, Tulsa, OK (April 15-18, 1984).
2. Wang, G.C., "A Laboratory Study of CO_2 Foam Properties and Displacement Mechanism," SPE/DOE paper 12645, presented at the SPE/DOE Forth Symposium on Enhanced Oil Recovery,Tulsa, OK (April 15-18, 1984).
3. Bae, J.H., "Viscosified CO_2 Process: Chemical Transport and Other Issues," SPE paper 28950, presented at the SPE International Symposium on Oilfield Chemistry, San Antonio, TX, (14-17 February 1995).
4. Martin, F.D., and Kovarik, F.S., "Chemical Gels for Diverting CO_2: Baseline Experiments," SPE paper 16271, presented at the 62nd Annual Technical Conference and Exhibition of the Society of Petroleum Engineers, Dallas, TX (September 27-30, 1987).
5. Martin, F.D., and Kovarik, F.S., "Gels for CO_2 Profile Modification," SPE/DOE paper 17330, presented at the SPE/DOE Enhanced Oil Recovery Symposium, Tulsa, OK (April 17-20, 1988).
6. Buller, C. S., and Vossoughi, S., "Subterranean Permeability Modification by Using Microbial Polysaccharide Polymers," U.S. Patent No. 4,941,533 (July 17, 1990).
7. Vossoughi, S., and Buller, C.S., "Permeability Modification by In Situ Gelation with a Newly Discovered Biopolymer," *SPERE* (November 1991) 485-489.
8. Vossoughi, S., Green, D.W., Willhite, G.P., Raje, M., and Asghari, K., "Gel Systems for Controlling CO_2 Mobility in Carbon Dioxide Miscible Flooding," Chapter 7 in "Improving Reservoir Conformance Using Gelled Polymer Systems" Annual Report for the Period September 25, 1994 to September 24, 1995, Chapter 7, DOE contract no. DE-AC22-92BC14881, report no. DOE/BC/14881-18, The University of Kansas.
9. Willhite, G.P., and Green, D.W., " Improving Reservoir Conformance Using Gelled Polymer Systems", Annual Report for the Period September 25, 1994 to September 24, 1995, DOE contract no. DE-AC22-92BC14881, report no. DOE/BC/14881-18, The University of Kansas.
10. Gales, J.R., Young, T.S., Willhite, G.P., and Green, D.W., "Equilibrium Swelling and Syneresis Properties of Xanthan Gum-Cr(III) Gels," SPE/DOE paper 17328, presented at SPE/DOE Enhanced Oil Recovery Symposium, Tulsa, OK (April 17-20, 1988).
11. Young, T.S., Green, D.W., Willhite, G.P., and Gales, J., "Stability and Properties of Gels and Polymers," Second Annual Report for the Period October 1986 to September 1987, DOE contract no. AC19-85BC10843, report no. DOE/BC/10834-10, The University of Kansas.

Chapter 7

Gel Treatments in Production Wells

Principal investigators: G.P. Willhite, D.W. Green and C.S. McCool
Graduate research assistant: Zhongchun Yan

Introduction

A successful application of a gel treatment to a production well usually requires that the treatment sharply reduce the water relative permeability while minimally affecting the oil relative permeability. Several researchers [1,2,3] have proposed a number of different mechanisms for the disproportionate permeability reduction although no specific mechanism is widely recognized as the cause.

This investigation is being conducted to determine the mechanisms responsible for disproportionate permeability reduction. Guidelines and gel parameters for application of gelled polymer systems for water control in production wells will be formulated from the results of this study.

The primary experimental data for this investigation are the relative permeabilities to oil and water before and after a gel treatment and the water saturations profiles along a core slab. In situ saturations were determined using microwave measurements during displacements. These data will be used to elucidate the mechanisms of disproportionate permeability reduction.

Experimental

The gelant formulation used contains 5000ppm polyacrylamide (Alcoflood 935), 1500ppm thiourea, 600ppm sodium dichromate and 2.0% NaCl. This system was selected from several series of bottle tests that were conducted to determine gel times. Viscosity of aliquots of samples was measured as a function of time. Gel times were defined as the time when the viscosity rapidly increased to values greater than 500 cp.

Flow experiments are conducted in Berea sandstone slabs (10.52 cm wide, 1.74 cm thick, 61.1 cm long) that were coated with epoxy. Pressure was limited to 80 psig in the slab. Three pressure taps spaced along the core segmented the slab into four equal length sections. Sections were labeled from 1 to 4. A schematic diagram for flow experiments using brine and/or oil is shown in Figure 7.1. Dodecane and 2.0% NaCl brine were the oil-water pair. Oil and water are separated in the effluent and collected in two graduated cylinders.

Water saturations in the core were determined using the microwave scanning equipment as shown in Figure 7.2. Power loss through the core slab is directly proportion to the water saturation in the core.[5] The microwave apparatus scans the core length and focuses the measurement on a one inch diameter area in the center of the core width. Scans were conducted at selected times to determine water saturation as a function of length. Gelant and/or gel were not distinguishable from brine and were detected as water saturation.

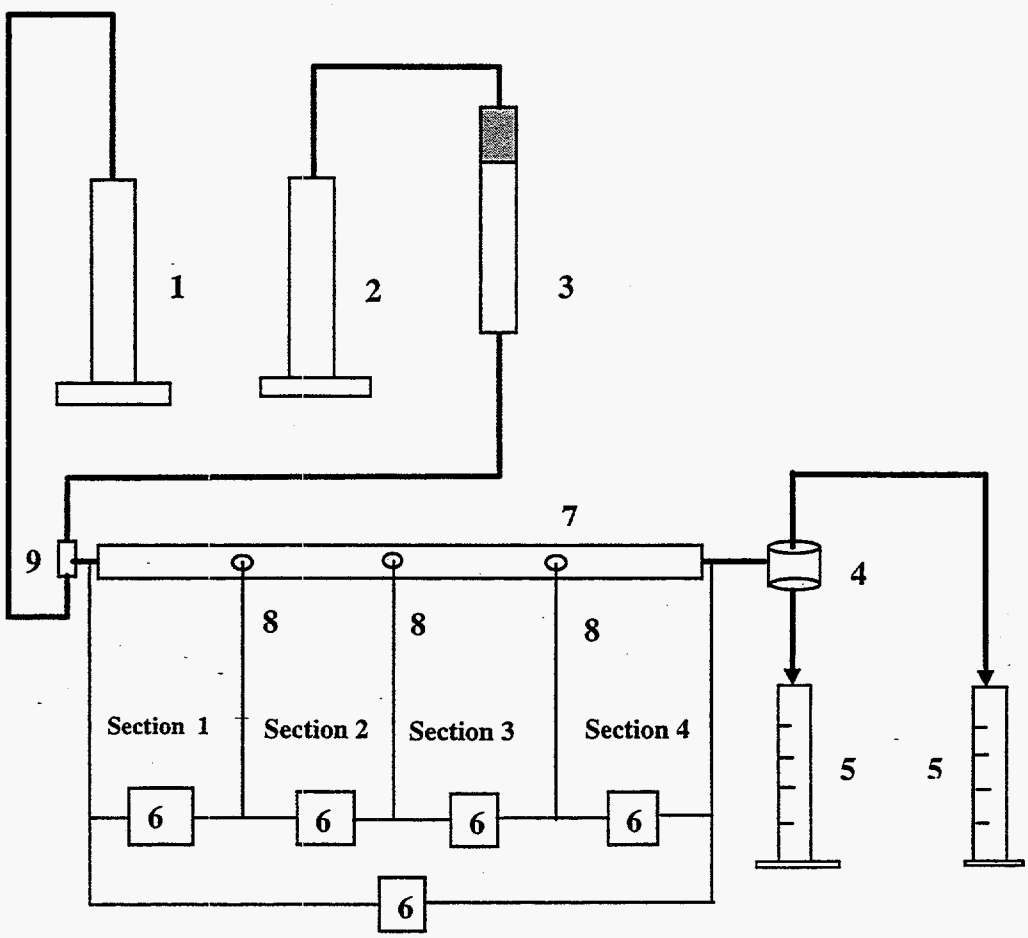

1. Oil pump
2. Water pump
3. Transfer cylinder
4. Water/oil separator
5. Graduated cylinders
6. Pressure transducers
7. Berea sandstone slab
8. Pressure taps
9. T-joint

Figure 7.1 : Schematic diagram of apparatus for flow experiments.

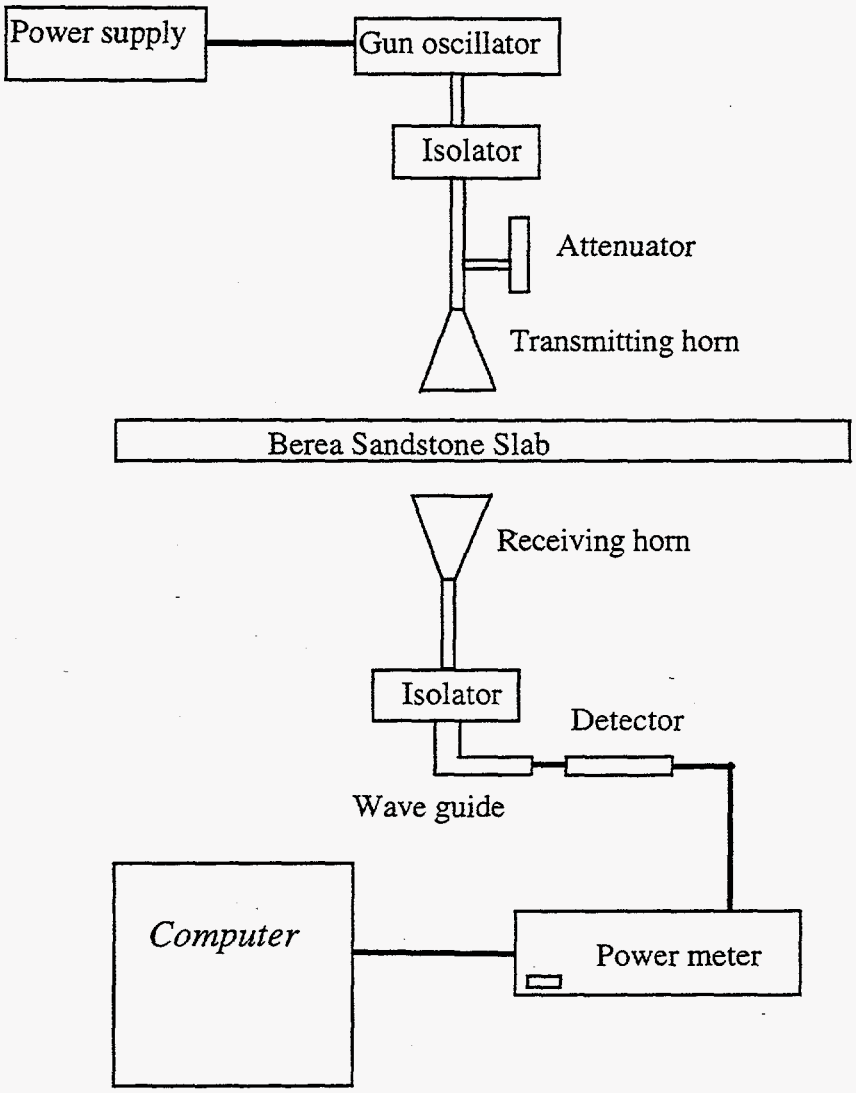

Figure 7.2 : Schematic diagram of microwave apparatus for determining in situ water saturations.

Calibration of the microwave data was achieved by scanning the core slab dry, fully brine saturated and after the initial oil and brine floods. Material balances were measured for the influent and effluent materials. The porosity of the slab was determined by weighing the core before and after brine saturation. Initial permeabilities of the core and individual sections were determined at 100 % brine saturation.

Fluids were injected into the core slab from both directions to simulate the flow directions during a treatment in a production well. Direction #1 (into Section 1) simulated the flow from the formation into the well and direction #2 (into Section 4) simulated the injection of fluids (gelant) into the formation from the well.

Relative permeability curves for oil and brine were determined prior to and after the gel treatment. Dodecane and/or 2.0% NaCl brine were injected from direction #1 at selected fractional flows of brine until steady-state was reached. In situ water saturations were determined from the microwave scans and the overall water saturations were determined from material balance. Permeabilities were determined for the total core length and the individual sections after the flow had reached steady-state. Relative permeability curves were determined for both increasing and decreasing water saturations.

Results and Discussion

Bottle Tests. The results of the bottle tests are given in Table 7.1. Criteria for selection of the gel system were a viscosity that was stable for 20 hours and a sufficient gel strength, i.e. the gel would not exit a 60 ml bottle upon inversion. The gel time was selected to allowed sufficient time for gelant injection without significant development of flow resistance. No pH adjustment was necessary for the selected system. Viscosity as a function of time for the selected system is shown Figure 7.3.

Displacement Experiments. Relative permeability curves for the drainage (water saturation decreasing) and imbibition (water saturation increasing) cycles were determined for the entire core slab and for the four sections and are shown in Figures 7.4 through 7.8. Some hysteresis in the curves was observed. The end-points at the residual oil saturation did not coincide. Injection of fluids for these experiments were from direction #1. Direction #1 is from the left, or zero side, of the core length in figures showing water saturation profiles in the slab.

Water saturations in the slab were measured several times during each experiment at the selected fractional flow. Water saturation profiles, at steady state and during the drainage cycle, for several fractional flows are shown in Figure 7.9. Most of the saturation change occurred at high oil cuts.

To prepare for gelant injection, the slab was injected with oil and water at a 60% fractional flow of water until steady-state was reached. This was done at increasing water-saturation mode and in direction #1. 0.144 pore volumes of gelant were then injected in direction #2 over 27.5 hours. 0.144 pore volumes correspond to the water saturation at residual oil in one quarter of the slab length. An overflush of 0.20 pore volumes of dodecane immediately followed gelant injection, again in direction #2. The slab was shut-in for 8 days to allow for gelation.

Table 7.1 : Gel times and strengths of gelants.

Thiourea Concentration	Sodium Dichromate	Initial PH	Stable Period* (hours)	Sufficient strength? **
1500ppm	400ppm	5.31 (not adjusted)	24	No
		=>4.82***	20	Yes
		=>4.49	12	Yes
		=>4.17	8	Yes
	600ppm	5.19 (not adjusted)	24	Yes
		=>4.80	16	Yes
		=>4.51	12	Yes
		=>4.19	8	Yes
	800ppm	5.15 (not adjusted)	16	Yes
		=>4.81	12	Yes
		=>4.50	8	Yes
		=>4.18	4	Yes
2000ppm	400ppm	5.21 (not adjusted)	23	No
		=>4.81	18	Yes
		=>4.49	14	Yes
		=>4.18	14	Yes
	600ppm	5.17 (not adjusted)	23	Yes
		=>4.82	14.7	Yes
		=>4.52	14.7	Yes
		=>4.814.12	4	Yes
	800ppm	5.10 (not adjusted)	18	Yes
		=>4.80	13.5	Yes
		=>4.50	9	Yes
		=>4.20	4	Yes

* No significant viscosity increase during time period.

** Strength is sufficient when 50 ml of gel will not exit a 60 ml jar upon inversion a couple days after the gel time.

*** Initial pH of solution was adjusted.

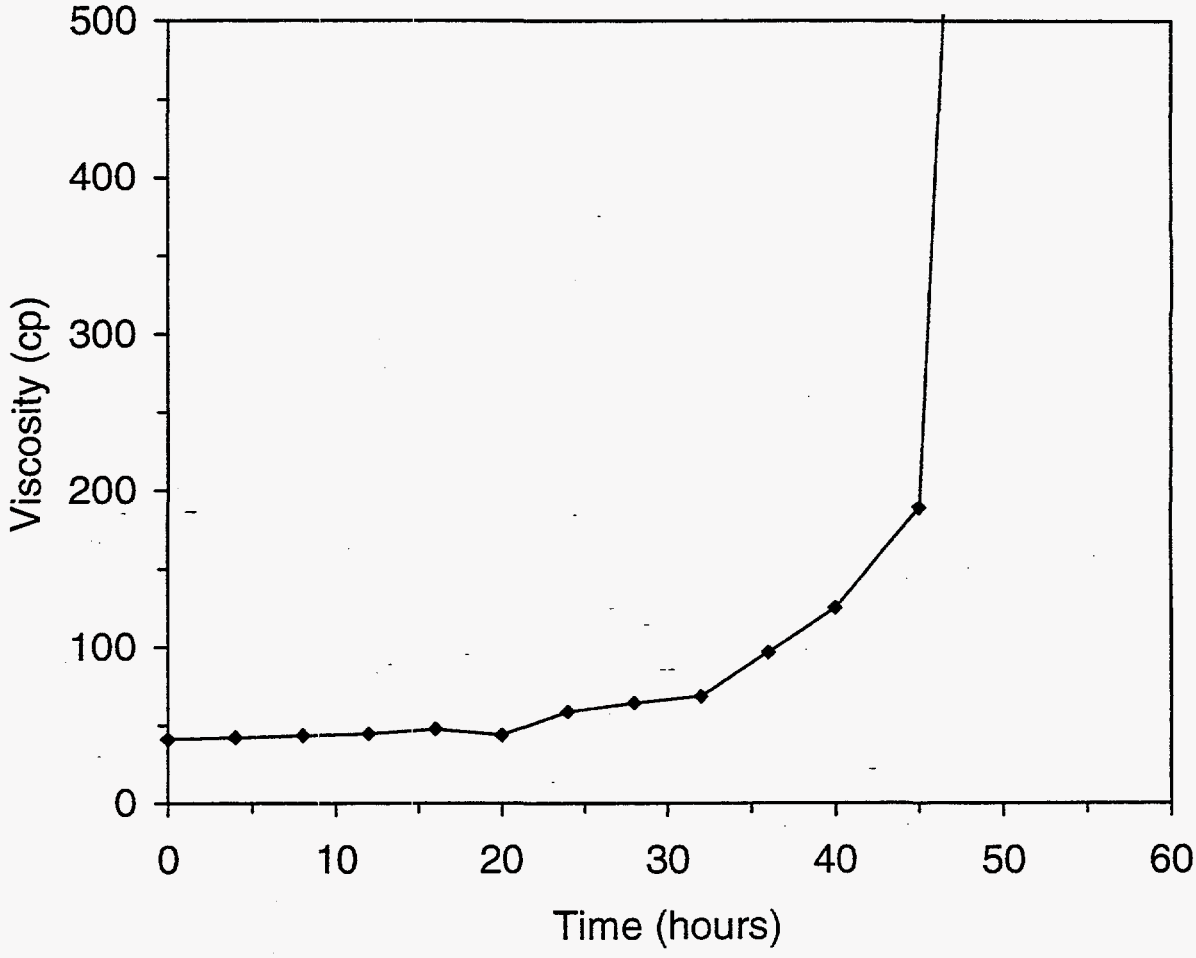

Figure 7.3 : Viscosity behavior of gelant containing 5000 ppm Alcoflood 935, 1500 ppm thiourea, 600 ppm sodium dichromate and 2.0% NaCl; Shear rate = 11.25 s^{-1}.

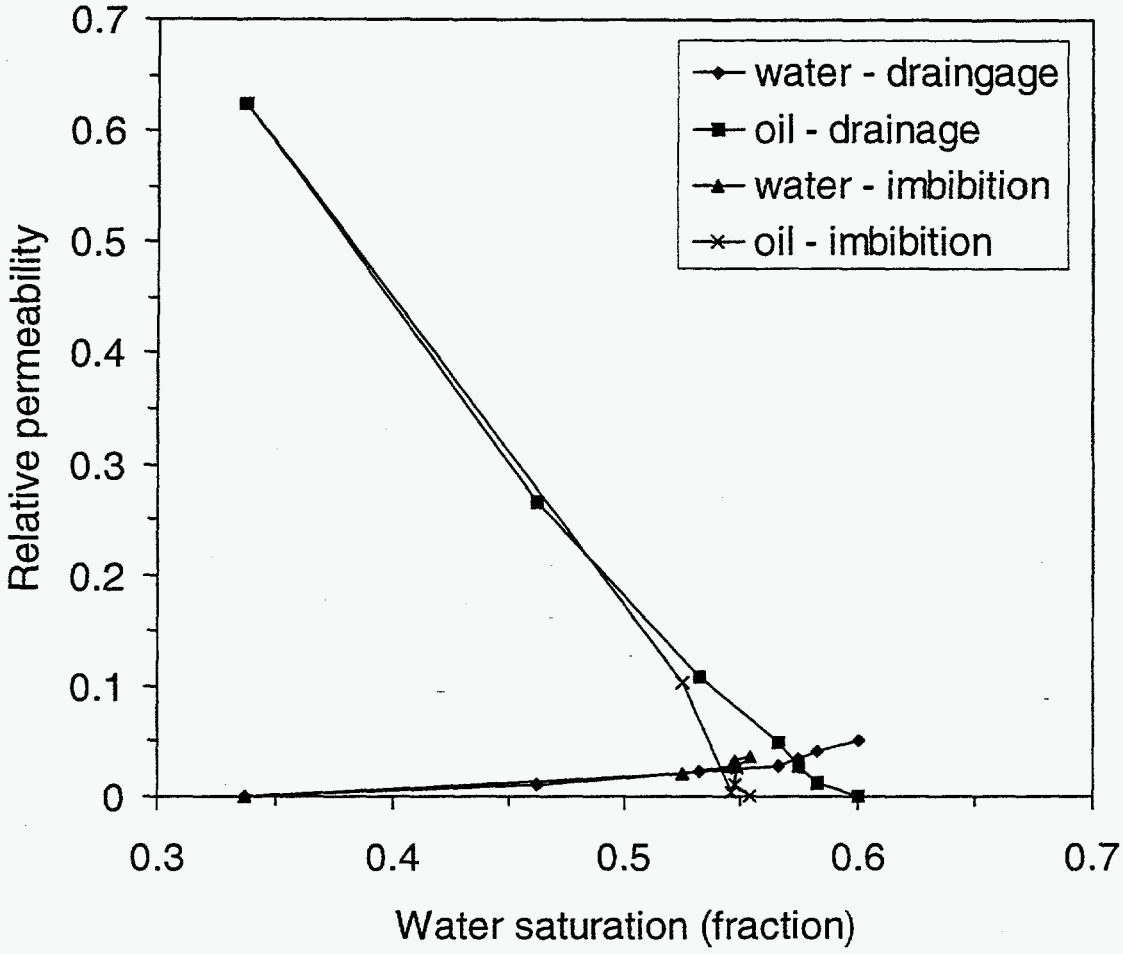

Figure 7.4 : Relative permeability curves before gel treatment - Total slab length;
- Base permeability = 184 md at 100% water saturation.

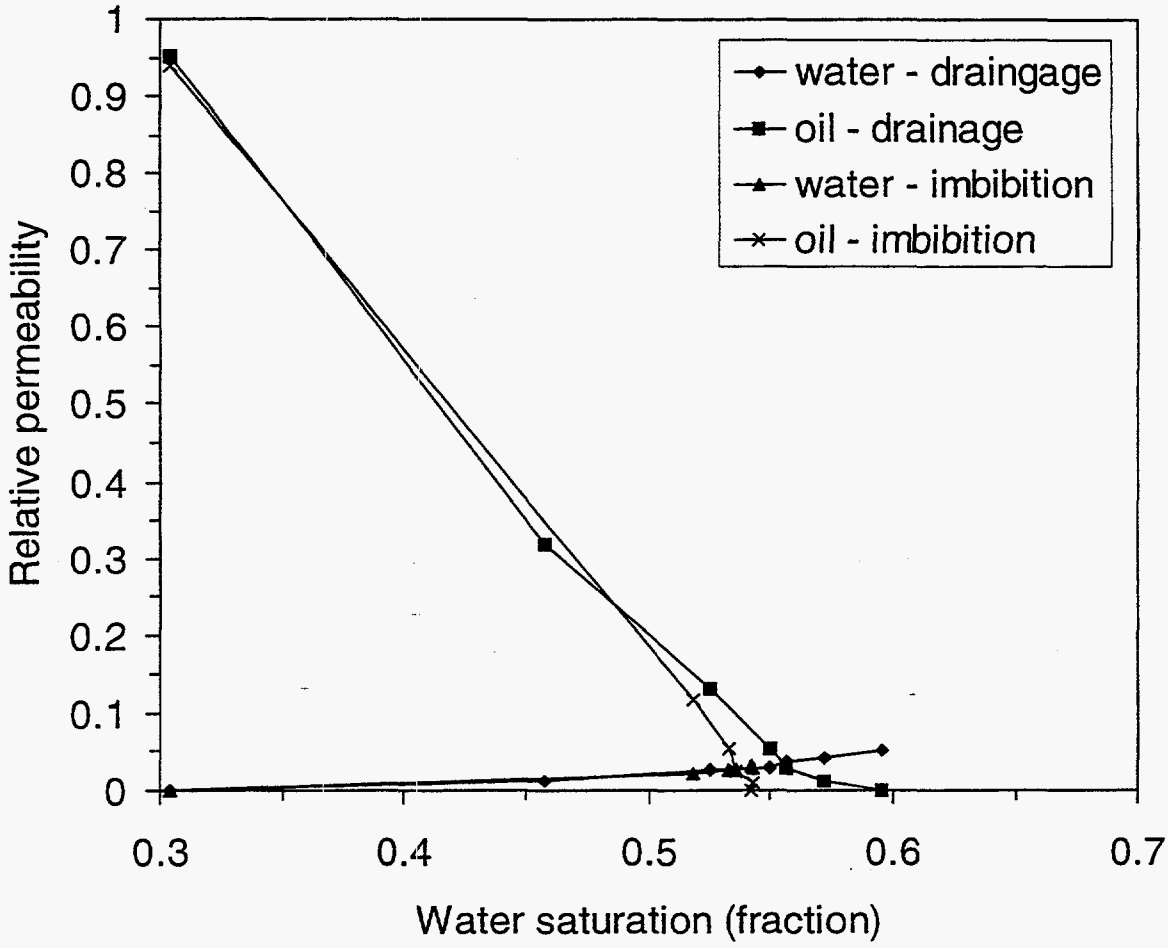

Figure 7.5 : Relative permeability curves before gel treatment - Section 1;
- Base permeability = 172 md at 100% water saturation.

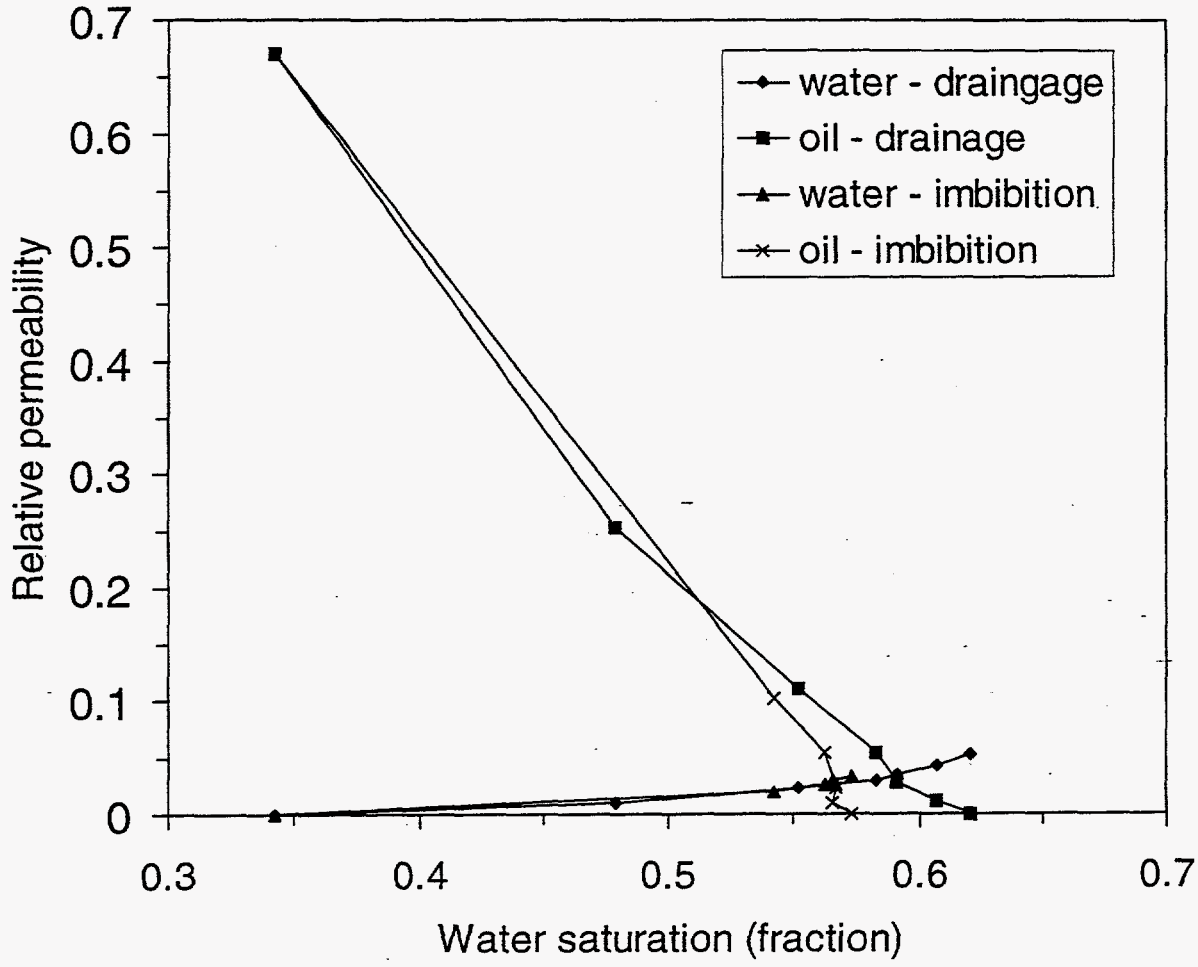

Figure 7.6 : Relative permeability curves before gel treatment - Section 2;
- Base permeability = 223 md at 100% water saturation.

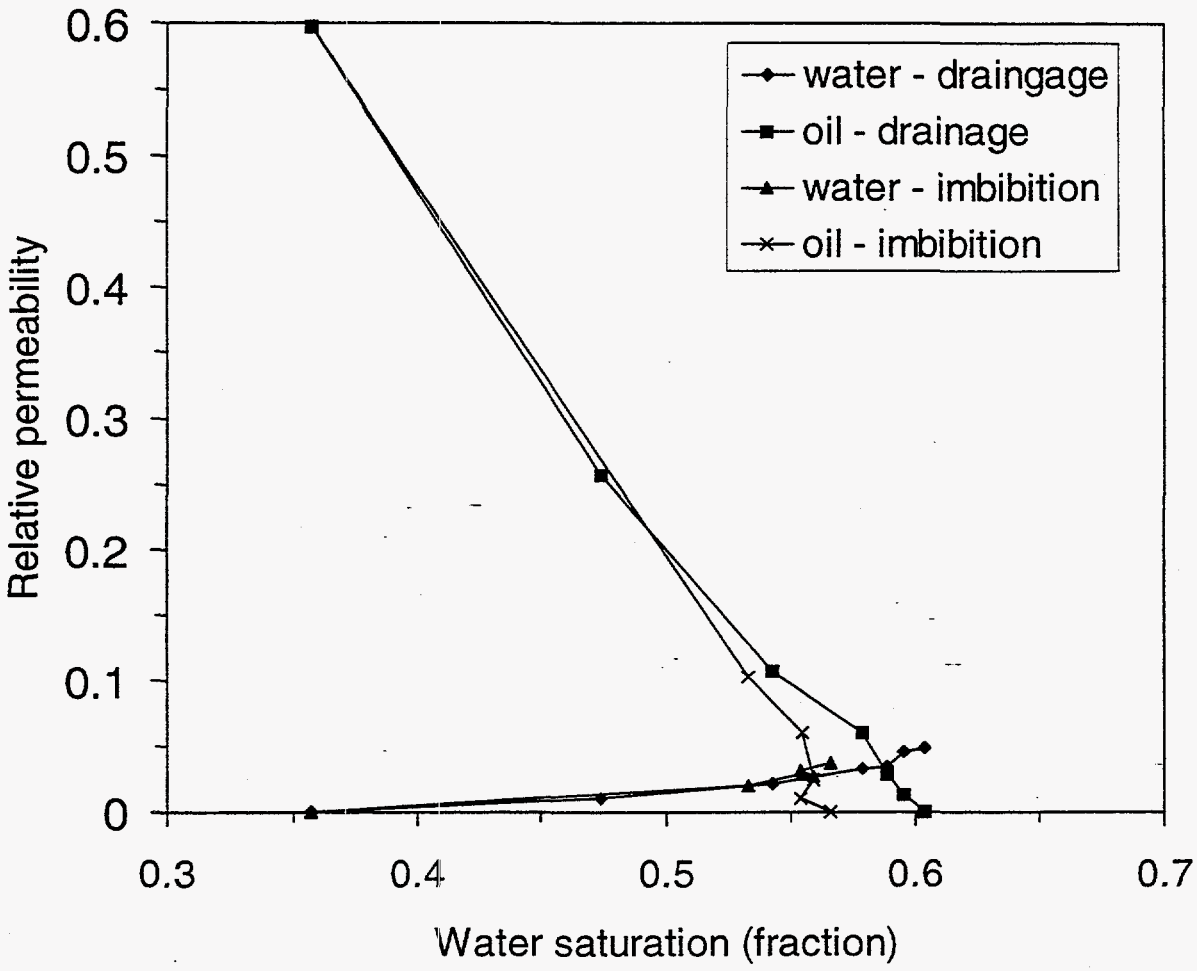

Figure 7.7 : Relative permeability curves before gel treatment - Section 3;
- Base permeability = 182 md at 100% water saturation.

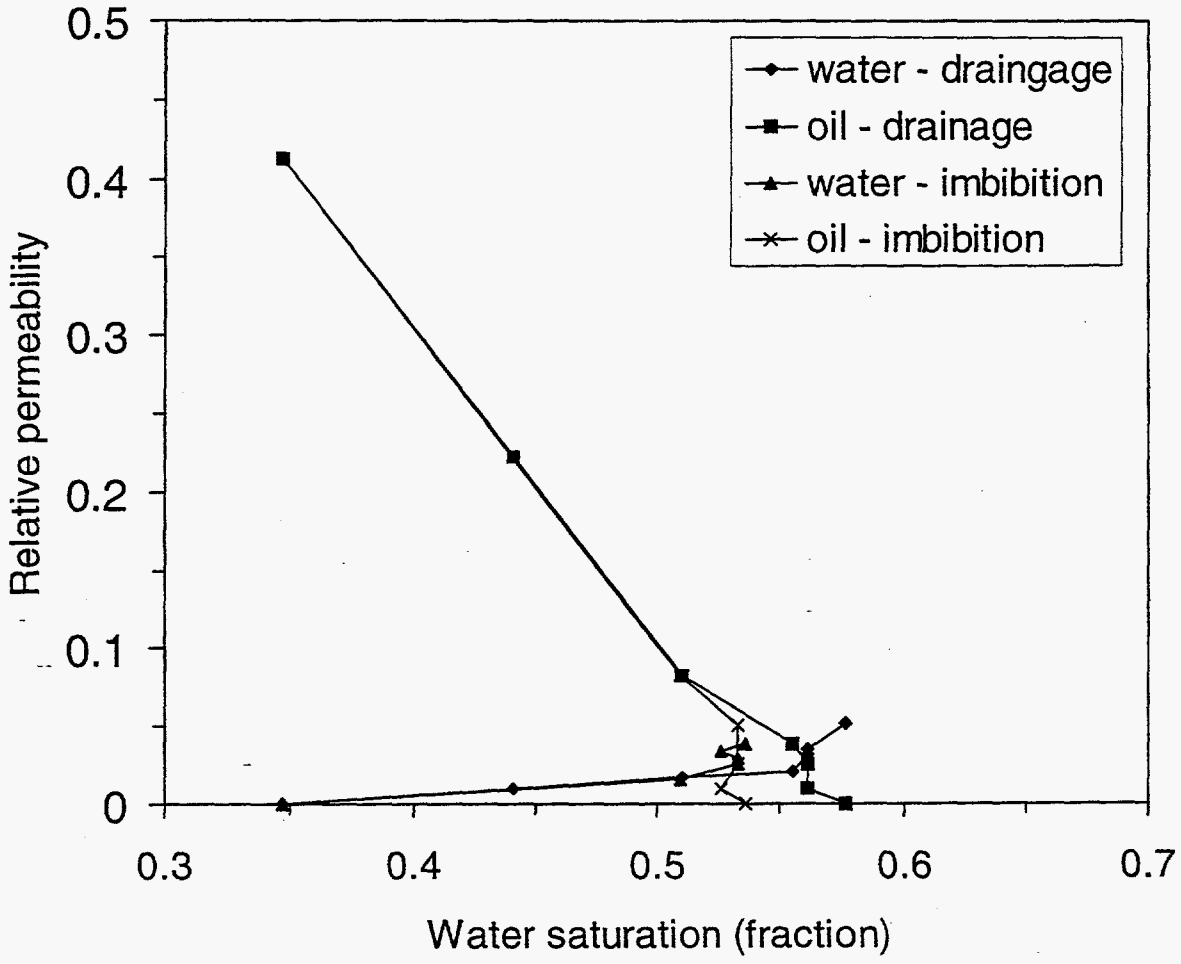

Figure 7.8 : Relative permeability curves before gel treatment - Section 4;
- Base permeability = 181 md at 100% water saturation.

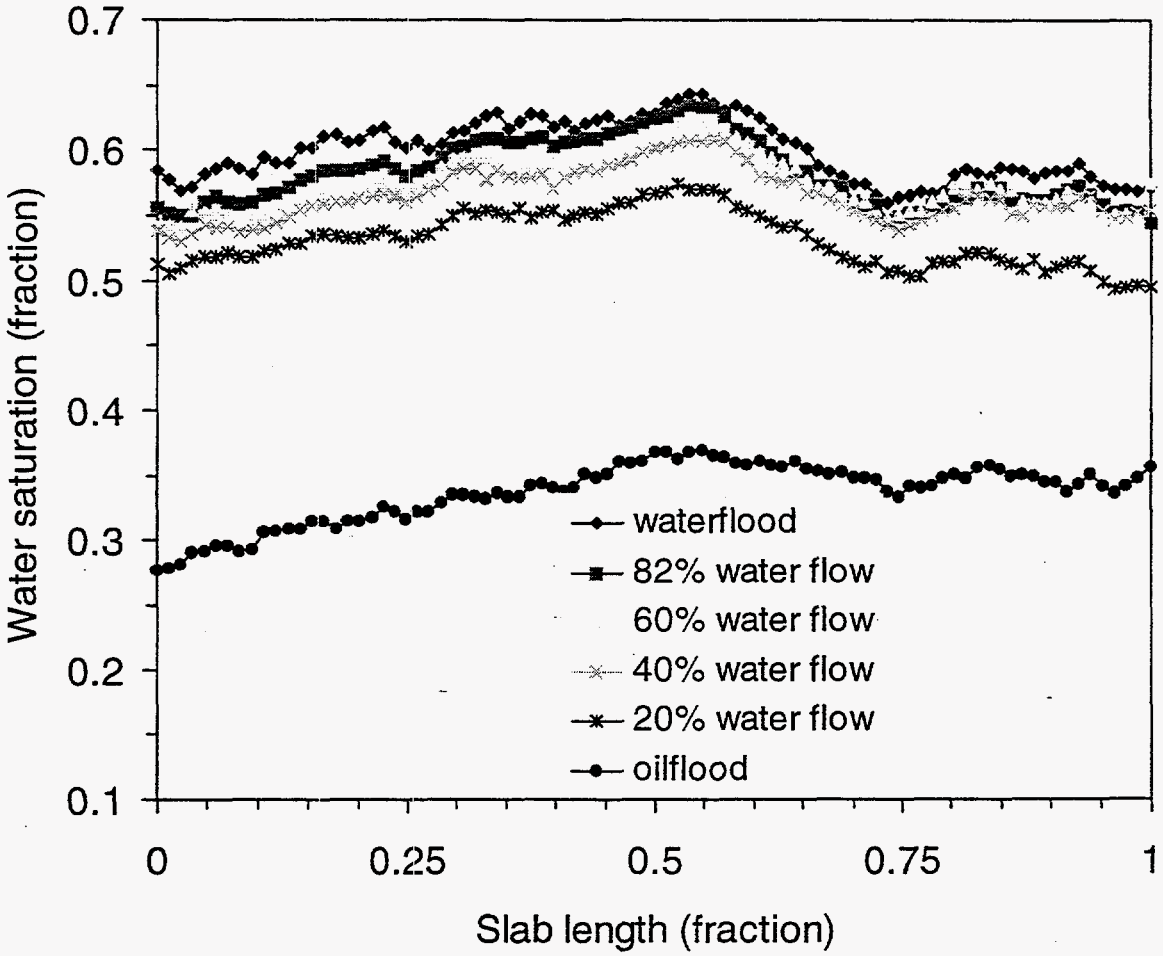

Figure 7.9 : Water saturation profiles at selected fractional flows before gel treatment - drainage cycle and steady-state.

Saturation profiles during gelant injection and during the oil overflush are shown in Figures 7.10 and 7.11, respectively. The gelant and the oil overflush were injected in direction #2, from the right side in Figures 7.10 and 7.11. The gelant displays as water saturation in the profiles. Small saturation changes were observed during gelant injection as shown in Figure 7.10. An oil bank was observed to progress through the core slab during the oil overflush (Figure 7.11).

Post-treatment injections were from direction #1. Dodecane was injected until steady-state was reached. Water saturations in the slab after the oil flood reached steady-state are shown in Figure 7.12. The oil flood decreased the water saturation in sections 1, 2 and 3 (up to 0.75 of core length), but slightly increased the water saturation in the gel-treated section (0.75 to 1.0 of core length).

Residual water saturations and permeabilities to oil at residual water saturations before and after the gel treatment are presented in Table 7.2. The gel significantly reduced the oil permeability in Section 4 (the treated section) but also reduced in the permeability in the other three sections. The treatment also increased the residual water saturations in all sections.

Future Work

Injections of oil, water and both will be conducted in the core slab in order to determine the relative permeability curves after the gel treatment. These curves along with the saturation profiles will be used to interpret the behavior of the gel system for use in production wells.

References

1. Seright, R. S., *Improved Techniques for Fluid Diversion in Oil Recovery*, U.S. Department of Energy Contract No. DE-AC22-92BC14880, Report No. DOE/BC/14880-5 (December 1993).
2. Liang, J., Sun, H., and Seright, R. S., *Why Do Gels Reduce Water Permeability More Than Oil Permeability?* SPE/DOE 27829 presented at the 9th Symposium on Improved Oil Recovery, Tulsa, Oklahoma (17-20 April 1994).
3. Zaitoun, A , Rahbari, R., and Kohler, N., *Thin Polyacrylamide Gels for Water Control in High_Permeability Production Wells* , SPE22785 presented at the 66th Annual Technical Conference and Exhibition of the Society of Petroleum Engineer held in Dallas, TX (October 6-9, 1991).
4. Maxcy T. A., *A Kinetic Study of the Reduction of Chromium(VI) to Chromium(III) by Thiourea*, PhD Dissertation, University of Kansas (1991).
5. Harnboonzong, P., *Microwave Attenuation for Monitoring Saturations in a Linear System during Liquid-Liquid Immiscible Displacement*, MS Thesis, University of Kansas (1990).

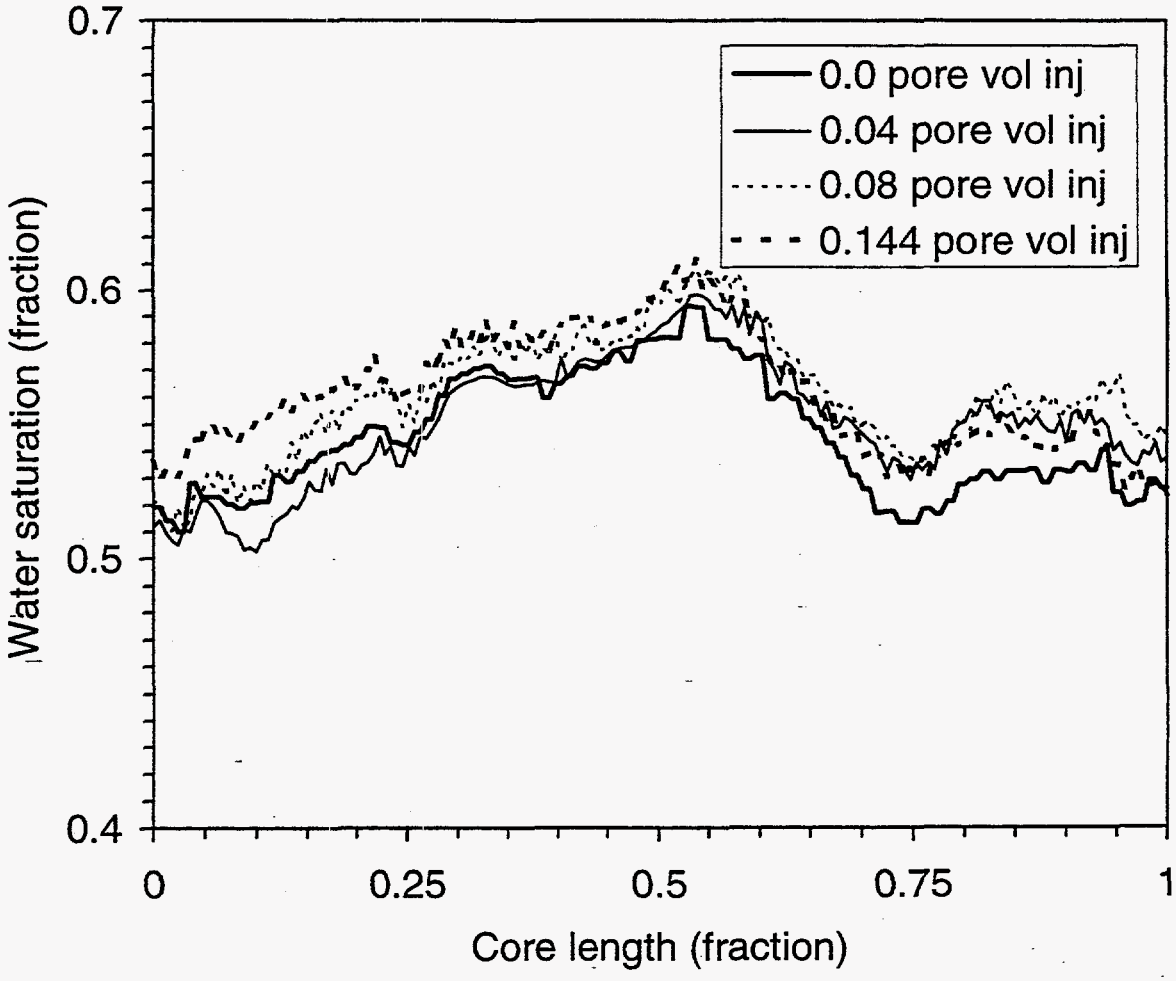

Figure 7.10 :Water saturation profiles during gelant injection; Injection from right side (direction #2).

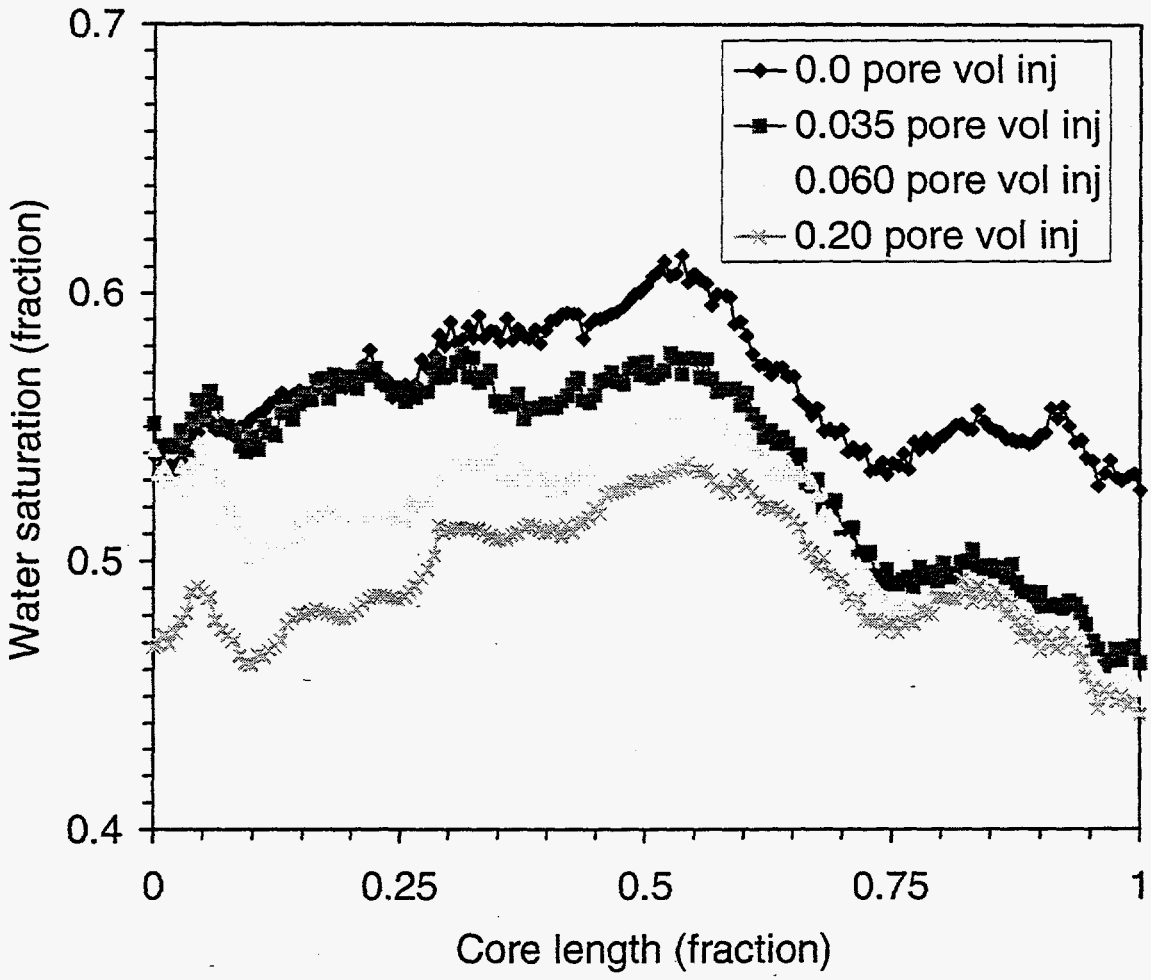

Figure 7.11 : Water saturation profiles during injection of oil overflush; Injection from right side (direction #2).

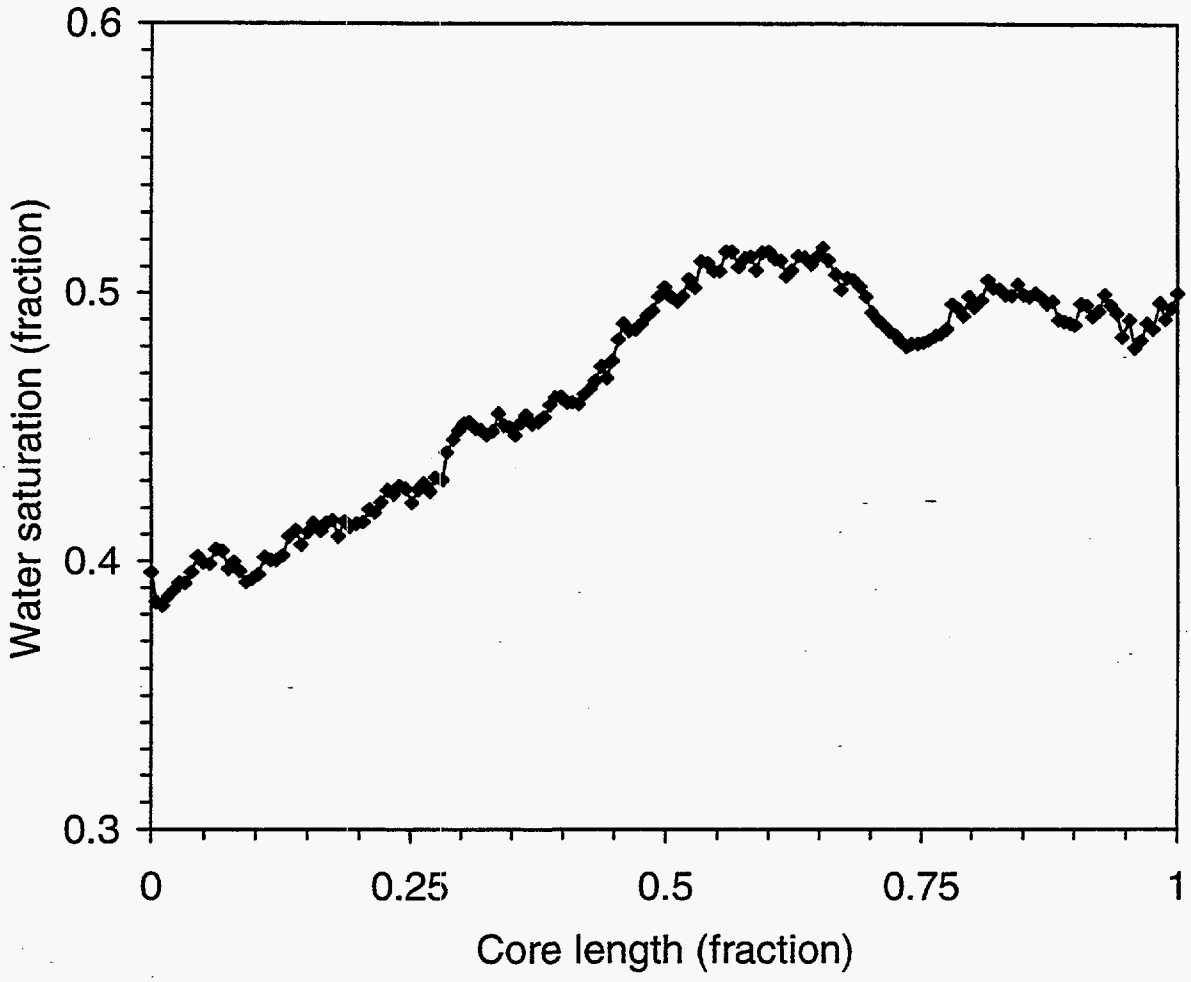

Figure 7.12 : Water saturation profiles after post-treatment oilflood; Injection from left side (direction #1).

Table 7.2 : Residual water saturations and oil permeabilities at residual water saturation before and after the gel treatment.

	Pre-gel treatment		Post- gel treatment		
	Residual water saturation	Oil permeability at residual water saturation (md)	Residual water saturation	Oil permeability at residual water saturation (md)	Permeability ratio (pre-/post-)
Overall	0.32	153	0.47	1.0	150
Section 1	0.28	205	0.41	40	5.1
Section 2	0.32	202	0.46	31	6.5
Section 3	0.34	142	0.51	21	6.8
Section 4*	0.33	117	0.49	0.26	450

* Section 4 was treated with gel.